

# **KC-135 Flight Testing of Void Fraction Capacitance Probe for Microgravity Two-Phase Flow**

Dr. Frederick R. Best  
Texas A&M University  
Department of Nuclear Engineering  
College Station, Texas 77843-3133  
(409) 845-4108

Under NASA JSC Grant: NAG 9-787

## **GOVERNMENT PURPOSE LICENSE RIGHTS**

This technical data shall be subject to the restrictions contained in the definition of "Limited Rights" in DFARS clause at 252.227-7013. After two year period, the data shall be subject to restrictions contained in the definition of "Government Purpose License Rights" in DFARS clause at 252.227-7013. The Government assumes no liability for the unauthorized use or disclosure by others. This legend, together with the indications of the portions of the data which are subject to such limitations, shall be included on any reproduction hereof which contains any portions subject to such limitations and shall be honored only long as the data continues to meet the definition on Government Purpose License Rights.

## **ABSTRACT**

This report describes the work performed under a NASA Johnson Space Center grant to perform flight testing of a void fraction capacitance probe in the microgravity environment aboard the KC-135. The overall goal of this project is to validate and calibrate the capacitance sensor in a microgravity environment. This project has been conducted with the cooperation of Goddard Space Flight Center (test bed), Lewis Research Center and Creare Inc. (capacitance void fraction sensors and instrumentation), Johnson Space Center, Texas A&M Center for Space Power, and the Interphase Transport Phenomena Laboratory (data acquisition and integration of equipment for KC-135 flights). Twelve KC-135 flights were conducted in three series. Test points were collected over a wide range of void fractions (0 % - 90 %). Data were collected from stratified, slug, and annular flow regimes. Void fraction measurements from the capacitance sensors were compared with the void fractions from a trapped volume in the test section between two quick closing valves. Under the annular flow regime, void fractions measured by the capacitance sensors compared well with values from the trapped volume. In slug flow regime, some discrepancies between the sensors and trapped volumes were found. However, when the working fluid (Suva) mass flow rate increased from 0.416 lb./min. to 1.00 lb./min., the void fraction measurements between the capacitance sensors and the trapped volume had better agreement. Overall, the FRIM experimental package produced satisfactory test conditions in the microgravity conditions of the KC-135 aircraft, to validate and calibrate the Creare capacitance void fraction sensors.

## CONTENTS

	Page
1.0 Introduction .....	1
2.0 Equipment Description .....	5
2.1 Flow Regime In Microgravity (FRIM) .....	5
2.2 ITP Mechanical .....	9
3.0 Flight Test Effort.....	10
3.1 Preflight Activities .....	11
3.2 July 1995, Flight Chronology .....	13
3.2.1 Flight 1 - July 11 .....	13
3.2.2 Flight 2 - July 12 .....	16
3.2.3 Flight 3 - July 13 .....	17
3.2.4 Flight 4 - July 14 .....	17
3.3 Equipment Modifications.....	17
3.4 January 1996, Flight Chronology.....	18
3.4.1 Flight 5 - January 23.....	19
3.4.2 Flight 6 - January 24.....	20
3.4.3 Flight 7 - January 25.....	20
3.4.4 Flight 8 - January 27.....	20
3.5 Equipment Modification .....	21
3.6 May 1996 Flight Chronology.....	22
3.6.1 Flight 9 - May 21.....	23
3.6.2 Flight 10 - May 22.....	23
3.6.3 Flight 11 - May 23.....	23
3.6.4 Flight 12 - May 24.....	24
4.0 Results .....	25
4.1 Instrumentation Validation .....	25
4.2 July 1995, Flight Results.....	37
4.3 January 1996, Flight Results .....	41
4.3 May 1996, Flight Results .....	43
4.4 Fill Calibration Test.....	47
5.0 Summary .....	49
References.....	51

## FIGURES

	<b>Page</b>
Figure 1. FRIM schematic .....	6
Figure 2. Tri-axial accelerations for initialization parabola set.....	27
Figure 3. Tri-axial accelerations for parabola 1 .....	28
Figure 4. Tri-axial accelerations for 0 g period of parabola 1 .....	29
Figure 5. Liquid Suva mass flow rate .....	30
Figure 6. Ambient temperature .....	31
Figure 7. Coolant inlet and outlet temperatures .....	32
Figure 8. Temperatures before and after test section .....	33
Figure 9. Absolute pressure .....	34
Figure 10. Evaporator power.....	35
Figure 11. Void fraction sensors .....	36
Figure 12. Average void fraction from July 1995, flights .....	38
Figure 13. Flow regime map for microgravity .....	39
Figure 14. Flow regime map for 2 g .....	40
Figure 15. Average void fractions from January 1996, flights .....	42
Figure 16. Average void fractions from May 1996, flights .....	46
Figure 17. Sensor fill test .....	48

## Tables

	Page
Table 1. Test points May 22, 1996.....	44
Table 2. Test points May 23, 1996.....	44
Table 3. Test points May 24, 1996.....	45

## 1.0 Introduction

Currently, the space program uses gravity independent, single-phase flow for high power thermal management purposes. Since technology for space applications is sensitive to volume, mass, and power, future space missions should take advantage of two phase flow systems (co-current vapor and liquid flow). This technology has the ability to carry more energy per unit mass than single-phase flows, while simultaneously operating at a constant temperature. A two-phase system also requires less pumping power per unit thermal energy carried and has better heat transfer characteristics than single-phase systems. All of these features lead directly to improved performance and smaller mass requirement than a single-phase system.

In traditional two-phase flow studies, the flow regime refers to the physical location of the gas and liquid in a conduit. The flow configuration is important for engineering data correlation such as heat and mass transfer, pressure drop, and wall shear. However, it is somewhat subjective since it is mostly defined by the experimenter's eye, which results in an approximate definition. Thus, there is a need for better discretizing instrumentation. In designing a thermal management system, one can usually estimate the phasic flow rates. However, the topological configurations of the phases are unknown. Hence, most investigations performed on this subject have tried to determine, through

experimental and empirical means, when each flow regime configuration is likely to occur given the system parameters.

Several tools have been developed over the years to identify the flow regime in two-phase flows. Such approaches include the study of pressure drop measurements, gamma densitometry, resistive and capacitance sensors as well as intrusive probes. Recently, with the advent of powerful personal computers and the development of technologies based on non-destructive evaluation, new technologies have been developed for non-intrusive monitoring. One such technology is the capacitance method developed by Creare Inc. for the purpose of void fraction measurements.<sup>1</sup>

Knowledge of the two-phase flow state is fundamental for two-phase flow systems. This is especially true in the microgravity acceleration environment of an orbital spacecraft. To a first order (or assuming a homogeneous flow exists), the void fraction is directly related to the energy carried by the two-phase mixture. Therefore, the void fraction is a key parameter in monitoring the operating state of a two-phase flow system. Furthermore, two phase flows in microgravity are known to be different from 1 g flows.<sup>2</sup> Therefore, it is essential to calibrate the void fraction sensors under a microgravity environment.

This report describes the work performed under a research grant funded by the NASA Johnson Space Center (JSC). This project is specifically aimed at

supporting the technological effort of the JSC Two-Phase Extended Evaluation in Microgravity (TEEM) experiment<sup>3</sup> and the Goddard Space Flight Center (GSFC) breadboard experiment.<sup>4</sup> The overall goal of this work is to validate and calibrate capacitance sensor operation in a microgravity environment.

This program was conducted jointly with JSC, GSFC, Lewis Research Center (LeRC), Creare Inc., the Interphase Transport Phenomena (ITP) group of Texas A&M University (TAMU), and the Center for Space Power (CSP) at TAMU. This program was funded at TAMU by a NASA JSC Grant, which also provided for eight days of flying aboard the KC-135.

GSFC provided the Flow Regime In Microgravity (FRIM) experiment test bed, which produced the two phase flow mixture. The FRIM is a modification of the breadboard experiment by Benner et al. at GSFC.<sup>4</sup>

LeRC provided a capacitance sensor transducer and two remote electronics boxes. In support, Creare Inc. loaned a second sensor to the program. Creare Inc. also provided flight support and analysis of the void fraction sensor results from the first two flight series.

The TAMU team carried out modifications to the FRIM for flight testing on the KC-135. These included integration into an ITP test system, which supplied data acquisition, digital imagery, pressurized gases, and cooling water. ITP lab was

responsible for the data acquisition and data reduction. Additional funds provided by the CSP allowed for four additional days of flying.

The following sections of the report detail the work that was performed under this research grant. The test system hardware, both the FRIM and ITP KC-135 support packages, is described in section 2.0. Preflight activities, including the preparation and submission of the Test Equipment Data Package (TEDP), are described in section 3.1. Flight activities and chronology are described in sections 3.2 to 3.6. Additionally, post flight equipment modifications are also described in these sections. Results from the flights and data analysis are described in section 4.0. A full calibration of the two capacitance sensors was completed and is described in section 4.4. Finally, a summary of the work is discussed in section 5.0.

## **2.0 Equipment Description**

The following sections provide a description of the test system that was used in flight and ground testing. This includes the FRIM, ITP's mechanical hardware and the data acquisition equipment.

### ***2.1 Flow Regime In Microgravity (FRIM)***

The FRIM is a modification of the breadboard experiment of GSFC described by Benner et al.<sup>4</sup> The breadboard was modified to include two void fraction sensors, a clear sight tube, and quick closing valves. Figure 1 is a schematic diagram of the modified FRIM. A detailed description of the capacitance sensors is given by Crowley et al.<sup>1</sup>

The following discussion describes the major components of the FRIM.

The FRIM uses R-134a, also called Suva, an environmentally benign tetrafluoroethane, as the working fluid. The description begins at the pump discharge manifold. From the outlet of the Suva pumps, subcooled Suva enters the evaporator. The evaporator is a bored rod evaporator, which can provide up to 2 kW of electrical power input. The function of the evaporator is to produce a

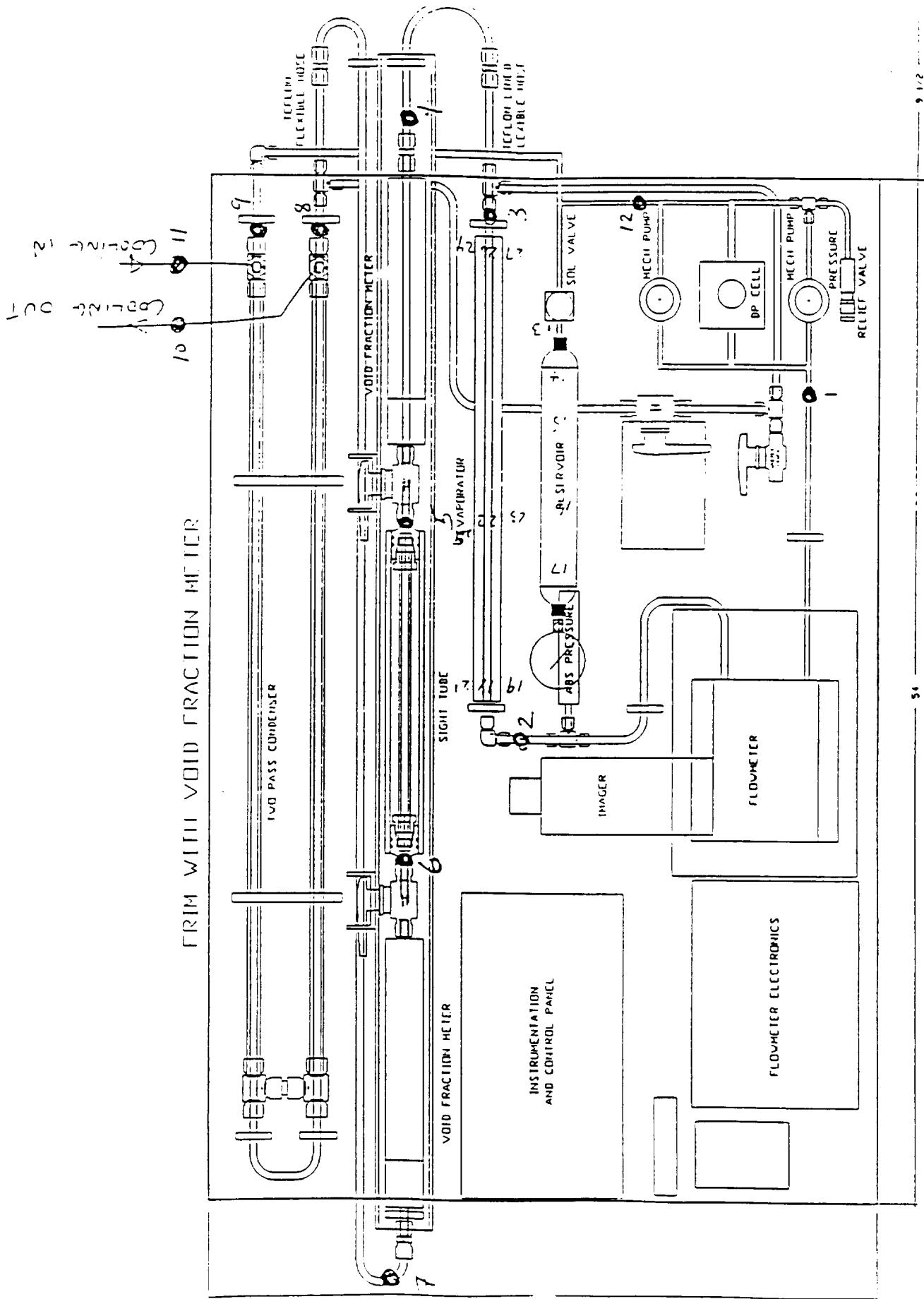


FIG. 1. FRIMV002  
DATE: MAY 9 1995

• The location

Figure 1. FRIM schematic

two phase mixture from the inlet subcooled liquid. The evaporator is insulated with Nomex cloth to limit ambient losses. The two phase flow from the evaporator passes through the test section. The test section consists of an upstream void fraction meter, a flow visualization tube, and a downstream void fraction meter.

After passing through the downstream void fraction meter, the flow enters the condenser section. The condenser is a two pass, tube-in-tube heat exchanger. Cold water was used as the coolant. The ultimate heat sink for the condenser coolant is an ice bath contained in a 10 gallon reservoir located on the bolt-down package (BDP). The subcooled liquid leaving the condenser returns to the pumps and begins the cycle again.

The flow rate is measured by a Coriolis mass flow meter, located on the outlet of the Suva pump manifold. A vertical, cylindrical vessel, located on the flow line after the condenser, is used to control the pressure in the test system. This accumulator is nominally filled half and half with liquid and vapor Suva. Pressure is regulated through external electrical heaters located on the outer walls of the accumulator. Temperature controllers, located on the instrumentation panel, regulate the temperatures of the accumulator heaters to produce the desired saturation temperature, thereby controlling pressure. A solenoid valve permits the isolation of the accumulator from the rest to the test loop when desired.

Absolute and differential pressure transducers provided absolute pressure reading for the system and differential pressure measurement across the pump. A bypass line was also included in the FRIM. When the quick closing valves shut, the bypass line opens, permitting the flow to bypass the test section and continue from the evaporator to the condenser. This helps to preserve constant system conditions and prevents dryout of the evaporator walls.

The quick closing valves, located at each end of the clear sight tube, allow the experimenters to isolate the two phase flow and measure the liquid level trapped in the sight tube. The test section was constructed to be rotated vertically for the mechanical measurements. The test section lies in the horizontal position during the 0 g periods of the flight. It will be raised into the vertical position after the quick closing valves are closed. The liquid level in the sight tube is measured during 2 g or level flight conditions.

Furthermore, 29 type T thermocouples were placed on the outer walls of the test system piping to monitor the temperatures in the system. Figure 1 shows the locations of the thermocouples. Another type T thermocouple was used to record ambient temperatures during the flight testing. Tri-axial accelerometers were mounted on the FRIM co-axially with the orientation of the test system piping. The accelerometers provide vertical, transverse, and axial acceleration profiles experienced by the test package during the flight test.

## ***2.2 ITP Mechanical***

The test system used on both the ground and on the KC-135 consists of three components, the FRIM, the “bolt-down package,” and the “ computer control console.” The FRIM contains the two-phase flow loop, as described in the previous section.

The bolt-down package (BDP) serves as 9 g structural support for the FRIM and the computer control console (CCC). The FRIM is mounted on aluminum I-beams, which are attached to the BDP. The BDP also contains the ice bath reservoir and the self-priming positive displacement cooling water pump. The BDP was bolted to the floor of the plane during flight testing. A cage of aluminum slide railing was constructed around the FRIM to protect the experiment and test personnel during flight testing.

The CCC is also attached to the BDP. The CCC contains the housekeeping computer, high speed instrumentation recorder, two Createc void fraction remote electronics boxes, two DC power supply boxes, one for the Suva pumps and the other for the positive displacement cooling water pump, and the central processor of the digital imager, Kodak Ektapro 1000 motion analyzer. The Ektapro 1000 is a high speed digital system, capable of capturing one frame of video every one thousandth of a second, and storing as many as 6 partial pictures per frame, with a recording rate of 6000 partial pictures per second.

### **3.0 Flight Test Effort**

The flight test effort consisted of twelve flights performed in three series on the NASA KC-135 test aircraft, which is based at Ellington Field in Houston, Texas.

The first test series of four flights was conducted on July 11-14, 1995. The second series of four flights was conducted on January 23, 24, 25, and 27, of 1996. The third series was conducted on May 21-24, 1996. The first and third test series were funded by the JSC grant. The second series was funded by the CSP.

The in-flight positions were as follows:

- Test coordinator (ITP)
- Void fraction sensor operator (Creare)
- Digital imager operator (ITP or JSC)
- Test section operator (ITP)
- Data collection computer operator (ITP)

The following sections describe the preflight activities and a brief chronology of the flights, including problems that were encountered and modifications made to the test package as the flights unfolded.

### **3.1 Preflight Activities**

The GSFC FRIM arrived at Texas A&M during the first week of June 1995. The Creare sensor remote electronics boxes arrived shortly after. From the arrival of the FRIM to the first day of KC-135 flight testing, the following activities were carried out.

- Charging the system

The FRIM was shipped from Goddard with nitrogen in the flow loop. The system was evacuated and charged with 1.1 kg of R-134a (Suva) at the ITP lab.

- Modification of BDP and CCC structures

Aluminum I-beams were mounted on the BDP to support the FRIM test bed. A nitrogen tank was installed on the BDP. Nitrogen was used to actuate the quick closing valves that isolate the sight tube. The CCC was modified to accommodate the void fraction sensor remote electronics boxes, housekeeping computer, digital imager processor, instrumentation recorder and DC power supplies.

- Completing the Test Equipment Data Package (TEDP)

The TEDP<sup>5</sup> is required by the NASA Flight Readiness Review prior to obtaining flight approval. This document includes the test plan, engineering drawings, schematics, structural analysis, electrical load analysis, and analysis of any identifiable hazards.

- Construction of the cooling water system

A cooling water reservoir, bath system was modified from a previous KC-135 experiment conducted by the ITP group. A positive displacement pump was used to pump cold water through the condenser of the FRIM. The system used an Omega rotameter to monitor coolant flow. A globe valve was used to adjust the flow rate of the cooling water.

- Integration of ITP data acquisition with the FRIM

MetraByte Exp-16 multiplexer cards were installed to receive thermocouple signals, evaporator power, mass flow rate, acceleration profiles from the tri-axial accelerometers, absolute and differential pressure readings. The signals from the MetraByte Exp-16 cards were digitized and stored on a personal computer via a MetraByte DAS8, analog to digital converter card. The instrumentation recorder was calibrated to receive voltage signals from the void fraction sensors and the tri-axial accelerometers.

- Construction of the protective cage

A protective cage of aluminum railing was constructed to prevent experimenters from flying into the sensitive test equipment during KC-135 flight testing. Also, the digital imager, with the halogen light source, was installed on the cage above the clear sight tube to record visually the flow regime in the test section.

Since there was limited time between the arrival of the FRIM and the flight schedule, ground tests were limited to a full-up run to check the instrumentation.

During these tests, one of the tri-axial accelerometers malfunctioned. An electrical short between two of its internal leads caused the accelerometer to be inoperable. A replacement accelerometer could not be obtained prior to the flight series. Therefore, it was decided to use only two accelerometers (vertical and axial) for the first flight series. Also, it was noticed that the LED from the second void fraction sensor remote electronics box periodically locked up when the quick closing valves were actuated. Creare was notified of this problem and another remote electronics box and sensor circuit board was brought to Ellington Field for the flight tests. The entire test system was packed and shipped by truck to Ellington Field.

### ***3.2 July 1995, Flight Chronology***

#### **3.2.1 Flight 1 - July 11**

A NASA JSC Safety and Test Readiness Review was conducted to ensure that all NASA safety regulations were satisfied. After passing the inspection, the test package was bolted to the KC-135 deck. The experiment was placed in the middle of the plane, with the FRIM forward of the CCC.

Prior to flight, the condenser coolant bath was filled with ice and water, then sealed to prevent leakage. An initial check of the system instrumentation revealed that the void fraction sensors were not responding properly. It was determined that the high humidity in the plane was causing condensation within

the void fraction instrumentation. When the remote electronics boxes were left on and heated up, the condensation evaporated and the boxes operated properly. Also, condensation on the digital imager lens blurred the focus at 500 frames per second.

For the first three parabolas, the housekeeping computer and void fraction recorder were operating, while rest of the system was shutdown, i.e., no flow and the evaporator was turned off. These null parabolas were used to verify the operating behavior of the instrumentation in the KC-135 flight environment in the absence of two-phase flow. For parabolas 4-6, the same conditions existed as for the null parabolas, except the accumulator was isolated during these parabolas. For the next four parabolas (7-10), the high flow Suva pump was turned to the maximum measurable flow rate of 0.416 lb./min.

Sets of ten parabolas were flown during this flight. The following is the test procedure that was intended for this flight:

- The operating conditions for the system were set prior to entering the first 0 g period. These conditions included the evaporator power, the liquid Suva mass flow rate, condenser coolant flow rate and the accumulator temperature setting. The goal was to set the test system under a steady operating condition prior to isolation of the sight tube.

- Data collection of the housekeeping data and the instrumentation recorder for the void fraction sensors was initiated prior to entering the first 0 g period. The data collection continued until the end of the parabola set.
- During the last 4 to 8 seconds of the 0 g period of the fourth parabola, an imager shot of the sight tube was taken. The sight tube was then isolated with quick closing valves prior to exiting the 0 g period. The test section was raised to the vertical position during the fifth 0 g period, with the liquid level being measured during the ensuing 2 g period.
- While the sight tube was isolated, the system settings were adjusted to the next test point conditions.
- A second imager shot and isolation were taken on the tenth 0 g period of the parabola set. After the tenth 0 g period, the plane returned to level flight (1 g) for several minutes. The test section was then raised to the vertical position and measurement of the liquid level in the sight tube was made. Also, during this time, housekeeping data stored in RAM was written to a floppy disk.

During this flight, the flight test personnel were unable to follow the proceeding test procedure due to various equipment failures. After the first set of ten parabolas, the system began experiencing power trips. These power trips occurred periodically throughout this flight. All housekeeping data prior to these trips were lost. Also, the quick closing valves opened after the lost of power to the system. Therefore, liquid level measurements were impossible after a power trip. The source of the power trips was isolated to a faulty power strip. A

replacement power strip was used for the next flight. The downstream Creare void fraction sensor remote electronics box locked up occasionally during the flight as experienced before in the ITP lab. The remote electronics box was cycled off and on to return to normal operational mode.

Finally, it was discovered after flight that erroneous vertical acceleration readings were recorded. The leads from the accelerometer were dislodged from the data acquisition card during the flight. Therefore, the instrumentation recorder recorded no voltage signal from the vertical accelerometer. This problem was rectified prior to the next flight.

### 3.2.2 Flight 2 - July 12

The same pre-flight activities were conducted for this flight as the first flight. The electrical and accelerometer problems from the previous flight were corrected and did not reoccur on subsequent flights. For this flight, only the first five parabolas of the first set of ten were used as initialization parabolas. The last five of the set were used for a test point. The flight procedure described in the previous section was utilized. However, the instrumentation recorder, a scientific tape recorder, used to record the void fraction sensor data, malfunctioned during this flight. The tape to the recorder was misfed at the start of the flight. Most of the void fraction readings from the capacitance sensors and vertical acceleration data were lost for this flight.

### 3.2.3 Flight 3 - July 13

For this flight, an analog to digital recorder was borrowed from a NASA contractor to record void fraction readings in parallel with the instrumentation recorder. While the instrumentation recorder recorded continuously throughout the parabola set, the analog to digital recorder only activated during 0 g periods of test points. The flight was cut short due to turbulent weather. Four test points were collected for this flight.

### 3.2.4 Flight 4 - July 14

On the fourth day of flying, no major equipment failures occurred. The void fraction remote electronics boxes occasionally locked up after the sight tube was isolated, but returned to normal operational mode after cycling their power switches. The maximum possible of eight test points was collected using the test procedure outlined in Flight 1. Both the analog to digital recorder and the instrumentation recorder operated satisfactory during the flight.

## **3.3 Equipment Modifications**

After gaining experience on the test package from the July flights, several modifications were made prior to the second series of flights in January of 1996. It was decided to use a PC to record the signals from the void fraction sensors

instead of the instrumentation tape recorder. A second analog to digital card (MetraByte DAS8) was purchased and used with a Hyundai 386 computer, the house keeping computer from the previous flight series, to record void fraction readings. An IBM 286 compatible computer was used for the house keeping data. Furthermore, Creare used their own notebook computer to record data from the void fraction sensors during the flight. The test package was evacuated and recharged with 1.1 kg of Suva. A new, third accelerometer was ordered and installed in the test package prior to the second flight series.

### ***3.4 January 1996, Flight Chronology***

Since the first flight series consisted of test points with high void fractions, test points with low void fractions were attempted for this flight series. As before, the evaporator power was varied to achieve different test conditions. Suva temperatures around the test system were monitored to ensure that the evaporator did not reach critical heat flux conditions and that vapor did not enter the Suva pumps. The condenser coolant water pump was cycled on and off to keep the Suva sub-cooled exiting the condenser. Also, to minimize ambient losses, the accumulator saturation temperature setpoint was set to the approximate ambient temperature of the plane during flight.

### 3.4.1 Flight 5 - January 23

Prior to flight, the coolant reservoir was filled with ice and water, then sealed.

The digital imager was set at 250 frames per second for this flight. The lower shutter speed permitted for better picture quality than the first the flight series (500 frames per second) with the light source used on the experimental package.

The first set of eight parabolas was used as initialization parabolas. The sight tube was isolated during the third 0 g period. An imager shot was taken just prior to the isolation.

Due to other experiments on the plane, the number of parabolas per set varied. Generally, there were eight parabolas per set. Occasionally, there were parabola sets of two parabolas when the plane was making a turn. Therefore, the test procedure from the first flight series was slightly modified. The sight tube was isolated during the third and the eighth 0 g periods of the set. The void fraction remote electronics boxes continued to periodically lock up after the sight tube was isolated. As before, the remote electronics box power was cycled off and on. Five test points were collected on this flight. Two test points were lost because the isolation occurred after exiting the 0 g period.

#### 3.4.2 Flight 6 - January 24

No initialization parabolas were taken for this flight. The conditions for the first test point were set prior to entering the first parabola. The same test procedures were used as before. Seven test points were collected from this flight.

#### 3.4.3 Flight 7 - January 25

Instead of being inside the hanger, the KC-135 aircraft remained outside during the night. The ambient temperature on the aircraft and in the FRIM was initially 44 °F. The ambient temperature climbed from 64 °F from the first parabola to 78 °F on the last parabola. The flight sequence was slightly different from the previous flights. Due to constraints from another experiment on the plane, each parabola set consisted of twelve parabolas. The first eight parabolas had small positive vertical accelerations, while the last four parabolas were close to 0 g. Therefore, the sight tube was isolated once during the first eight parabolas and twice (ninth and twelfth) during the last four parabolas of the set. Twelve test points were recorded for this flight.

#### 3.4.4 Flight 8 - January 27

It was decided for this flight to vary the coolant water flow rate instead of the evaporator power to set the test conditions. Each parabola set consisted of eight

parabolas. The sight tube was isolated on the third and the eighth parabolas. Fifteen test points were recorded from 64 parabolas flown for this flight.

### ***3.5 Equipment Modification***

Since Creare was not able to participate in the third flight series, a second 386 computer was acquired to record the void fraction readings continuously throughout a parabola set. The new PC was integrated into the CCC.

During the second flight series, it was usually not possible for the test system to reach equilibrium in a given parabola due to the low Suva mass flow rate used in the system. The maximum Suva mass flow rate was limited by the Coriolis flow meter. The flow meter was calibrated up to 0.416 lb./min. From the imager visualization shots, the velocity of the two phase flow varied from 1 to 2 inches per second. Therefore, the transit time of the two phase fluid through the upstream void fraction sensor, the sight tube, and the downstream void fraction sensor would be 25 to 50 seconds. Since the average 0 g period is only 18 seconds, it was not possible for the system to reach equilibrium conditions.

However, the high flow Suva pump was capable of higher mass flow rates. A new Coriolis flow meter was obtained from GSFC. The flow meter was sent to JSC to be calibrated. However, the JSC calibration lab was unable to calibrate the flow meter prior to the third flight series in May 1996. Therefore, a pre-calibrated flow meter and transmitter were borrowed from JSC. The borrowed flow meter and transmitter were integrated into the test system. With the new

flow meter, the Suva mass flow rate was increased by a factor of two. The test package was evacuated and charged with 1.1 kg of Suva.

Considering previous flight experience, control of the void fraction was easily established by controlling the cooling water flow rate. Modifications to the cooling system were installed that would allow control of the cooling water flow rate through the condenser as well as the ability to vary the cooling water temperature. An arrangement of valves and by-pass lines allowed the cooling water to cycle between the pump, condenser, and reservoir.

### ***3.6 May 1996 Flight Chronology***

The emphasis in this flight series was on low void fractions. The modifications made to the test package permitted higher Suva flow rate and better control of the cooling water temperature. Instead of varying the evaporator power to set the test conditions, the cooling water to the condenser was used to set the test conditions in the system. Prior to take off, the accumulator temperature controller was turned on and the heater temperature set to the approximate ambient temperature of the plane. This minimized the difference between the temperature of the Suva and the ambient temperature.

### 3.6.1 Flight 9 - May 21

At the conclusion of the first parabola set, the house keeping computer malfunctioned and all data from this set were lost. The problem was isolated to a burned out power supply. Since a spare power supply was not available in flight, the rest of this flight was scratched.

### 3.6.2 Flight 10 - May 22

The power supply to the house keeping computer was replaced prior to this flight. The accumulator was turned on prior to flight as before. The evaporator was set to 150 W to produce a two phase flow in the Suva system. Test points were collected during parabolas 3, 10, 13, 19, and 23. The flight was aborted during parabola 25 due to mechanical problems with the KC-135 aircraft.

### 3.6.3 Flight 11 - May 23

To expedite the production of two phase flow during startup, the accumulator heater controller was kept on during take-off. Therefore, vapor was generated prior to the first parabola and the system was ready for isolation during the first 0 g period. The sight tube was isolated during the second, sixth, and tenth 0 g periods of each parabola set (10 parabolas). During this flight, 17 test points were collected from 56 parabolas.

#### 3.6.4 Flight 12 - May 24

The same flight procedure was used as the previous flight. Twelve test points were collected from 40 parabolas.

In this section, the preflight activities, flight activities, and post flight modifications to the experiment were described. Also presented in this section was the evolving test procedure used aboard the KC-135 as the experimenters gained experience with the test package and the flight environment.

## **4.0 Results**

The following sections present results and analysis of the data. The validation of the instrumentation in the KC-135 aircraft environment is described in section 4.1. Creare conducted analysis of the void fraction sensor data from the July 1995 and January 1996 flight series. Brief descriptions of the results of the Creare analysis are included in sections 4.2 and 4.3, respectively. The results from the May 1996 flight series are described section 4.4 and were analyzed by the ITP group with assistance from Creare. Section 4.5, describes the verification of the capacitance sensor outputs in a fill test of the test section.

### ***4.1 Instrumentation Validation***

The test environment on the KC-135 is very different than a ground based laboratory. The aircraft acceleration varies in time and direction. Cabin pressure varies through each parabola and cabin temperature varies throughout the flight. For these reasons, it is important to understand instrument responses to environmental conditions in the KC-135. Therefore, initialization parabolas, where special experimental conditions are set, e.g., no mass flow rate or power to the evaporator, are flown to quantify instrument responses in the aircraft.

The following section is a description of the instrumentation responses during the initialization parabola set flown on January 23, 1996. The test package was at near ambient temperature with single phase liquid Suva in the test system. The

Suva pump and the positive displacement pump for the coolant water were turned off. The evaporator was also turned off. Both upstream and downstream void fraction sensors were energized and the data acquisition computer recorded the output voltages. The house keeping data computer was recording FRIM instrumentation and temperature readings.

Figure 2 is a plot of the tri-axial accelerations for the initialization parabola set. In a KC-135 flight, the initial 1 g level flight period is followed by a 2 g pull-up which transitions into the 0 g period. The 2 g to 0 g cycle is repeated eight times before the plane returns to 1 g level flight. There is a 0.2 g acceleration in the axial (fore-and-aft) direction (ACCY) just prior to entering the 0 g period. To minimize the effect of this acceleration to the experiment, the axis of the test section is set perpendicular to the flight direction.

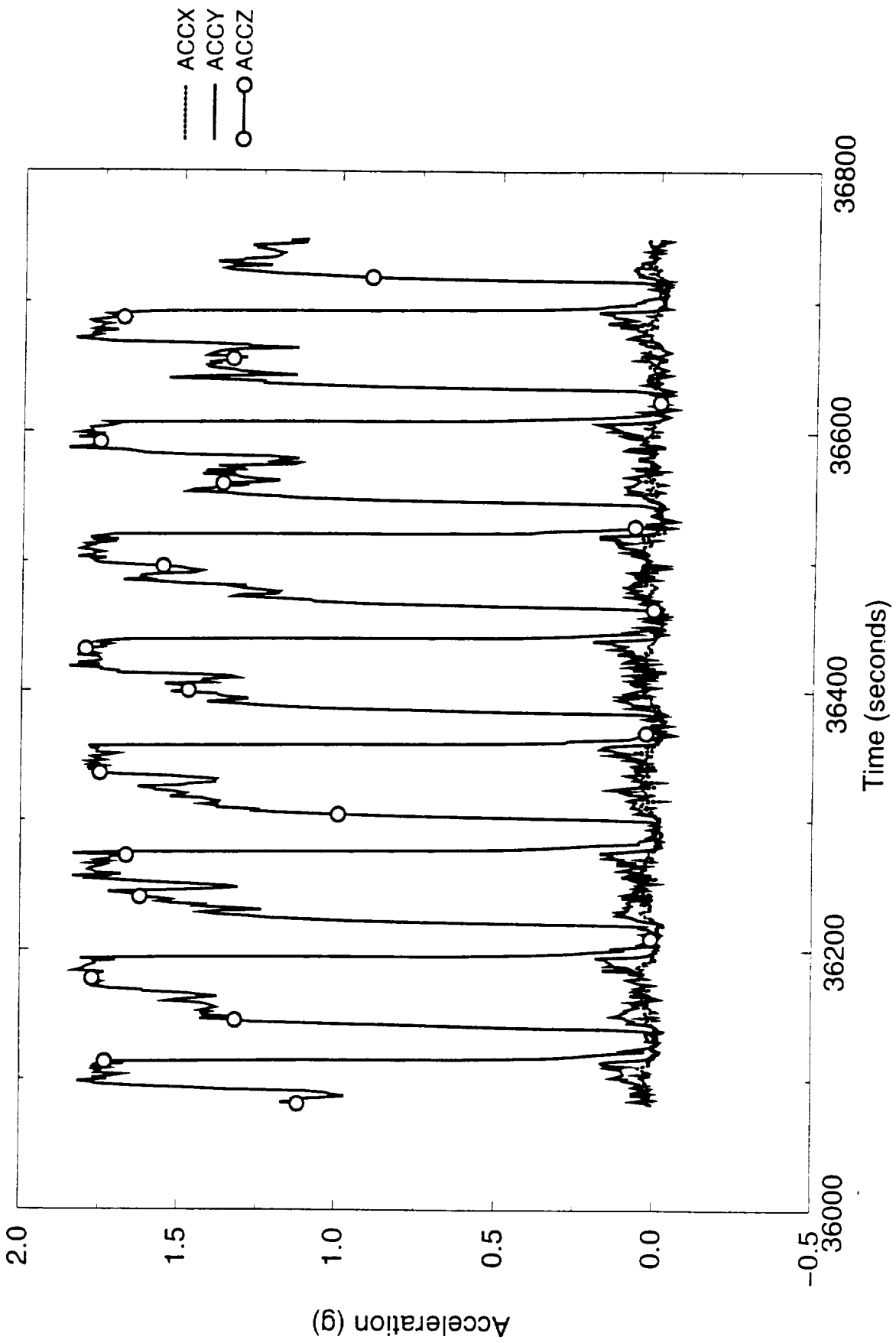
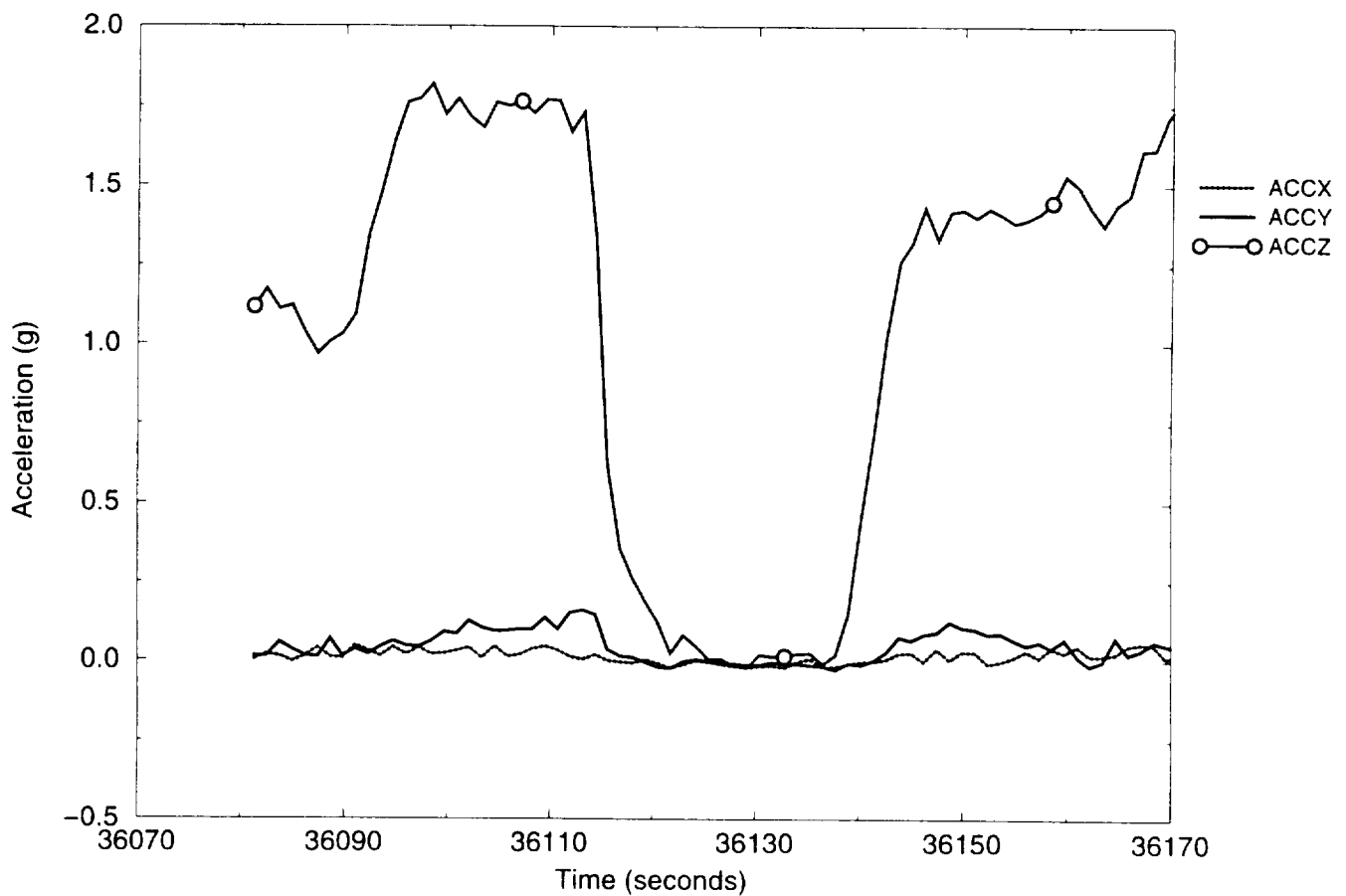


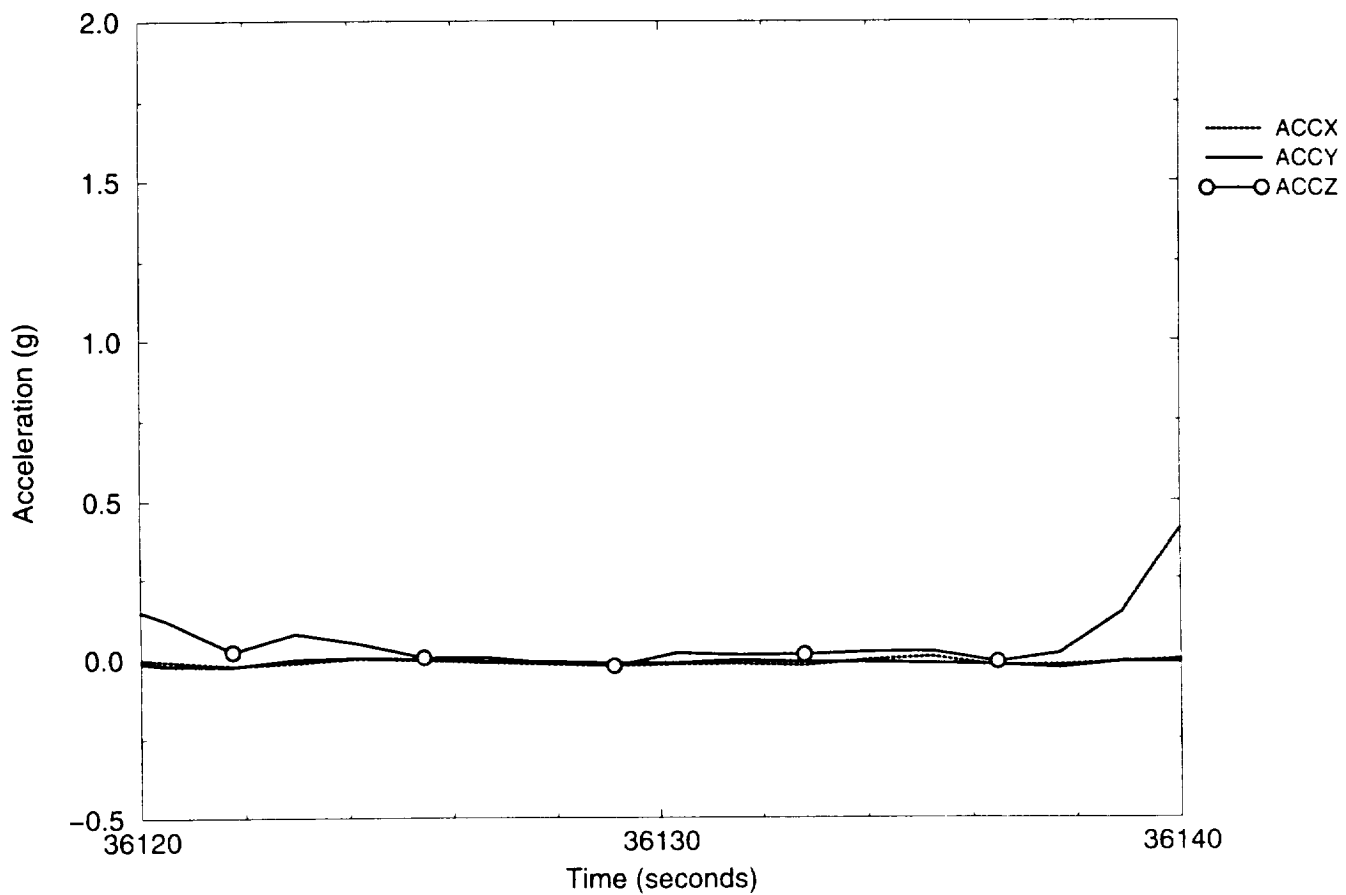
Figure 2. Tri-axial accelerations for initialization parabola set

Figure 3 is a plot of the tri-axial accelerations for the first parabola of the initialization set. This figure shows how the three accelerations approach 0 g. The transverse acceleration (ACCX) is usually  $<0.01g$  throughout the parabola set. The axial acceleration increases to about 0.2g during the 2 g pull-up and then approaches 0 g just before the vertical acceleration (ACCZ) reaches 0 g.



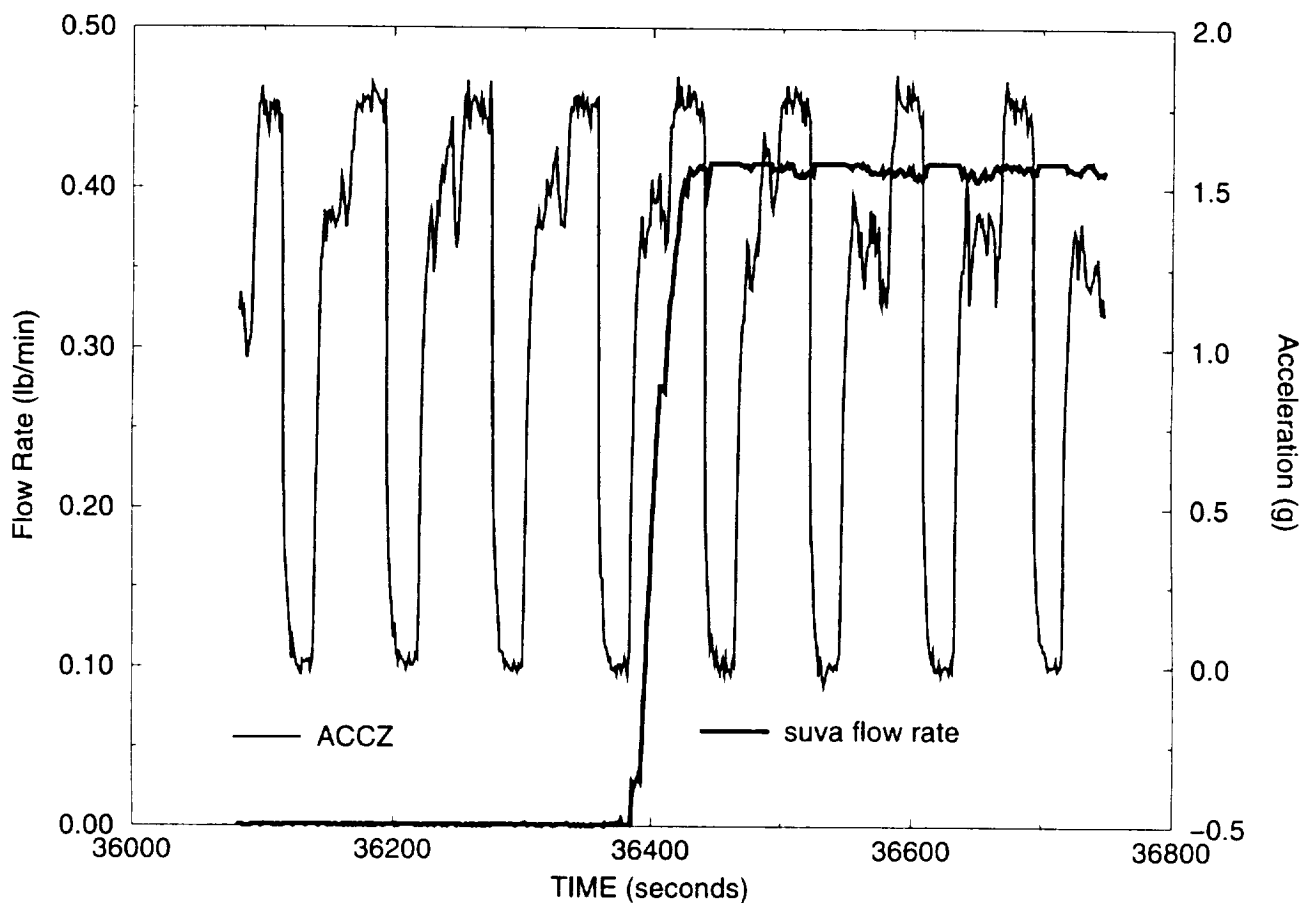
**Figure 3. Tri-axial accelerations for parabola 1**

Figure 4 is a plot of the near 0 g portion of the first parabola. This figure shows that the 0 g period lasts about 15 seconds and all the accelerations are uniformly small. The 0 g period ends with a rapid increase in the vertical acceleration corresponding to the start of the 2 g pull-up of the aircraft.



**Figure 4. Tri-axial accelerations for 0 g period of parabola 1**

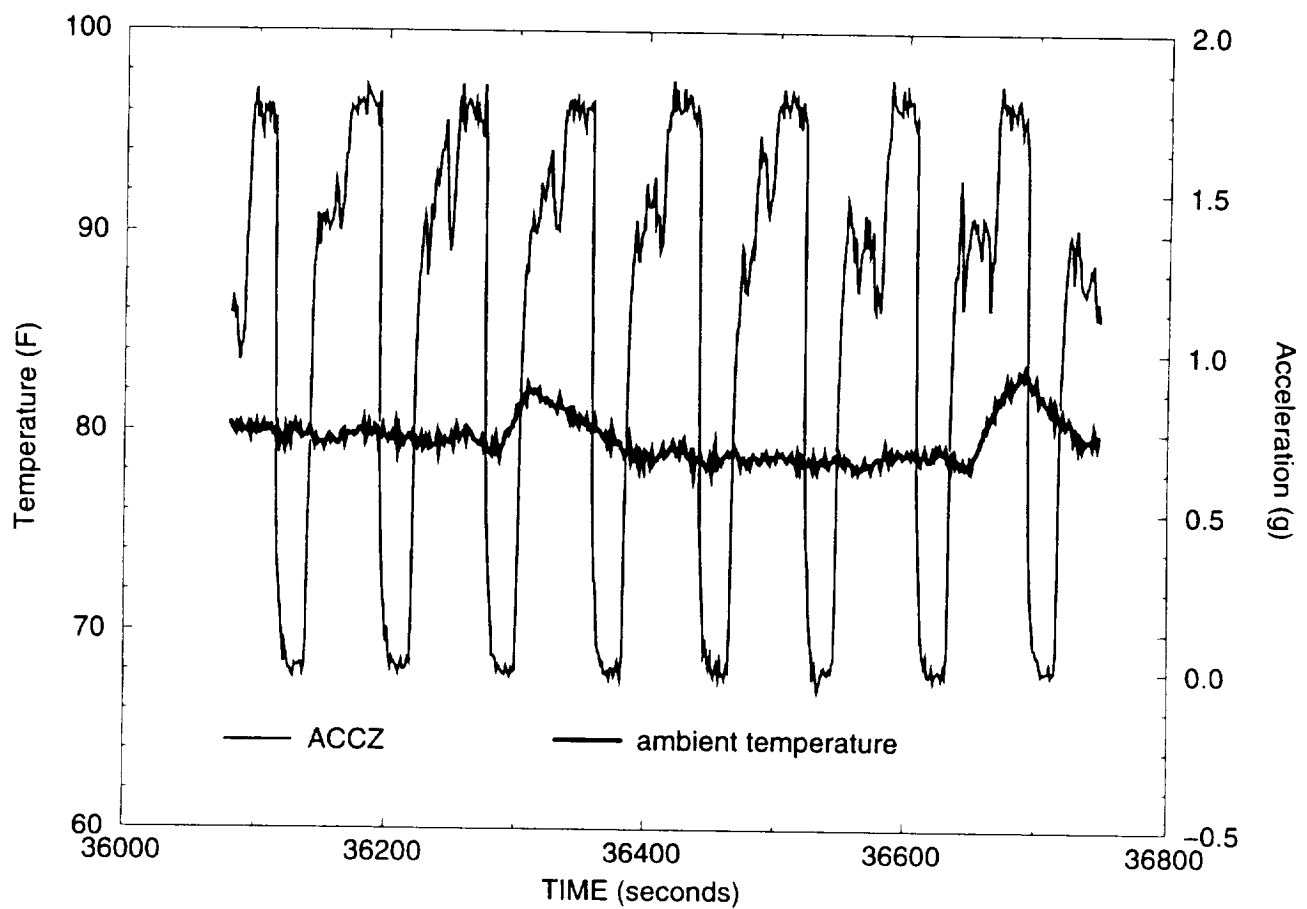
Figure 5 is a plot of liquid Suva mass flow rate and vertical acceleration versus time. Initially, the liquid Suva mass flow rate is zero. After the fourth 0 g period, the liquid Suva mass flow rate was set at the maximum value of 0.416 lb./min. This figure shows that the liquid flow is substantially independent of acceleration.



**Figure 5. Liquid Suva mass flow rate**

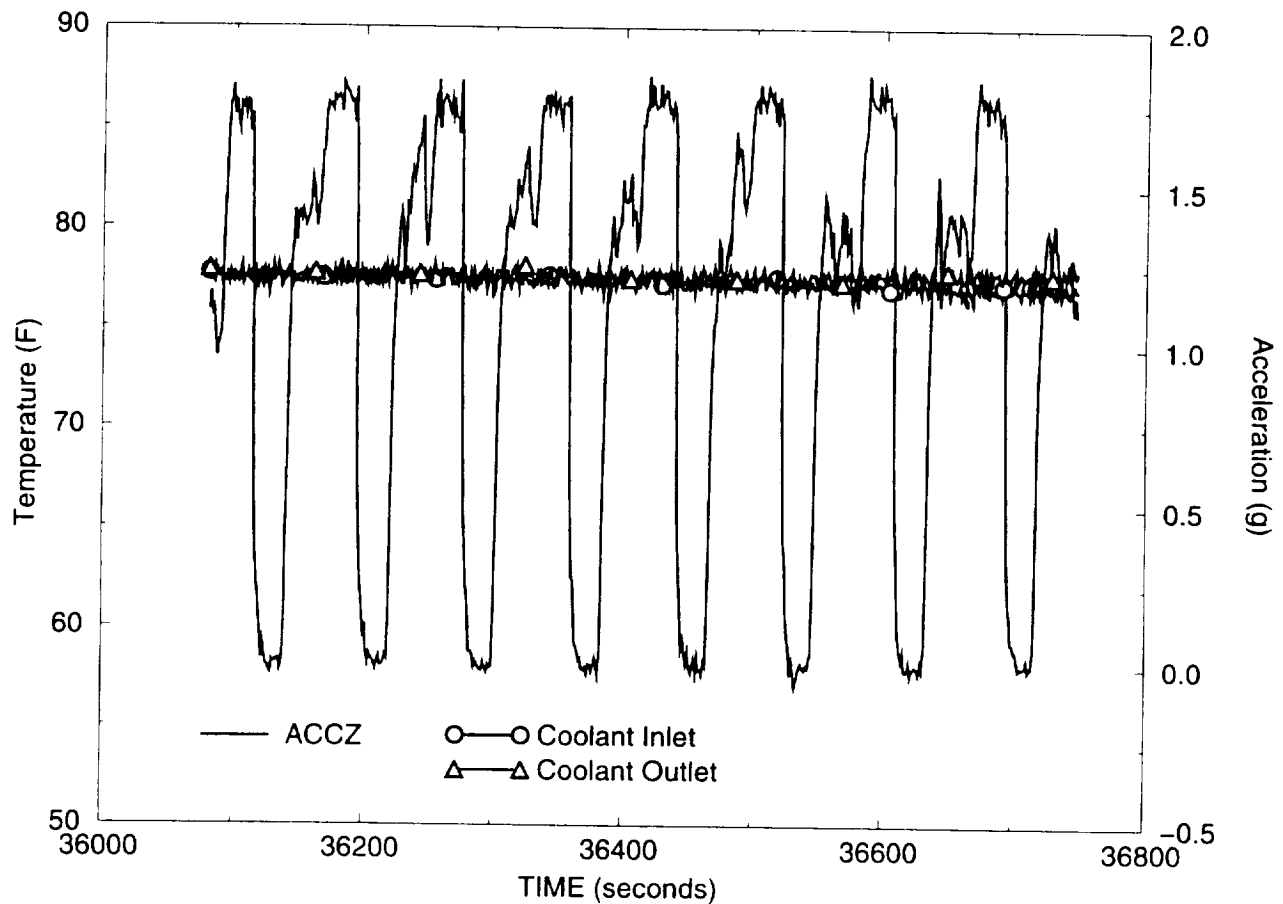
Figure 6 is a plot of ambient temperature and vertical acceleration versus time.

The increase in the ambient temperature following the third and seventh 0 g periods is due to the imager halogen light, which is turned on when a digital imager shot was taken.



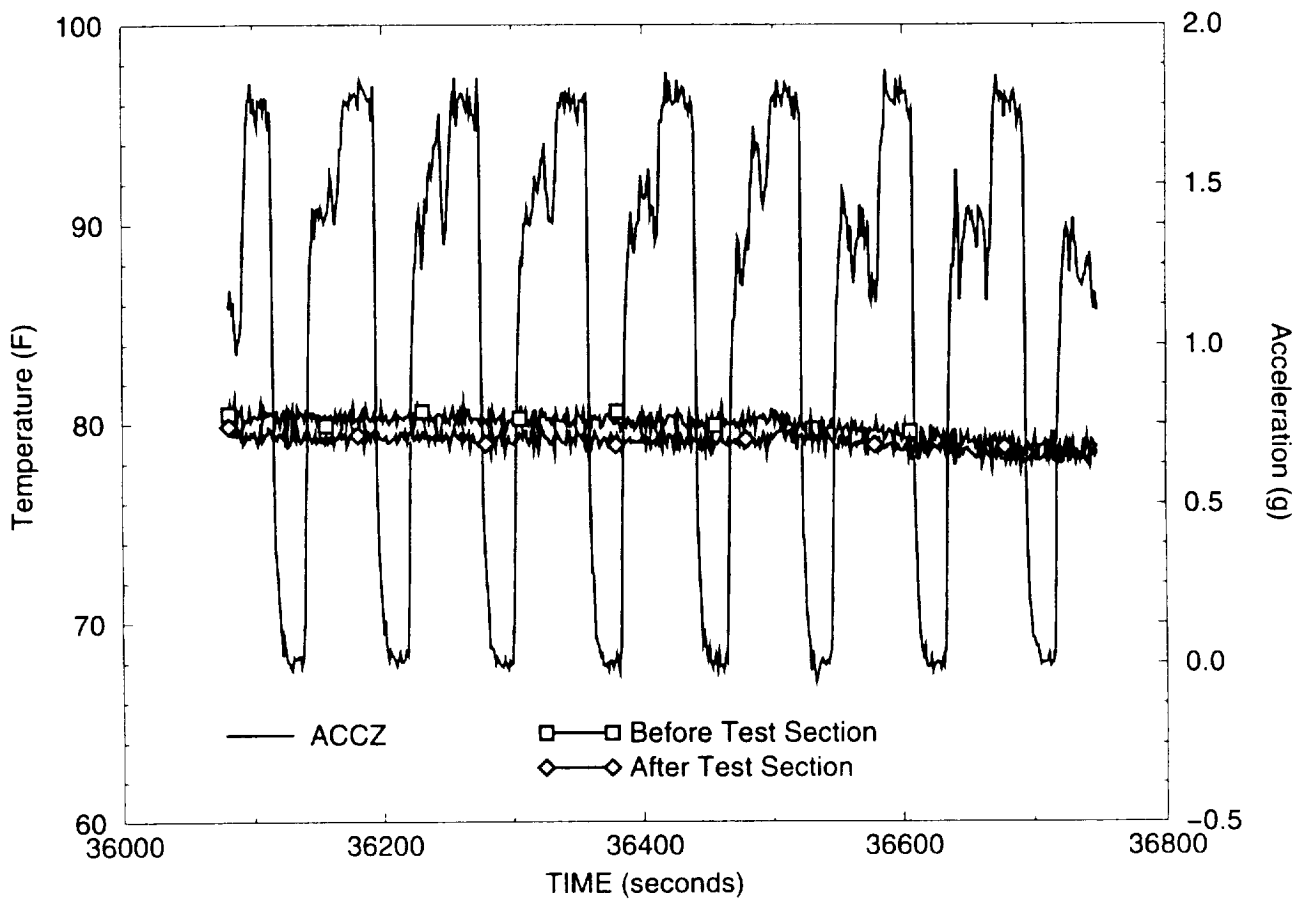
**Figure 6. Ambient temperature**

Figure 7 is a plot of condenser cooling water inlet and outlet temperatures and vertical acceleration versus time. This figure shows that the temperatures remain fairly constant throughout the parabola set. Since the cooling water pump was turned off during this parabola set, the temperatures should remain at a constant value.



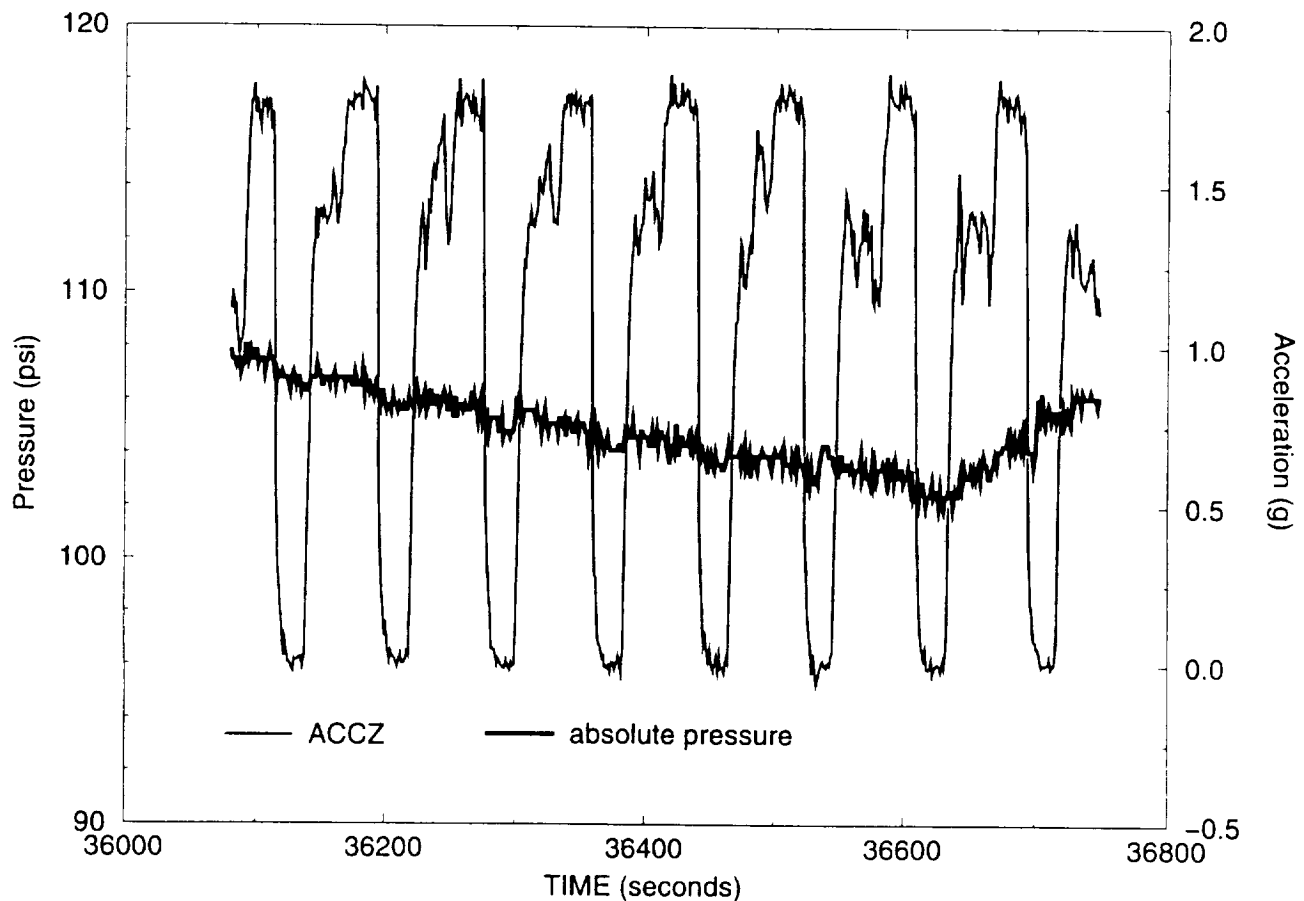
**Figure 7. Coolant inlet and outlet temperatures**

Figure 8 is a plot of Suva temperatures before and after the test section. This figure shows that the temperatures remain constant and are independent of acceleration. The slight temperature drop after the fourth 0 g period is due to the Suva pumps being activated and liquid Suva being pumped through the system.



**Figure 8. Temperatures before and after test section**

Figure 9 is a plot of the absolute pressure of the test package and vertical acceleration versus time. This figure shows that system pressure drops slowly until the last parabola, where it starts to rise. The probable reason for this is the heaters on the accumulator. Initially, the accumulator heaters over shoot the temperature setpoints, which increased the system pressure. Therefore, the heaters are cycled off, pressure decreased until the accumulator temperature reached below the setpoint. Once the temperature reached below the setpoint, the heaters cycled on and the system pressure began to rise.



**Figure 9. Absolute pressure**

Figure 10 is a plot of evaporator power and vertical acceleration versus time.

This figure shows evaporator power ranges from zero to two watts, even though power is turned off. This noise is due to fact that the evaporator was calibrated for 2 kW. The accuracy for the evaporator reading is about  $\pm 5$  W.

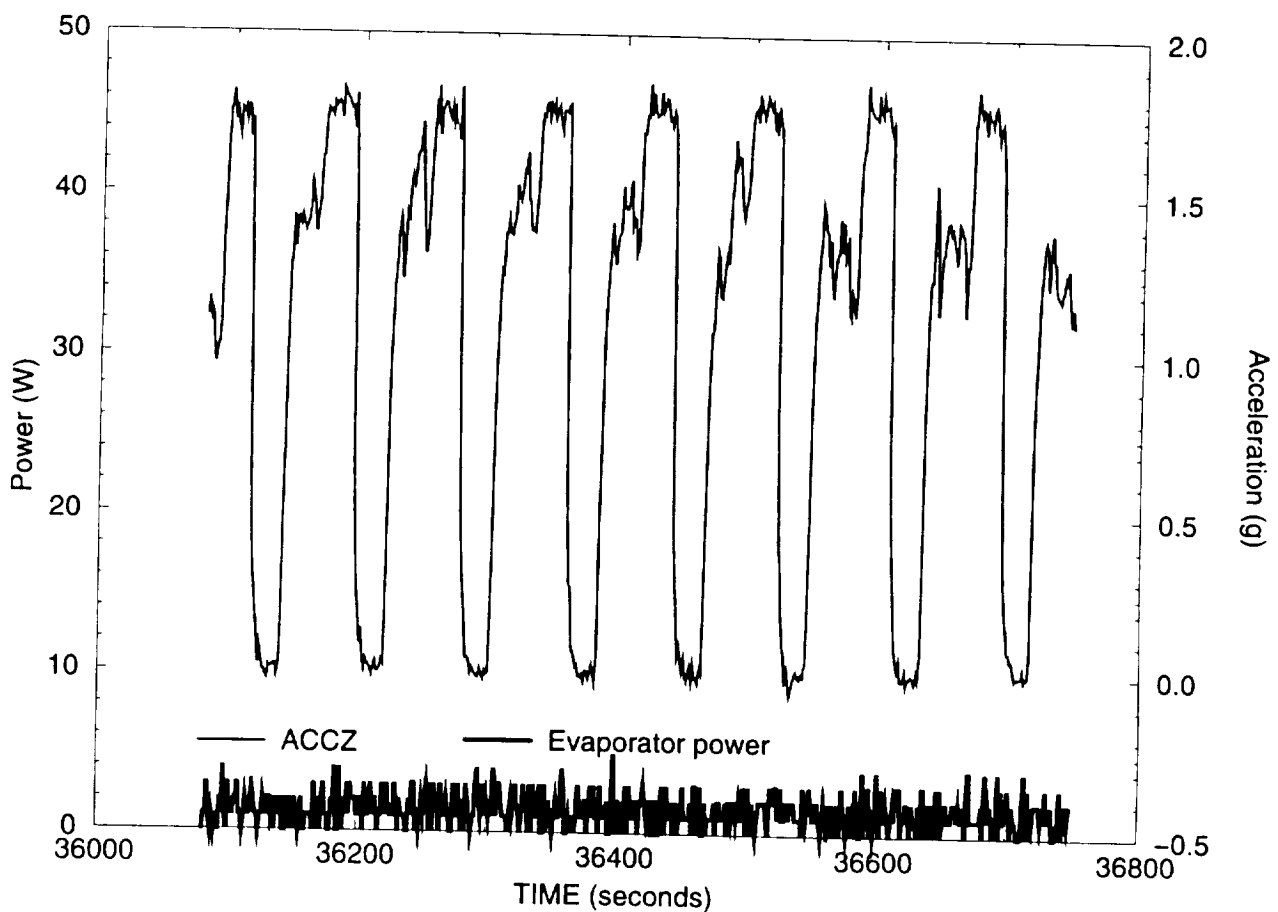
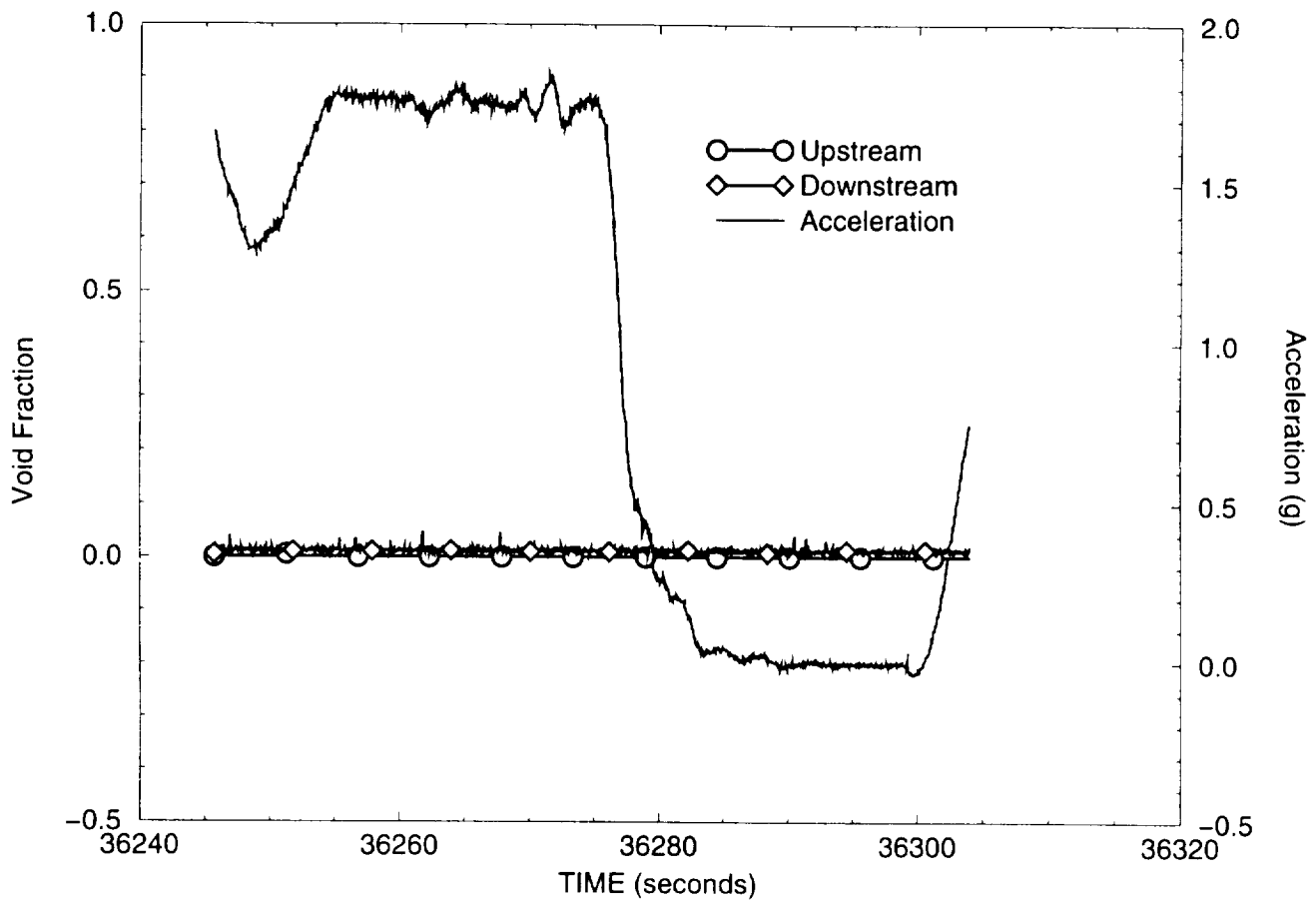


Figure 10. Evaporator power

Figure 11 is a plot of the void fraction data from the upstream and downstream sensors during parabola 3 of the initialization set. This figure show that outputs from the void fraction sensors are independent of aircraft accelerations and indicates zero void fraction, which the correct response when the system is filled with liquid Suva.



**Figure 11. Void fraction sensors**

#### ***4.2 July 1995, Flight Results***

The following is a summary of the Creare analysis of the July 1995 flight series (see Appendix A). The evaluation of data from the July 1995, flight series focused on the 8 data points obtained during the fourth day (July 14, 1995). Data were analyzed from microgravity ( $<0.01$  g) and 2 g periods. The flow regimes experienced in microgravity were slug, slug-annular, and annular with the average void fraction ranging from 0.47 to 0.97. Averaged void fraction for the 2 g period ranged from 0.18 to 0.99. Generally, there is significant amount of fluctuation in void fraction during the transition from 2 g to microgravity period. Often the transitional period will last for 10 seconds, about half of the microgravity period. Comparison of averaged void fraction measurements of the upstream and downstream void fraction sensors showed good agreement with the trapped volume void fraction within  $\pm 0.10$  of the void fraction. Void fraction measurements from the 2 g period were also analyzed. However, no measurements with the quick closing valves were made. Figure 12 is a plot of void fraction measurements from the quick closing valves and the two capacitance void fraction sensors from the July 1995, flight series.

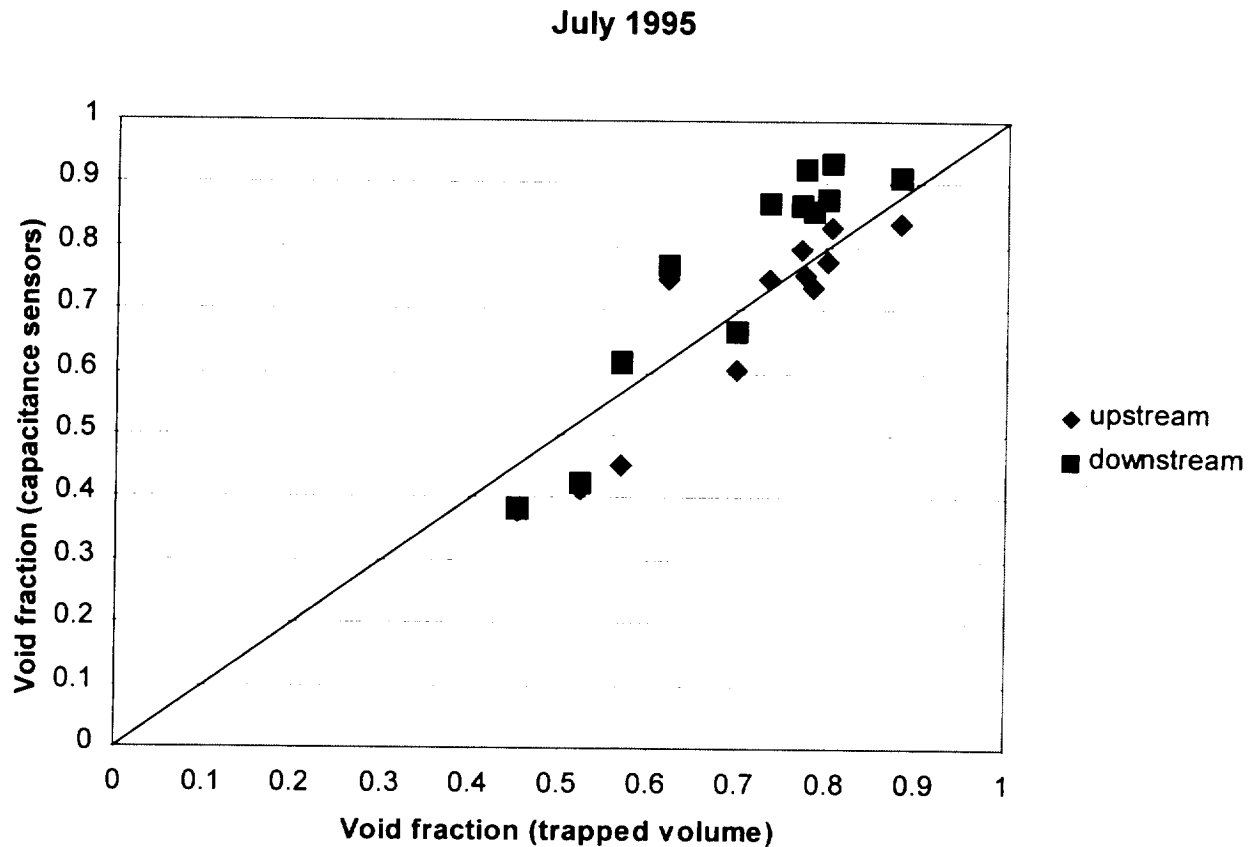


**Figure 12. Average void fraction from July 1995, flights**

Flight data were plotted on flow regime maps for microgravity and 2 g periods, Figure 13 and Figure 14, respectively. The flow regime maps were constructed with the Creare MICROREG software. Slug, slug-annular and annular flow regions were observed under the microgravity conditions. For the 2 g period, stratified flow region was observed for all conditions.

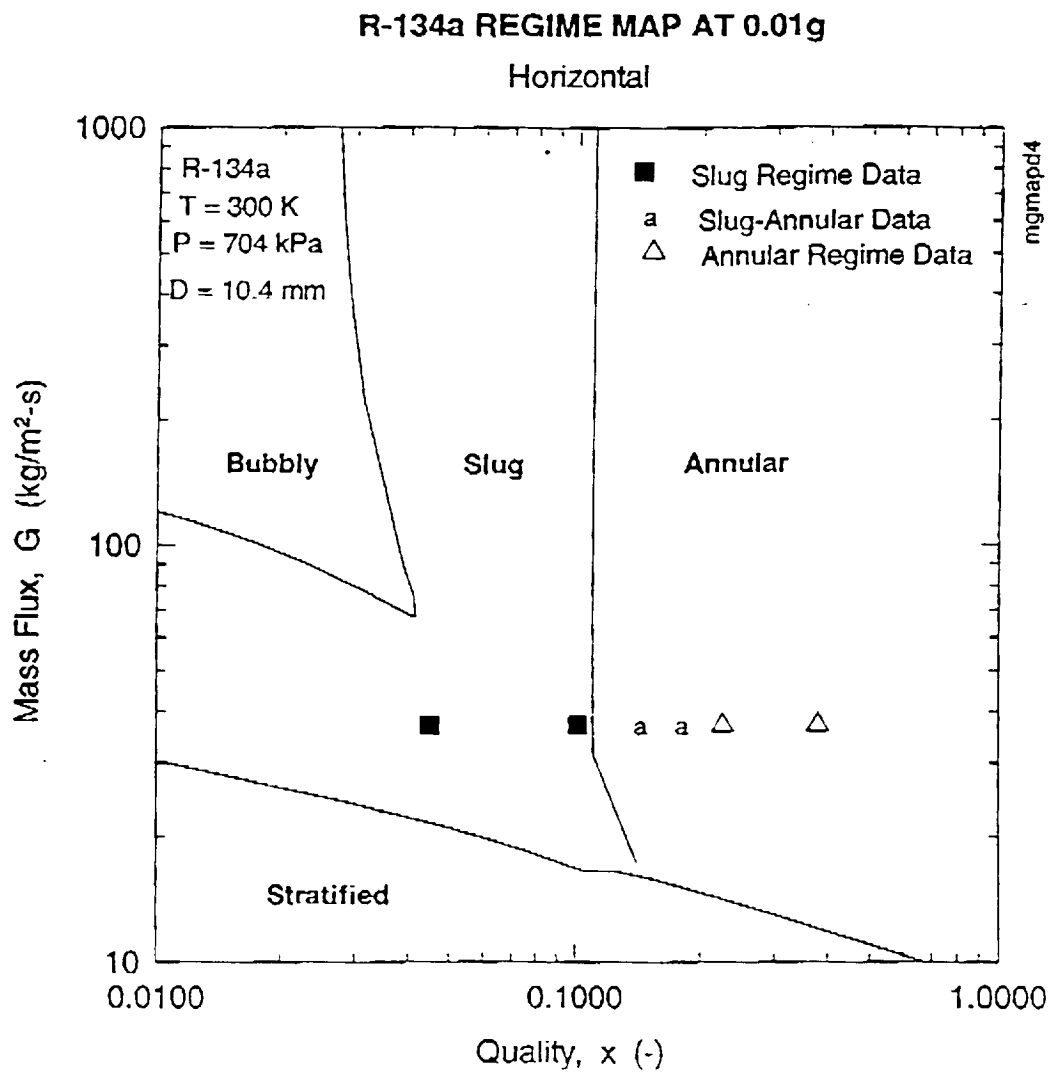


**Figure 13. Flow regime map for microgravity**

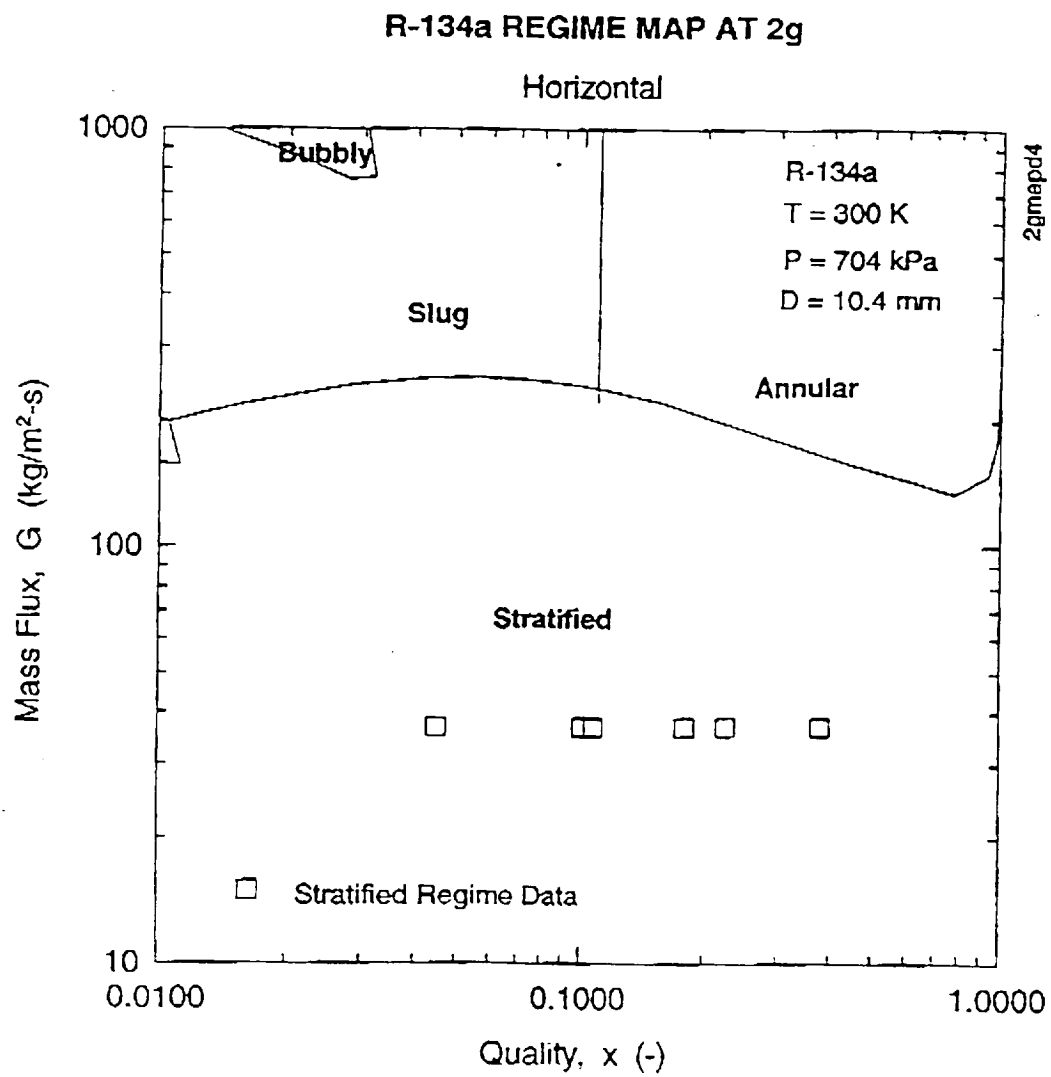


Figure 14. Flow regime map for 2 g

### **4.3 January 1996, Flight Results**

The following section is a summary of the Creare analysis of the January 1996, flight series (see Appendix B). The aim of the January 1996, flight series was to use lower power to produce void fractions less than 0.50 in the slug or bubbly flow regimes. It was difficult to draw conclusions from the results of this flight series with the difficulty obtaining steady flow conditions with low evaporator powers used during this flight series. Transient behavior and non-uniform distribution of vapor and liquid across the test tube during the microgravity periods were observed throughout the flight series. However, the following conclusions were derived from this flight series:

- The transient response of the void fraction sensors from these tests was in qualitative agreement with the visual observations of the sight tube.
- The average void fraction measurements from the upstream meter had better agreement than the downstream meter compared to the void fraction measurements from the quick closing valves.
- The calibration (empty and full readings from the sensors) of the void fractions sensors remain stable between the ground tests at GSFC in May 1995, through the January 1996 flights.

Figure 15 is a plot of the averaged void fraction measurements from the upstream and downstream sensors and the void fraction measurements from the quick closing valves. Due to the transient behavior observed during the

microgravity periods, it is difficult to conclude the significance of the correlation between the averaged void fraction measurements of the two sensors and the trapped volume from the quick closing valves.

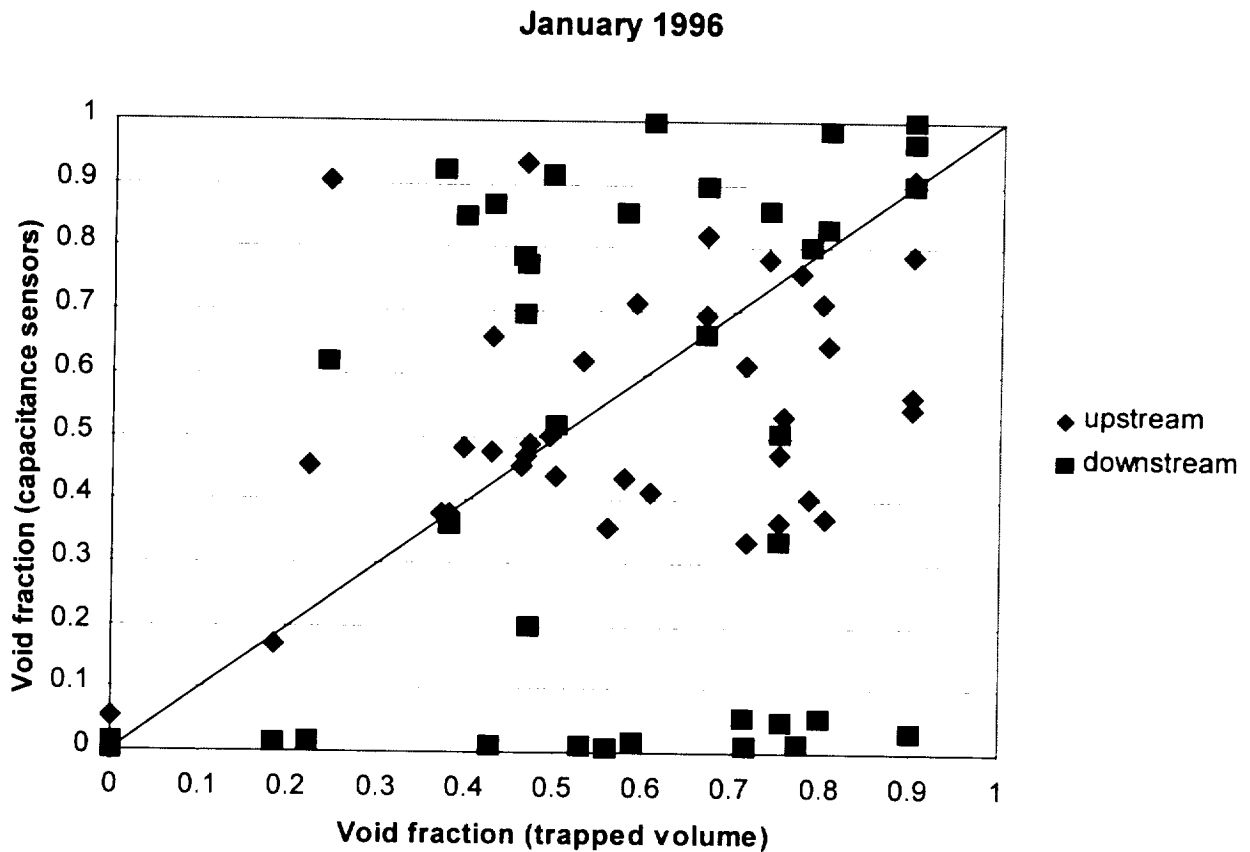


**Figure 15. Average void fractions from January 1996, flights**

Due to this large mismatch between the capacitance sensors and the trapped volume, an analysis of the transit time for the liquid/vapor front from the inlet of the evaporator to the end of the downstream sensor was completed by the ITP group (Appendix C). This analysis concluded that with the Suva mass flow rate and evaporator power used on this flight series, steady state conditions in the

test section were not possible. Therefore, the Suva mass flow rate was increased and higher evaporator power was used on the third flight series.

#### ***4.3 May 1996, Flight Results***

The emphasis in this flight series was on void fraction measurements in the slug flow regime. Tables 1 – 3 are listings of the test points and conditions from the three flight days. No data were taken on the first day of flying due to computer hardware failure.

A new Coriolis flow meter and transmitter were installed into the test system. With this flow meter system, the maximum measurable Suva mass flow rate was 1.00 lb./min. The higher Suva flow rate coupled with the higher evaporator power shortened the transit time of the two phase flow and increased the velocity of the fluid in the system. Based on the analysis in Appendix C, with the evaporator power at 150 W, the superficial velocity is about 11.8 inches per second and the transit time, from the inlet of the evaporator to the outlet of the downstream capacitance sensor, is about 8 seconds.

From the three days of flying, 34 test points were collected. All the test points were in the slug flow regime. The evaporator power ranged from 150 to 165 watts. The liquid Suva mass flow rate ranged from 0.86 to 1.00 lb./min.

**Table 1. Test points May 22, 1996**

Parabola Number	Evaporator Power (W)	Flow Rate (lb/min)	Absolute Pressure (psia)	Suva Temp. (°F)	Ambient Temp. (°F)	Void Fraction (trapped)	Void Fraction (upstream)	Void Fraction (downstream)
3	152	0.926	112	79.9	83.5	0.60	0.56	0.61
10	153	0.871	111	84.2	80.7	0.70	0.60	0.68
13	153	0.932	102	74.9	77.8	0.62	0.56	0.64
19	153	0.935	100	72.9	76.8	0.72	0.60	0.70
23	153	0.940	97	69.3	75.6	0.62	0.57	0.67

**Table 2. Test points May 23, 1996**

Parabola Number	Evaporator Power (W)	Flow Rate (lb/min)	Absolute Pressure (psia)	Suva Temp. (°F)	Ambient Temp. (°F)	Void Fraction (trapped)	Void Fraction (upstream)	Void Fraction (downstream)
2	151	0.861	110	73.3	82.3	0.62	0.59	0.63
6	154	0.948	113	74.2	81.7	0.40	0.39	0.44
10	151	0.944	111	73.9	80.5	0.55	0.51	0.57
12	151	0.943	110	70.9	77.5	0.58	0.47	0.57
16	152	0.938	113	72.0	75.7	0.44	0.38	0.48
20	152	0.938	111	70.1	75.1	0.25	0.26	0.50
22	152	0.939	110	72.2	72.5	0.53	0.50	0.58
26	152	0.940	110	71.2	73.7	0.43	0.39	0.42
30	152	0.946	108	70.9	72.4	0.61	0.52	0.57
32	153	0.950	108	66.6	71.3	0.51	0.40	0.52
36	153	0.949	108	66.9	70.4	0.46	0.39	0.46
40	153	0.949	110	67.1	69.6	0.37	0.33	0.36
42	153	0.951	110	64.5	68.0	0.23	0.17	0.46
46	153	0.957	109	63.7	68.1	<0.20	0.17	0.51
50	153	0.953	108	67.0	70.1	0.38	0.36	0.47
52	153	0.955	108	66.1	70.5	0.37	0.45	0.53
56	154	0.962	107	64.4	70.8	0.24	0.24	0.52

**Table 3. Test points May 24, 1996**

Parabola Number	Evaporator Power (W)	Flow Rate (lb/min)	Absolute Pressure (psia)	Suva Temp. (°F)	Ambient Temp. (°F)	Void Fraction (trapped)	Void Fraction (upstream)	Void Fraction (downstream)
2	164	0.988	114	69.7	85.2	0.39	0.39	0.38
6	164	0.982	113	71.0	84.3	0.50	0.45	0.43
10	164	0.973	115	75.3	82.9	0.60	0.55	0.52
12	164	0.992	112	65.8	80.8	0.29	0.27	0.49
16	165	0.992	109	64.1	79.8	0.34	0.32	0.47
20	165	1.000	110	62.7	78.2	< 0.20	0.18	0.52
22	165	0.999	109	62.0	74.9	< 0.20	0.17	0.40
26	166	0.993	111	64.2	74.7	0.26	0.24	0.48
30	165	0.987	111	68.4	73.9	0.53	0.41	0.48
32	165	0.993	109	65.1	72.6	0.40	0.33	0.43
36	165	0.993	109	63.8	71.6	0.32	0.33	0.54
40	165	0.997	109	62.9	71.3	0.25	0.24	0.50

Figure 16 is a comparison between the upstream and downstream void fraction sensor with the void fraction measurements from the quick closing valves for the May 1996, flight series. The upstream and the downstream void fraction measurements are averages of the last 8 seconds prior to the end of the microgravity period in the parabola. There was good agreement between the capacitance sensors and the void fraction measurements from the quick closing valves. The bubble velocities were determined to be around 9 – 11 inches per second from the digital imager tapes. This is the result of increasing the Suva pump mass flow rate from 0.416 lb./min to 0.950 lb./min. and the higher evaporator power. It can be seen from Figure 16, that the upstream void fraction sensor agrees well with the void fraction from the trapped volume for the entire

range tested (20% to 80% void). The downstream void fraction sensor shows good agreement with the trapped volume for void fractions above 35%.

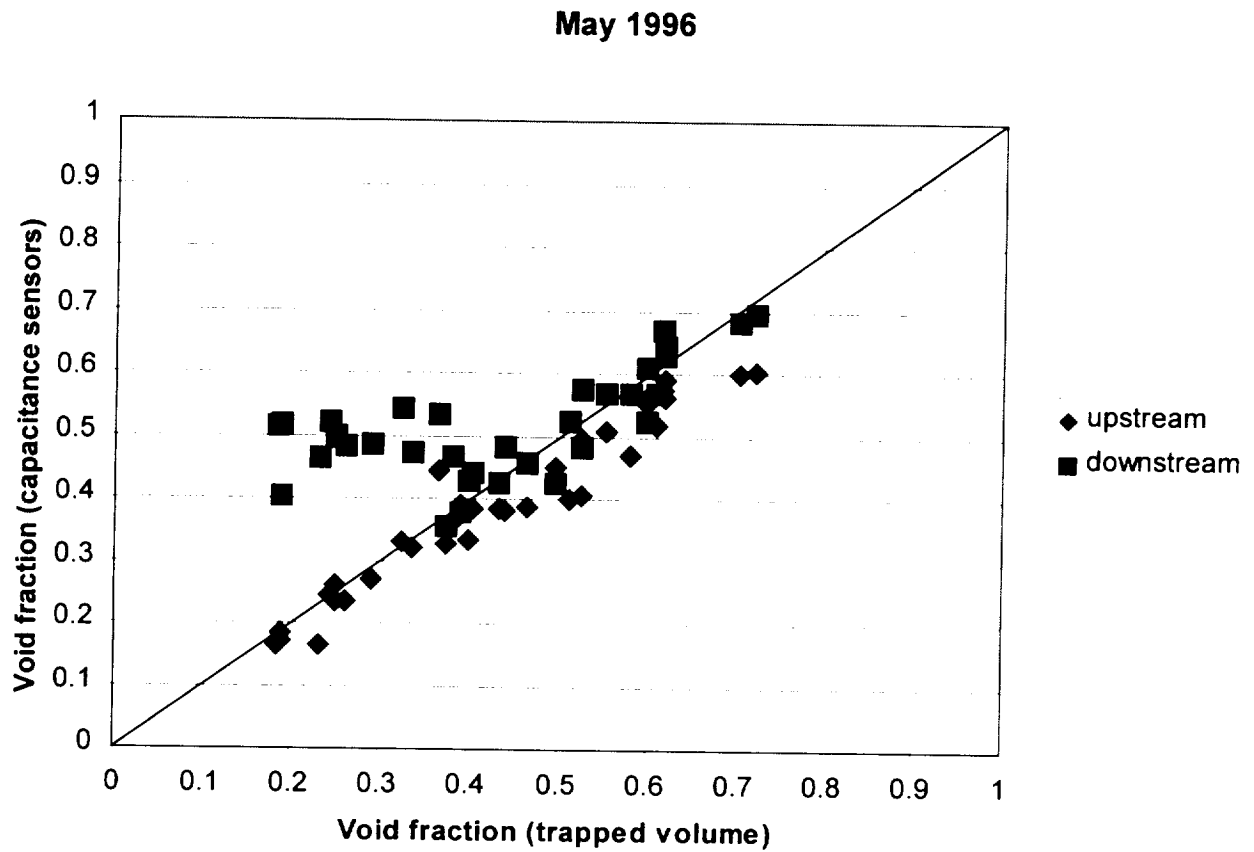


**Figure 16. Average void fractions from May 1996, flights**

#### **4.4 Fill Calibration Test**

Calibration tests of the capacitance void fractions sensors were performed in the ITP lab following the third flight series to check the performance of the sensors. The test section was rotated and set in the vertical position. A stable liquid vapor interface was achieved and then pumped up through the two sensors. Data acquisition system recorded the resulting signals and was plotted in Figure 17. Initially, both upstream and downstream sensors indicate 100% void. As the liquid Suva is pumped up through the upstream sensor, the void fraction measurement decreases to zero. This is repeated in the downstream sensor as the liquid moves through the sensor. The test confirmed that both sensors were producing the expected output signals without large fluctuations. The slight increase in the void fraction in the downstream sensor at 18555 seconds is due to the activation of the imager. An voltage signal from the imager was connected to the data acquisition system. At this time, the reason for the voltage drop (increased void fraction) for the downstream sensor is not known. However, the voltage drop is very small and may be neglected.

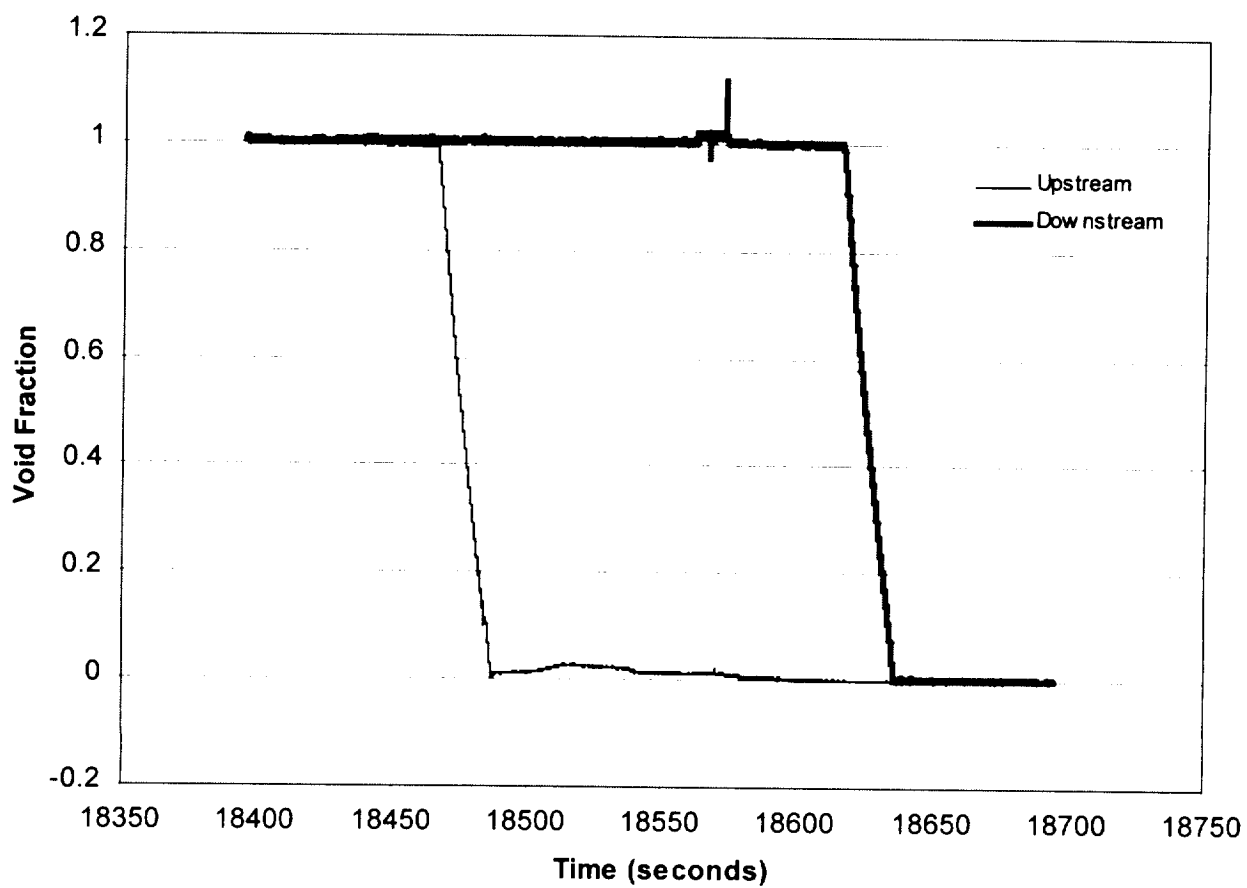


**Figure 17. Sensor fill test**

## 5.0 Summary

Three flight series were conducted in reduced gravity on the NASA KC-135 aircraft with the void fraction experimental package. The test package consisted of two Creare capacitance void fraction sensors, GSFC FRIM package, and the ITP data acquisition system and KC-135 test support system. Void fraction measurements from the capacitance void fraction sensors and trapped volume from the quick closing valves were collected. Furthermore, digital imager shots were recorded during the microgravity periods just prior to trapping of the sight tube. Over 70 test points were collected over 12 days of flying. Void fractions ranging from 0 % to 90% were measured. Stratified, slug, and annular flow regimes were observed during the flights. Average void fraction measurements from the capacitance sensors were compared to the void fraction measurement from trapped volume. Overall, the void fraction measurements from the sensors compared well with the trapped volume, especially in the annular flow regime. However, some discrepancies existed in the slug regime. These discrepancies were due to the lack of steady state conditions in the test system with the low liquid Suva mass flow rates and low evaporator powers. With the higher Suva mass flow rates and evaporator powers, void fraction measurements from the sensors and the trapped volume compared well. The void fraction sensors did lock up intermittently during the electrical transient caused by pneumatic valve actuation. However, overall, the Creare void fraction sensors were found to produce the correct result whenever the test system achieved equilibrium.

The overall objective of this project, to validate the performance of the Creare void fraction sensors in microgravity conditions in the KC-135, was achieved. The capacitance sensors operated satisfactorily in the KC-135. Furthermore, the FRIM package produced satisfactory test conditions for calibrating the Creare void fraction sensors. They are expected to be valuable tools for both scientific applications and thermal management system monitoring.

## References

---

- <sup>1</sup> C. J. Crowley, P. J. Magari, C. M. Martin, and M. E. Hill, "A Void Fraction Instrument for Two-Phase Flow In Dielectric Liquids," *Proc. 34<sup>th</sup> Aerospace Sciences Meeting & Exhibit*, AIAA-96-0925 (1996).
- <sup>2</sup> T. Reinarts, *Adiabatic Two Phase Flow Regime Data and Modeling for Zero and Reduced (Horizontal Flow) Acceleration Fields*, Dissertation, Texas A&M University, College Station, Texas (1993).
- <sup>3</sup> K.M. Hurlbert, "Two-Phase Extended Evaluation in Microgravity (TEEM) Flight Experiment," Personal Communication, 1995.
- <sup>4</sup> S. Benner, G. Durback, K. Kolos, and R. Bayt, "A Breadboard Flight Experiment for Two-Phase Flow Visualization in Microgravity," *Proc. 33<sup>rd</sup> Aerospace Sciences Meeting & Exhibit*, AIAA-95-0696 (1995).
- <sup>5</sup> Best, F. R., Test Equipment Data Package for KC-135 Flight Testing of Void Fraction Capacitance Probe for Microgravity Two-Phase Flow, June, 1995.



Create Incorporated  
P.O. Box 71  
Hanover, NH 03755

Date 10/6/95

Number of pages including cover sheet 20

To: **Dr. Frederick R. Best**

Center for Space Power

Texas A&M University

College Station, TX

77843-3118

Phone 409-845-4108

Fax Phone 409-847-8857

CC:

From: **Christopher J. Crowley**

Extension 302

Phone 603-643-3800

Fax Phone 603-643-4657

**REMARKS:**

☐ Urgent ☒ For your review ☐ Reply ASAP ☐ Please comment

**SUBJECT: KC-135 FLIGHT #1**

Here is a (very) rough working draft of my write-up on the first round of tests. Feel free to use any figures or tables that you wish in your presentation. I would prefer, however, that you do not copy the text to anyone else just yet. This was a quick dump, and I want more time to work on this before it gets distributed. If you have any comments about it as is, I would factor them into the next version.

*cjc*

Original to Follow: No x Yes        Via       

We are transmitting from a Xerox Telecopier 7017. If you do not receive this entire telecopy please call Create Incorporated (603) 643-3800. Ask for Anne Hablitzel.

## RESULTS FROM THE FIRST FLIGHT SERIES

### 1. SUMMARY

On a Phase II SBIR contract (NAS3-26552) for NASA Lewis Research Center, Creare has developed an instrument for measuring void fraction in a two-phase flow of a dielectric liquid. An objective of this work has been to demonstrate the use of this capacitive void fraction instrument under microgravity conditions. This void fraction instrument is being tested under microgravity conditions aboard the NASA KC-135 airplane, in a joint effort by NASA Centers JSC, LeRC, and GSFC as well as Texas A&M University and Creare.

In this brief report we look at the results from the first series of flight tests. We had two primary objectives in this work:

- Demonstrate that the void fraction instruments worked in the environment of the KC-135. This was demonstrated.
- Compare the void fraction as measured by two of the Creare instruments against the void fraction as measured by a volume of liquid trapped between a pair of quick-closing valves in the experiment. The initial result is that we find good agreement between the two.

Preliminary validation of the Creare void fraction instrument is therefore successful. Further tests are planned, covering a wider range of flow conditions and other instrument configurations.

## 2. FLOW LOOP

Figure 1 is a schematic of the flow loop used in the testing. This facility was constructed at NASA GSFC, using equipment from a previous bench-top experiment of a two-phase flow loop. The facility was adapted for use on the KC-135 by Texas A&M University, under sponsorship of NASA JSC. NASA LeRC loaned the void fraction instruments to this project, and Creare has provided technical support.

The facility itself is a boiling and condensing heat transfer loop. Beginning with the mechanical fluid pump, the key elements in the flow loop are:

- The mechanical pump
- An electrically heated evaporator
- One void fraction instrument
- A test section consisting of an armored glass sight-tube (11.1 mm ID) with pneumatically actuated, quick-closing valves at each end
- A second void fraction instrument
- A water-cooled condenser

The working fluid in the loop is the HFC replacement R-134a (a.k.a. SUVA). Nominal operating conditions are a pressure of 700 kPa (100 psia) and 300 K (80°F). Subcooled R-134a is pumped into the evaporator where it is heated and boiled. Two-phase flow leaves the evaporator and flows through the void fraction instruments and the test section. Upon leaving the test section, the flow enters the water-cooled condenser, where energy is removed so that the fluid becomes subcooled. Water is the coolant circulated on the secondary side of the condenser.

The pressure in the system is controlled by the reservoir. The fluid temperature in the reservoir sets the saturation pressure in the system. Operation of an electrical heater in the reservoir maintains the temperature via a temperature-control loop.

The test section, including the void fraction instruments, is mounted on an inclinable beam. To isolate liquid in the test section, the quick-closing valves are triggered. This simultaneously traps liquid between the valves and diverts the flow from the evaporator directly through the condenser. The test section can be inclined to measure the height of liquid trapped in the test section and thereby determine the void fraction.

This flow loop and the support equipment are mounted on the Texas A&M University Bolt Down Plate (BDP). Data acquisition, computer control, and data recording equipment are mounted on a Computer Control Console (CCC).

### 3. INTERPRETATION OF TEST RESULTS

Time-wise Data. Figure 2 shows the typical profile of microgravity flights aboard the KC-135. The bottom plot in this figure shows the profile of the vertical acceleration aboard the plane. Following an initial period of level flight at 1g, the KC-135 alternately experiences periods of 2g acceleration for about 60 seconds and 0.01g acceleration for about 30 seconds. A total of about 10 cycles occurs before level flight is resumed. This pattern of 10 parabolas is generally repeated 4 times, for a total of 40 parabolas on a given day.

The upper two plots in Figure 2 show the output from the two void fraction instruments. Both of the instruments functioned well during the testing. All of the data were obtained with the void fraction instruments in Configuration 5, where the void fraction measurement is across the diameter of the tube. The instruments have other configurations, including Configuration 0. Configuration 0 is intended for measurement of the void fraction with thin liquid films in the annular flow regime. That configuration has not yet been tested.

Our nominal procedure in the testing was to obtain data for one operating condition over each 5 parabolas experienced. The procedure was

- Set the power input and flow conditions in the loop prior to the 2g period of the first parabola in a sequence of 5.
- Allow the system to equilibrate through 3 parabolas
- Activate the quick-closing valves at the end of the third low-g period
- Raise/incline the test section during the fourth low-g period
- Measure the liquid level in the test section in the 2g period prior to the fifth parabola
- Lower the test section during the 5th low-g parabola
- Set the conditions for the next data point

Our evaluation focuses on 8 data points obtained during 40 parabolas on Day 4 of the testing (July 14, 1995). Tables 1 and 2 summarize the test conditions and void fraction measurements from those 8 tests. The parabola numbers for which the data were obtained are indicated in these tables.

Figures 3, 4, and 5 show the void fraction results at an expanded time scale from Parabolas 3, 18, and 32, respectively. These tests encompass a range of void fractions. In general, we find that the void fraction tends to increase during the 0.01g period compared with the void fraction during the 2g period. Moreover, there can be significant fluctuations in the void fraction following the transition from 2g to 0.01g. These may last 10 seconds, or half of the microgravity period. In Figure 4 the oscillations are due to an observed slug flow. The regular pattern of the void fraction instruments is consistent with the slug flow, as is the good correlation in the patterns of the output between the upstream and downstream instruments.

Table 1. Microgravity Test Results

Parabola	Pressure (kPa)	Flow Rate (kg/s)	Power (W)	Average Upstream Void Fraction (-)	Average Downstream Void Fraction (-)	Void Fraction from Trapped Liquid (-)	Regime
3	700	0.0032	25	0.47	0.50	0.54	Slug
8	700	0.0032	25	0.41	0.54	0.51	Slug
13	700	0.0032	56	0.64	0.56	0.67	Slug
18	700	0.0032	80	0.77	0.79	0.77	Slug-Annular
23	700	0.0032	100	0.74	0.84	0.81	Slug-Annular
29	700	0.0032	100	0.77	0.87	0.76	Slug-Annular
32	700	0.0032	210	0.97	0.95	0.85	Annular
40	700	0.0032	125	0.81	0.87	0.75	Annular

Table 2. 2g Test Results

Parabola	Pressure (kPa)	Flow Rate (kg/s)	Power (W)	Average Upstream Void Fraction (-)	Average Downstream Void Fraction (-)	Void Fraction from Trapped Liquid (-)	Regime
3	700	0.0032	25	0.47	0.28	n/a	Stratified
8	700	0.0032	25	0.35	0.18	n/a	Stratified
13	700	0.0032	56	0.33	0.31	n/a	Stratified
18	700	0.0032	80	0.46	0.42	n/a	Stratified
23	700	0.0032	100	0.54	0.50	n/a	Stratified
29	700	0.0032	100	0.51	0.40	n/a	Stratified
32	700	0.0032	210	0.97	0.99	n/a	Stratified
40	700	0.0032	125	0.49	0.49	n/a	Stratified

[Discuss instrument response in null parabola.]

Time-Averaged Data. To get the average values of void fraction from the instruments during the microgravity period, as listed in Table 1, the output signals were time-averaged. The instrument output was averaged over the middle 20 seconds of the 30-second 0.01g period. This allowed 5 seconds during the transition periods. We found that it made negligible difference whether the output was averaged over this whole 20 seconds, or over the first or second 10 seconds of this 20-second window. The average instrument output was the same in any case.

To get the average values of the void fraction from the instruments during the 2g period, as listed in Table 2, the output signals were also time-averaged. In this case, we time-averaged the results over the 20-second period prior to the start of the transition to low gravity.

Figure 6 compares the average void fraction measurements from the upstream and downstream sensors with the void fraction measured by the quick-closing valves. The void fraction sensors track the overall trend of increasing void fraction with increasing power. Agreement is  $\pm 0.10$  of the void fraction.

Figure 7 compares the average void fraction measurements from the upstream and downstream sensors during the 2g and 0.01g periods. (We did not trap the liquid in the test section during the 2g periods, so there are no data from the quick-closing valves in 2g.) Figure 7 shows that the void fraction is significantly greater during the microgravity period than during the 2g period.

#### 4. COMPARISONS WITH TWO-PHASE THEORY

Flow Regime Maps. In Figures 8 and 9 we have plotted the observed data on the predicted flow regime maps. The analysis tool that we used to predict the flow regime maps is the Creare MICROREG software. Figure 8 shows that the observed flow regime in 2g is stratified for all conditions, as expected. Figure 9 shows that the observed flow regime ranges from slug to annular, with some data in the transition region. The transition from well-defined slug flow to the less-well-defined slug-annular transition occurs at approximately the expected location of  $x = 0.12$ .

Note: There is presently some uncertainty in the calculations of the quality for the test data. To estimate the quality, we have used the following expression:

$$x = \left[ \frac{P}{\dot{m}h_{fg}} - \frac{c_{pf}\Delta T_{sub}}{h_{fg}} \right]$$

where

- $P$  is the input power to the evaporator (W)
- $\dot{m}$  is the mass flow rate (kg/s)
- $h_{fg}$  is the latent heat of vaporization (J/kg)
- $c_{pf}$  is the liquid heat capacity (J/kg-K)
- $\Delta T_{sub}$  is the liquid subcooling entering the evaporator (K)

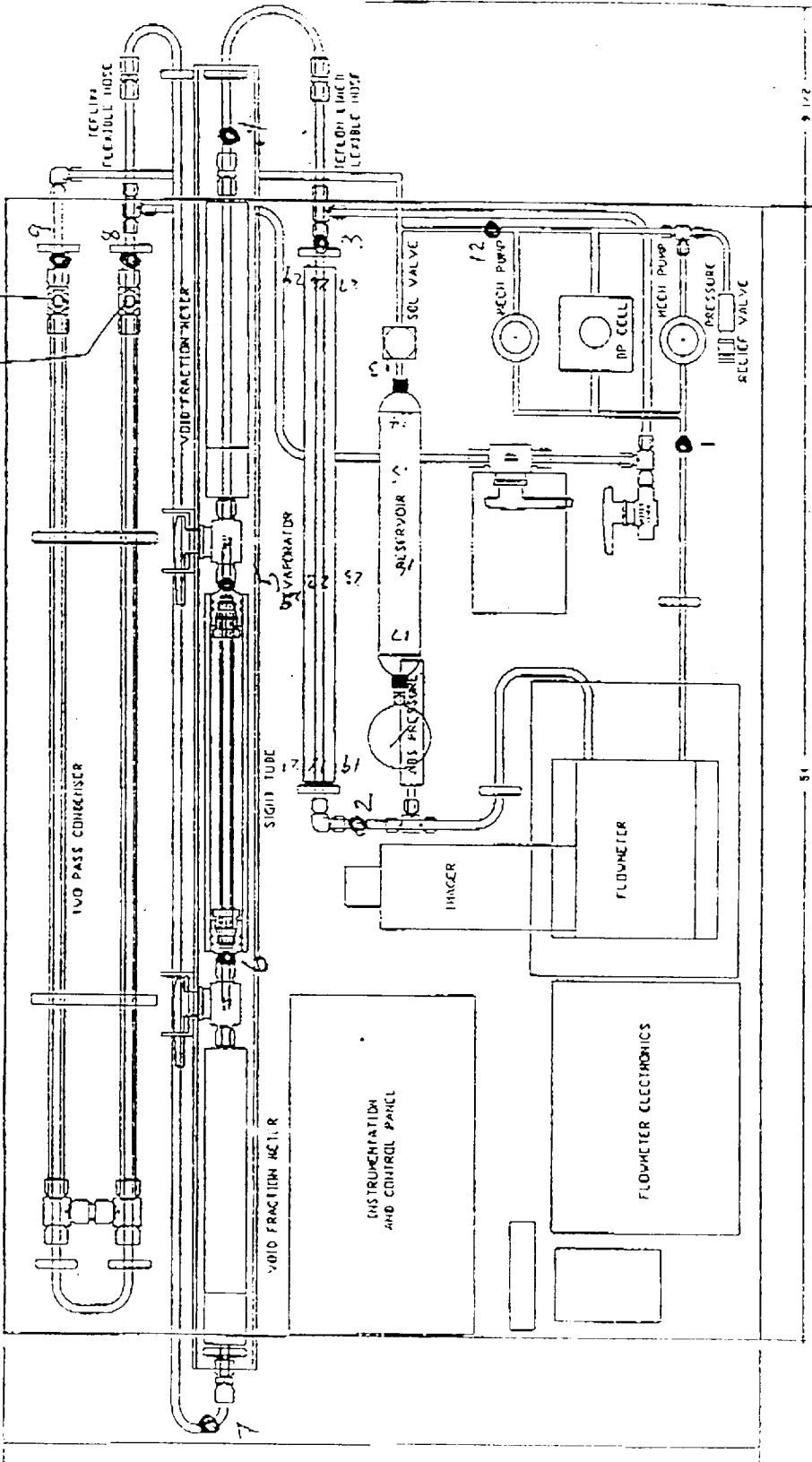
For this evaluation, we have assumed negligible subcooling entering the evaporator. We need to adjust the predictions for the actual subcooling from the recorded data when that becomes available. This expression does not account for heat losses or heat gains from the ambient. Adjustments for heat losses are currently being developed.

Void-Quality Analysis. The relationship between the void fraction and quality is determined by the characteristics of the two-phase flow. This relationship can be calculated for the different flow regimes. We have used the Creare software MICROP as the analysis tool for the predictions shown in Figures 10 and 11.

Figure 10 shows the predicted void fraction for microgravity conditions. Predictions are shown for both the slug and annular flow regimes. For these maps, the predicted quality is related to the power input using the equation shown above. The data at low power (25 W to 56 W) should compare with the predictions for slug flow. We see that the data lie at somewhat higher void fractions, indicating that the effective power input should be about 20 W greater. The data at high power ( $> 100$  W) should compare with the predictions for an annular flow. We see that there is fairly good agreement with the predictions for the annular flow. If the effective power input is adjusted by 20 W, this will have only a small effect on the comparison. Adjustment for heat gains from the ambient may therefore explain these data.

Figure 11 shows the predicted void fraction for the 2g conditions. Predictions are shown for the stratified flow regime. Two predictions are shown, one for a wavy stratified flow and one for a smooth stratified flow. The measured void fractions from the Creare sensors indicate that the void fraction is lower than expected during the 2g period. At present we do not have an explanation for this. We observe, however, that this result is consistent with the results from calibration tests at 1g (Figure 12). This needs further study.

# FRIM WITH VOID FRACTION METER

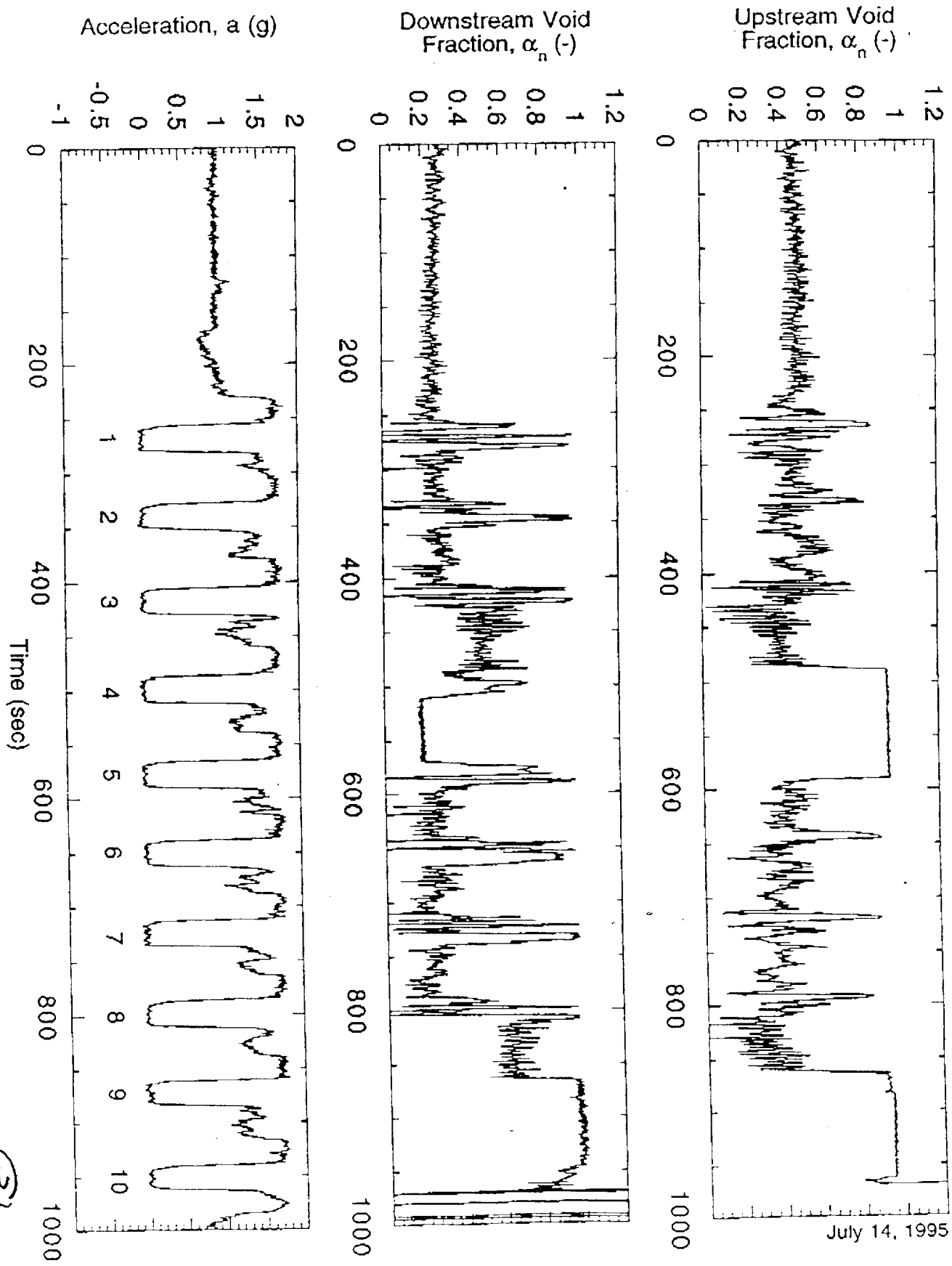


FILE: FRIM.FRIM.V002  
DATE: MAY 9, 1995

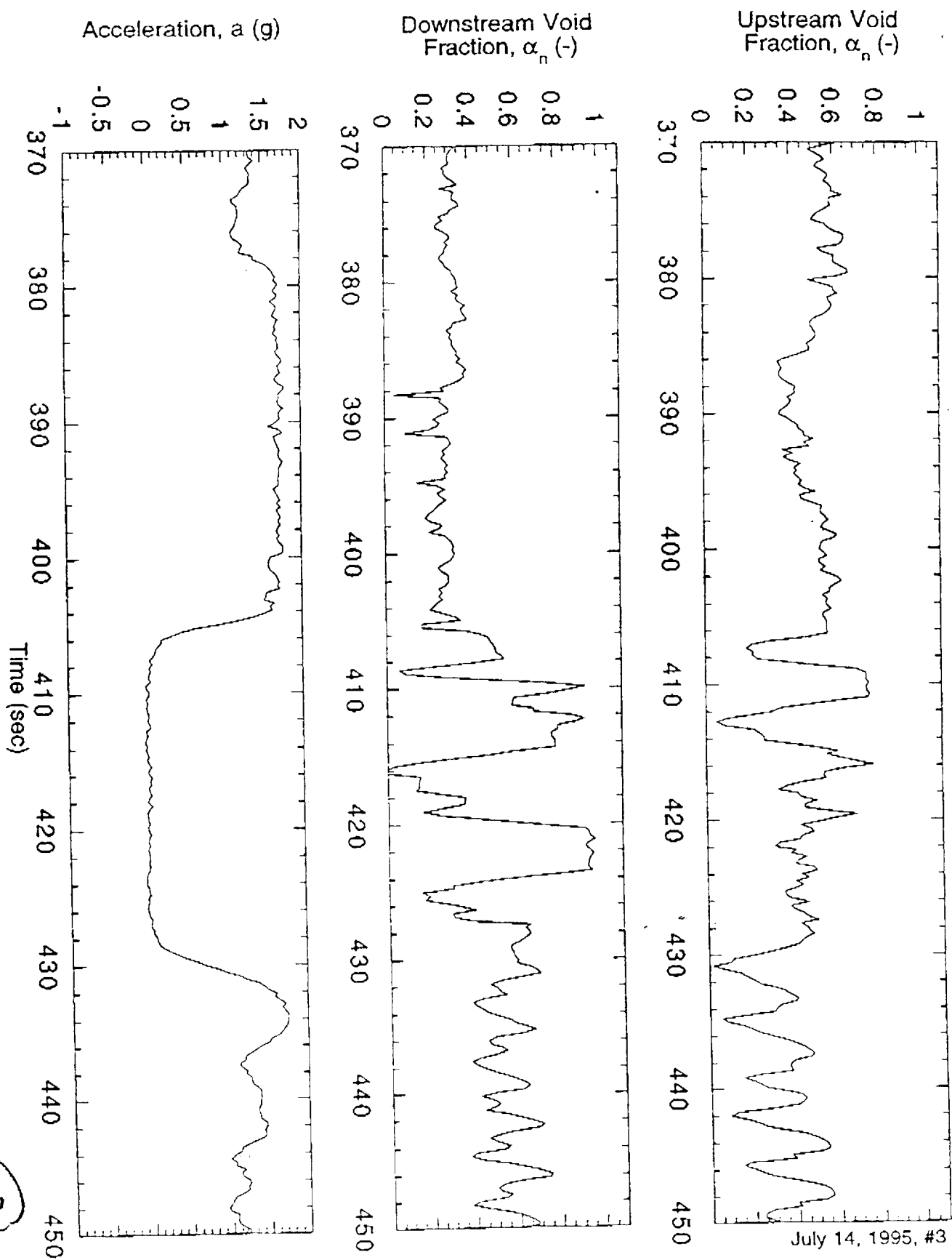
FIGURE 1  
Flow Regime in Microgravity (FRIM)

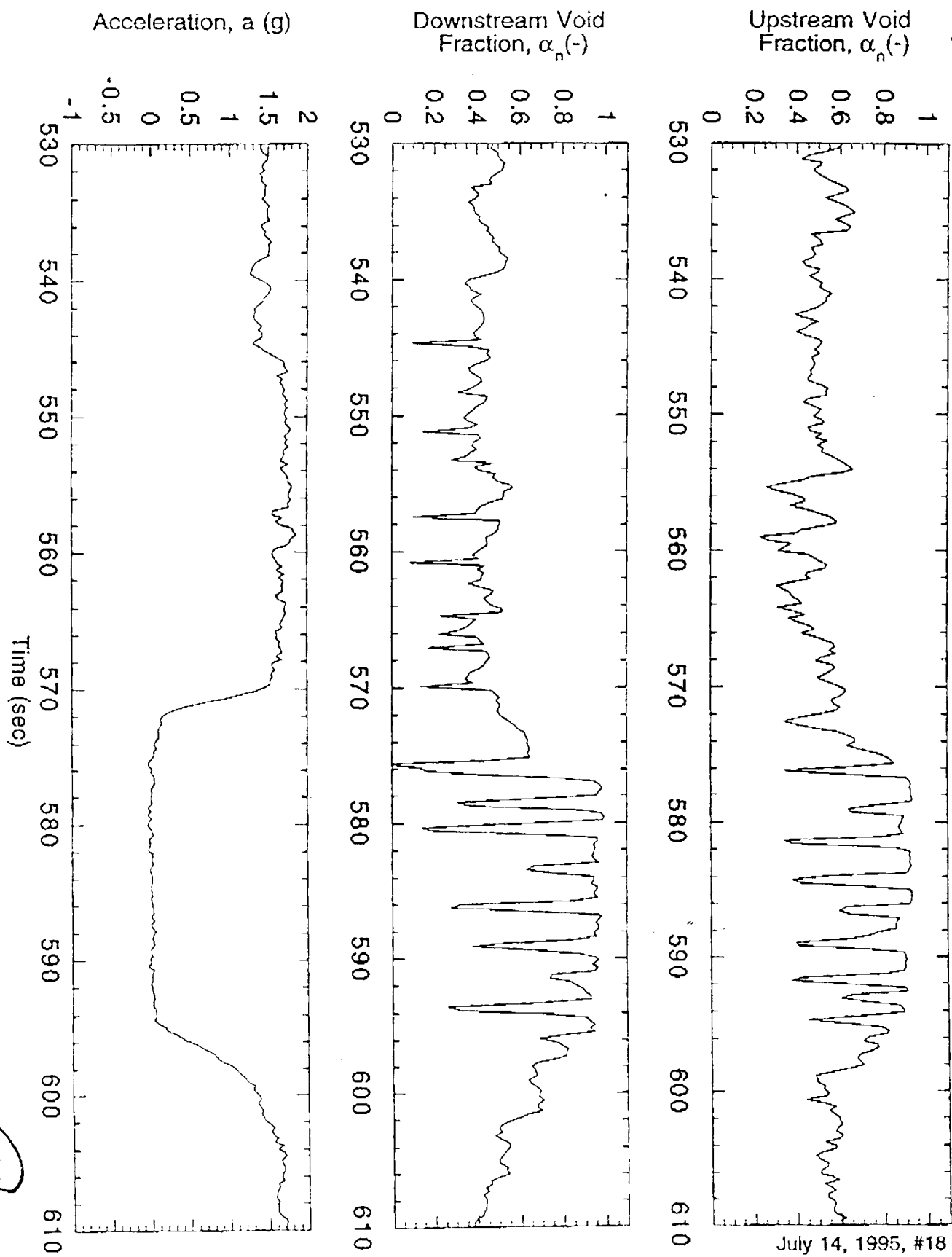
• The Location

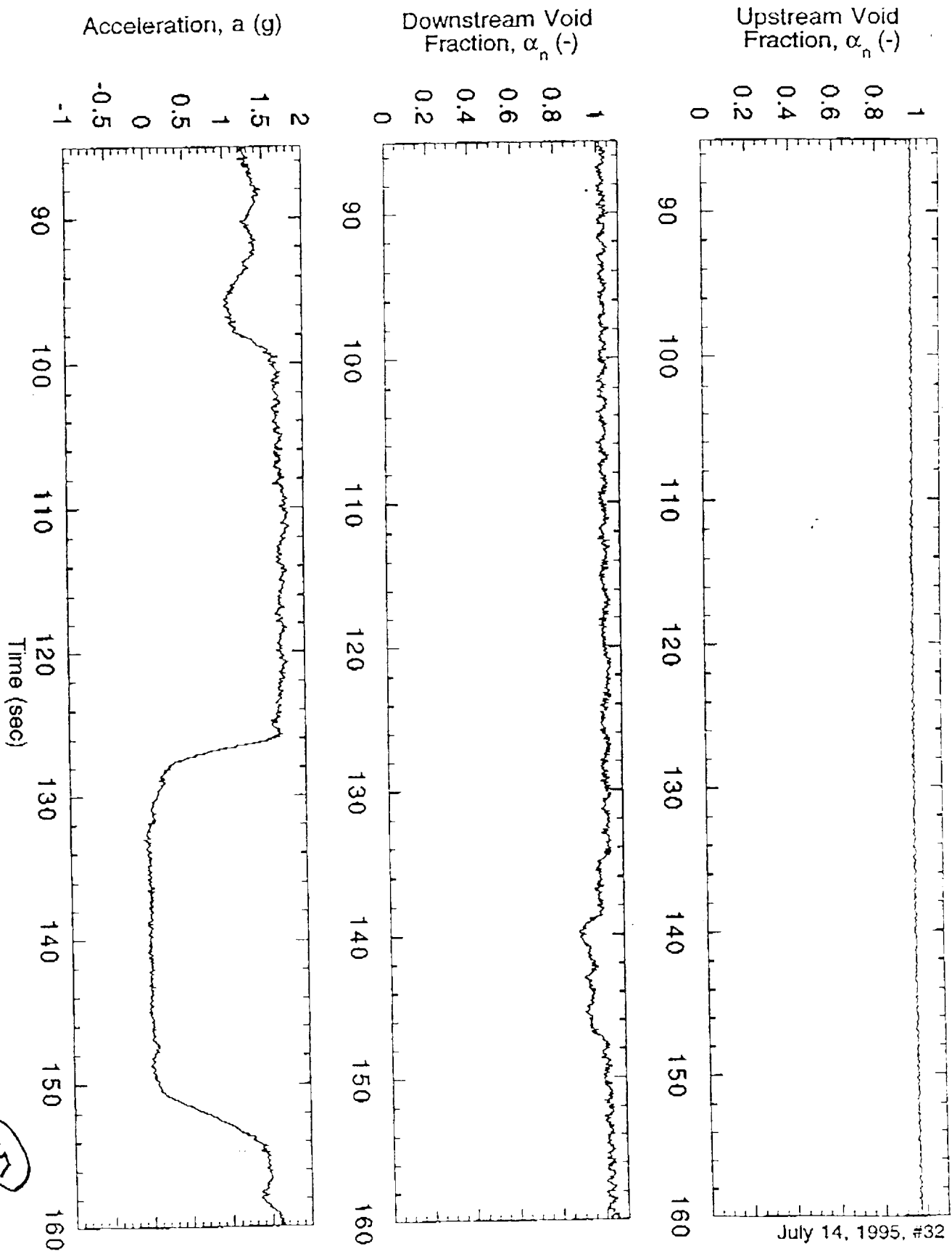
1

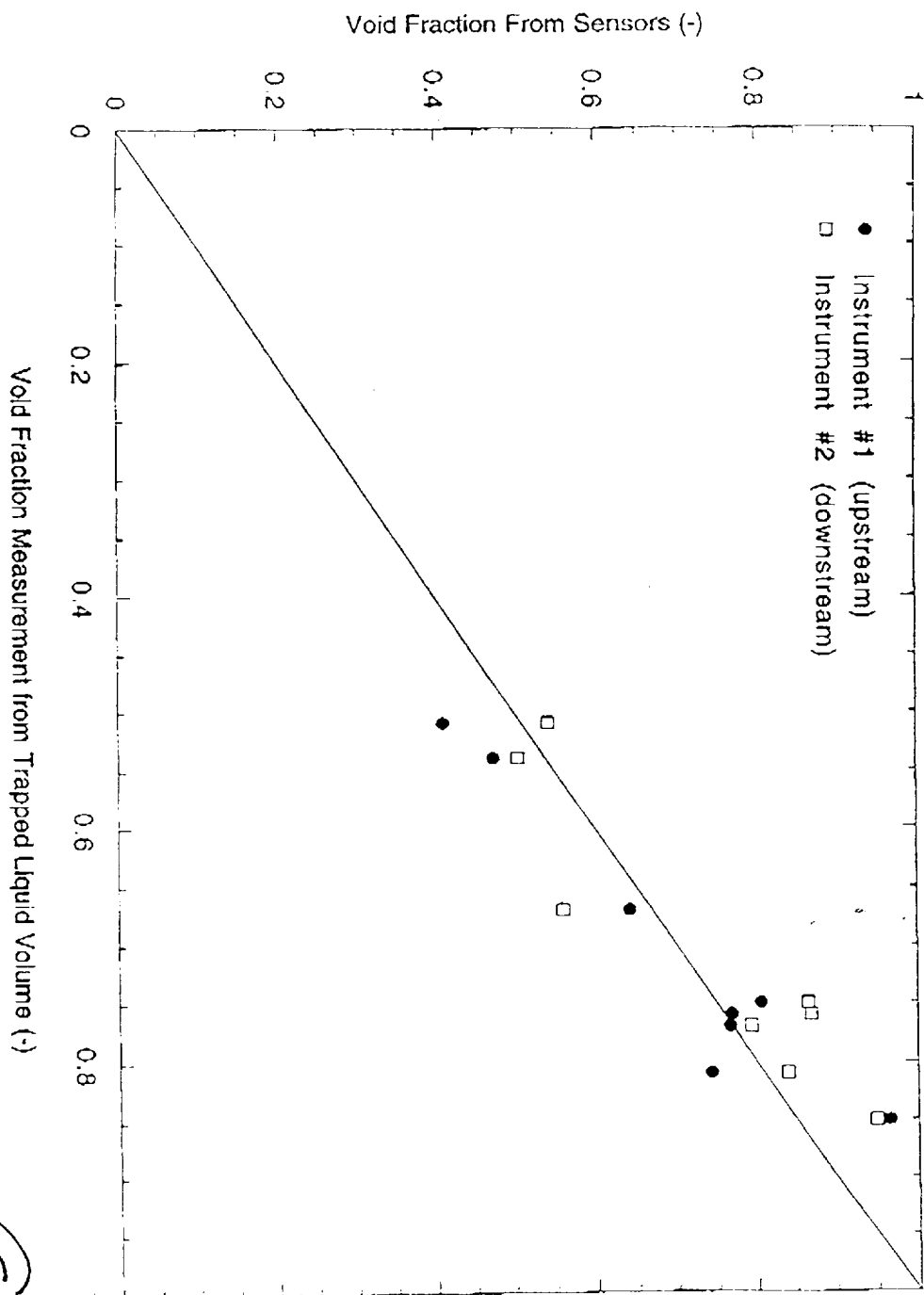


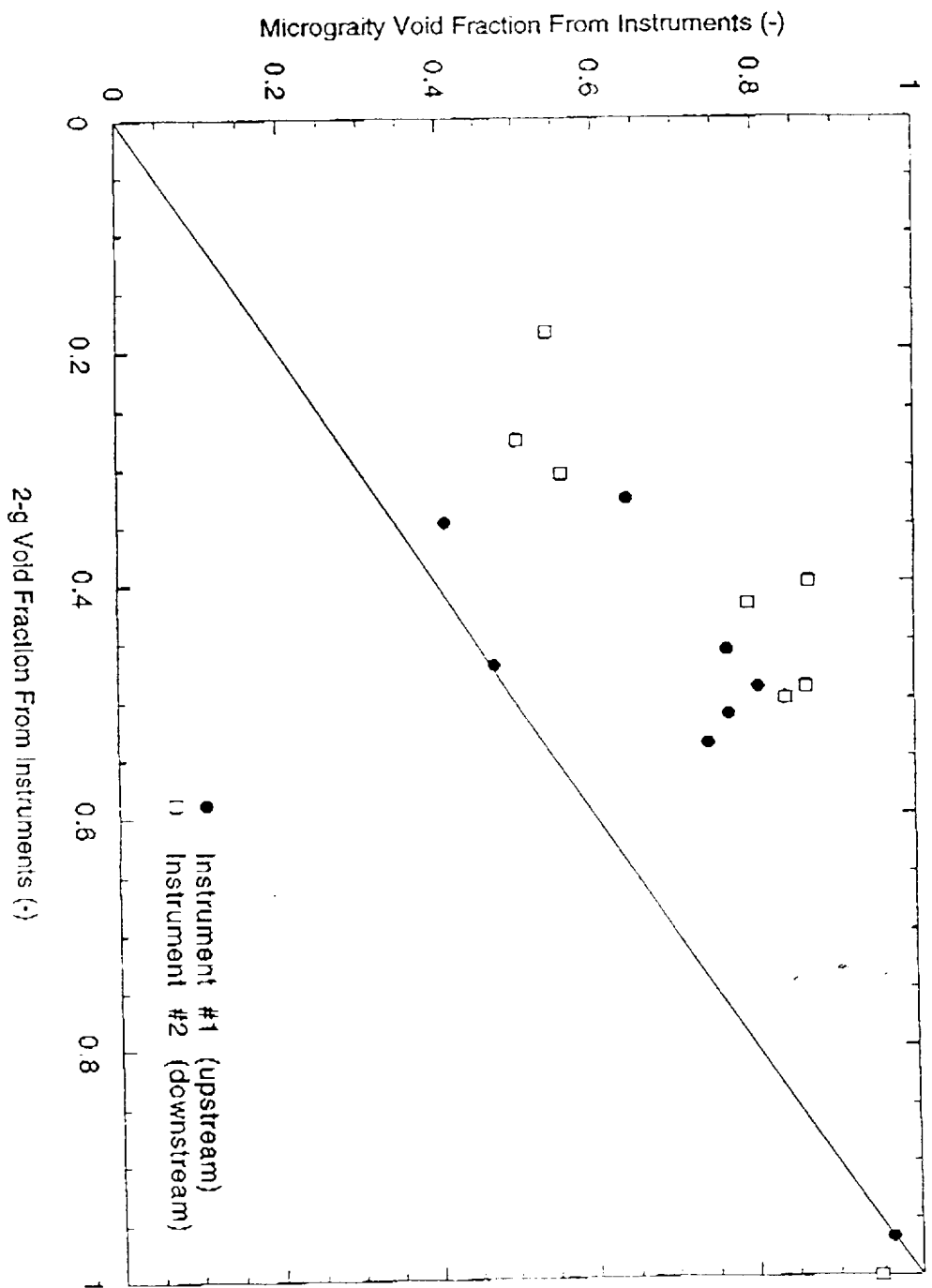
July 14, 1995





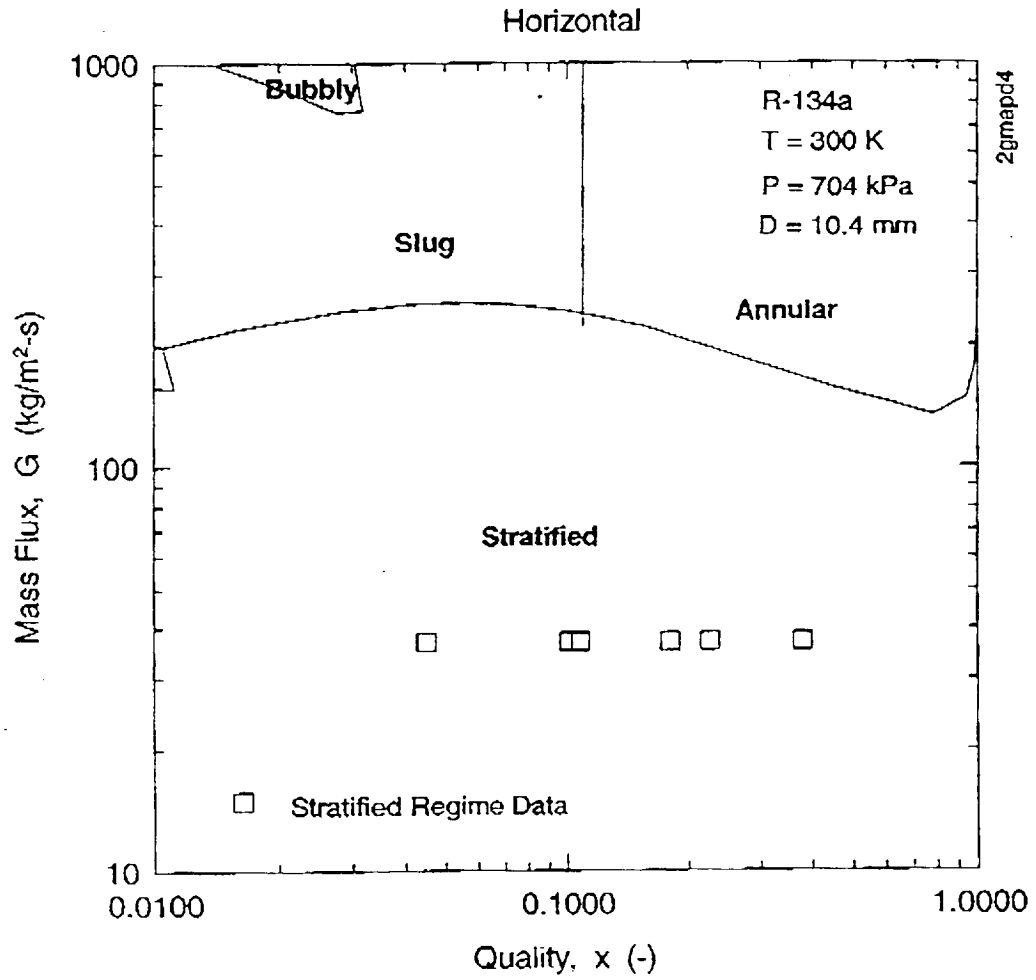






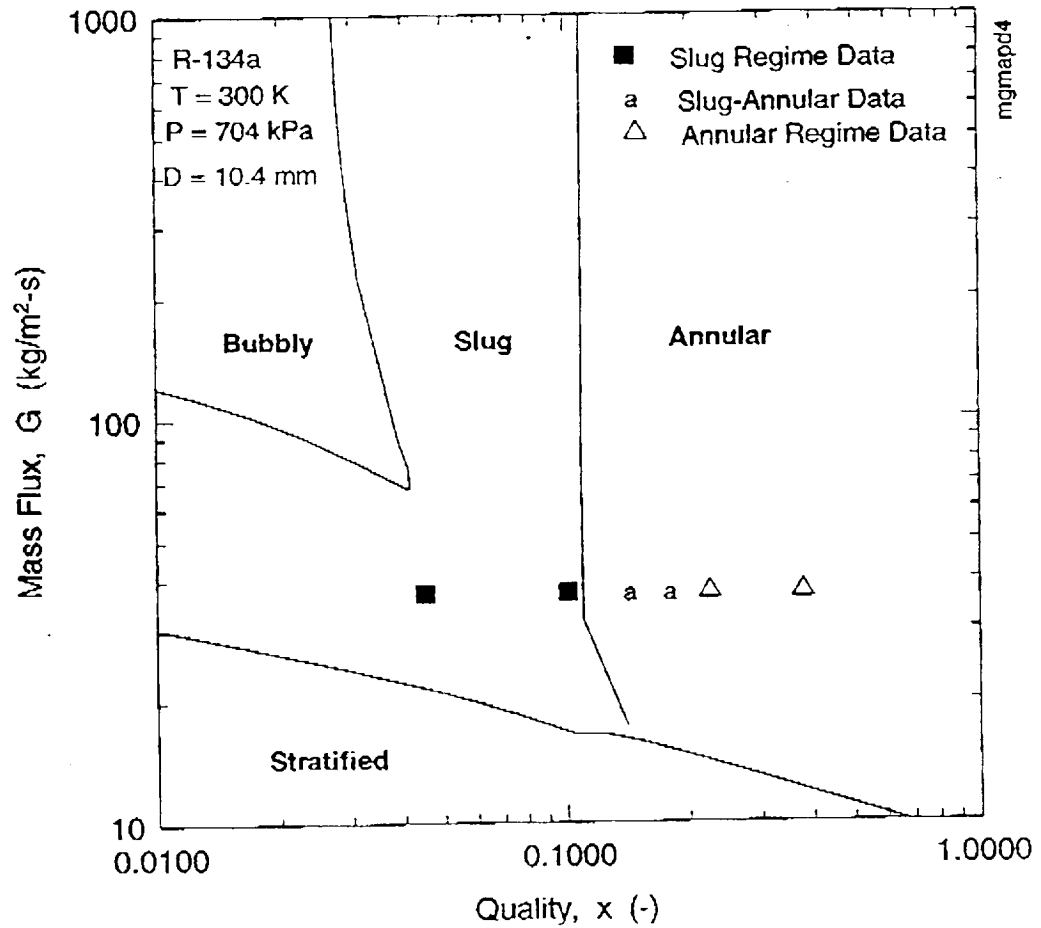
7

# R-134a REGIME MAP AT 2g

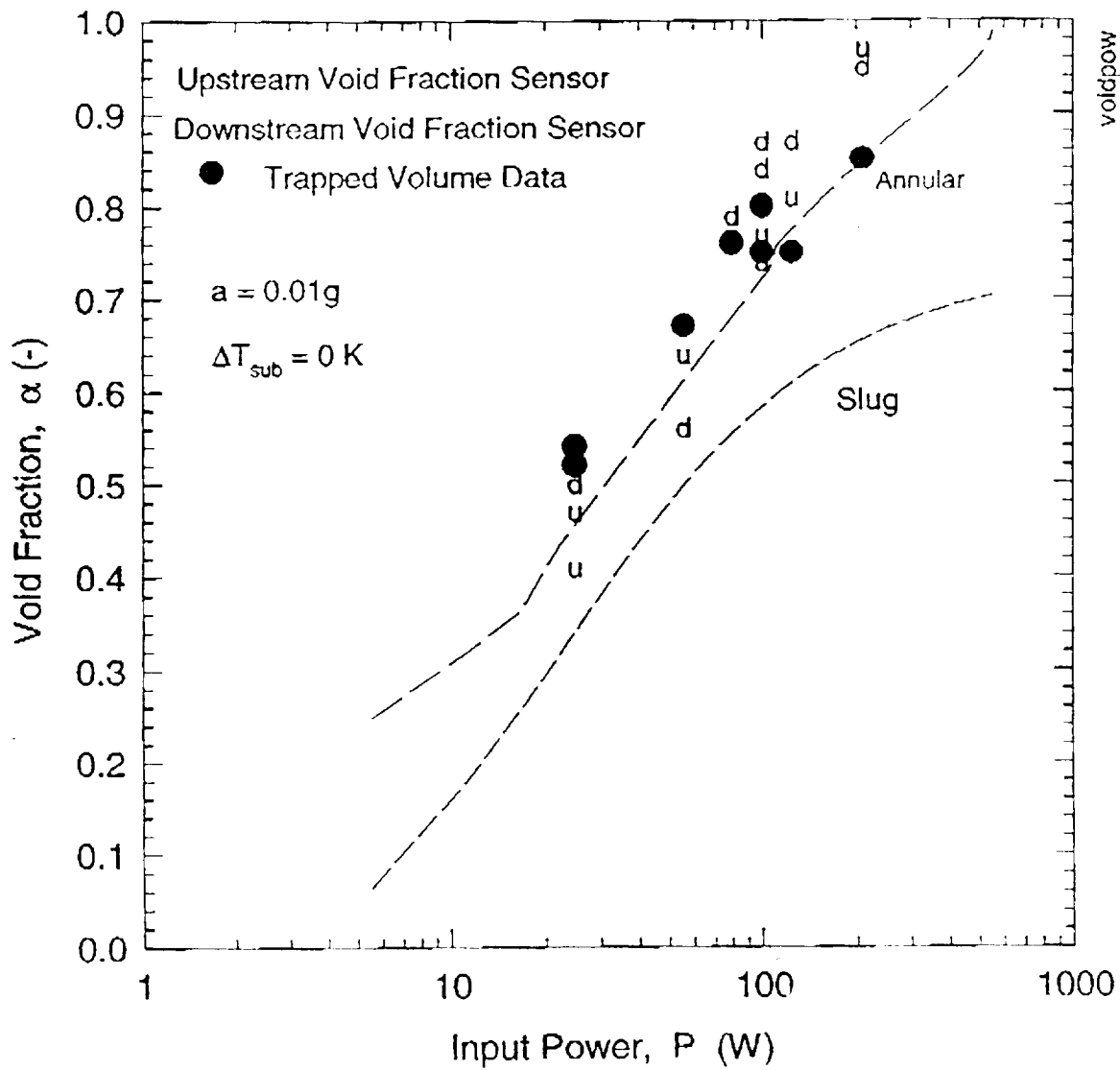


**R-134a REGIME MAP AT 0.01g**

Horizontal

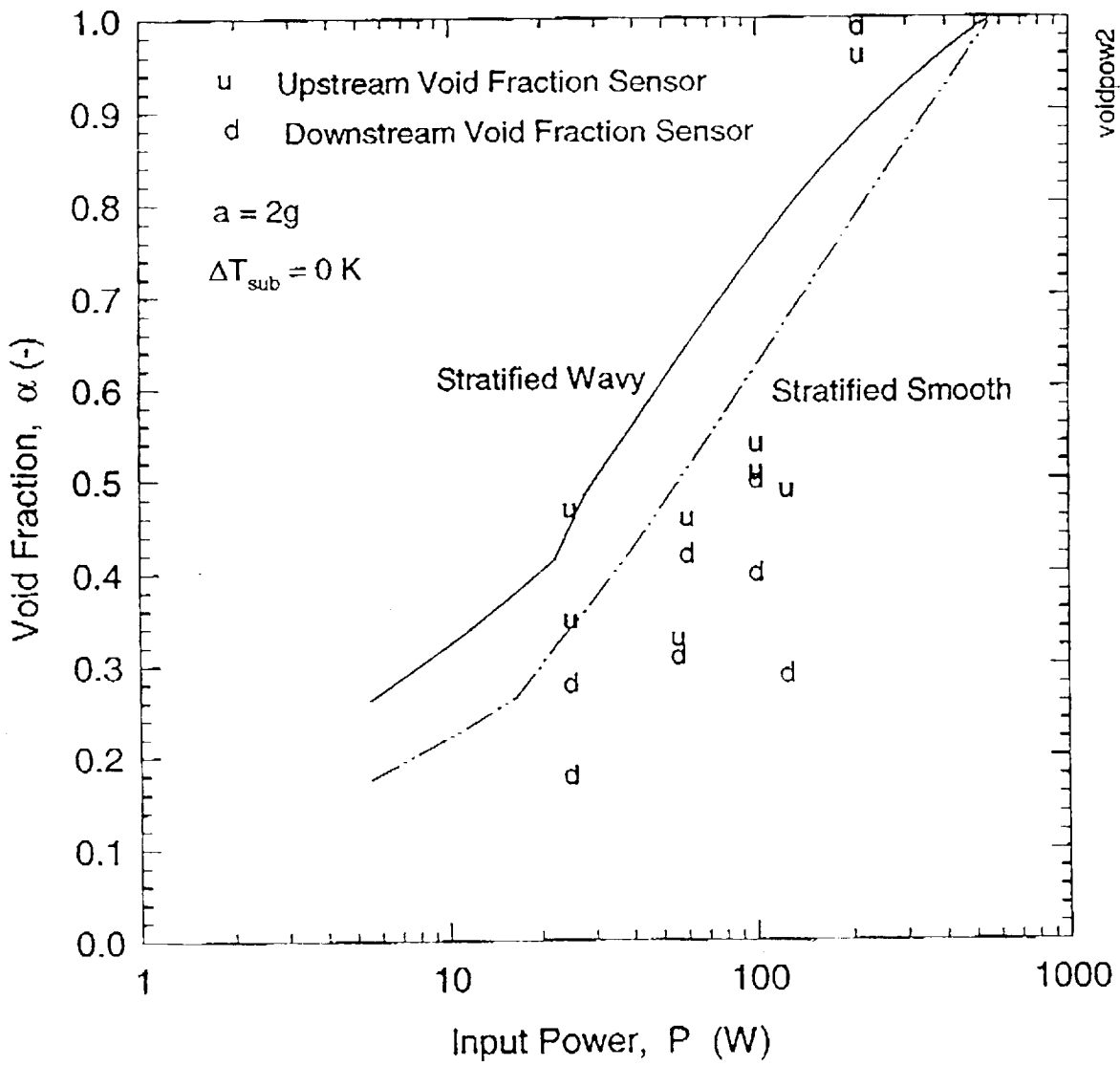


## Void Fraction Plot



6

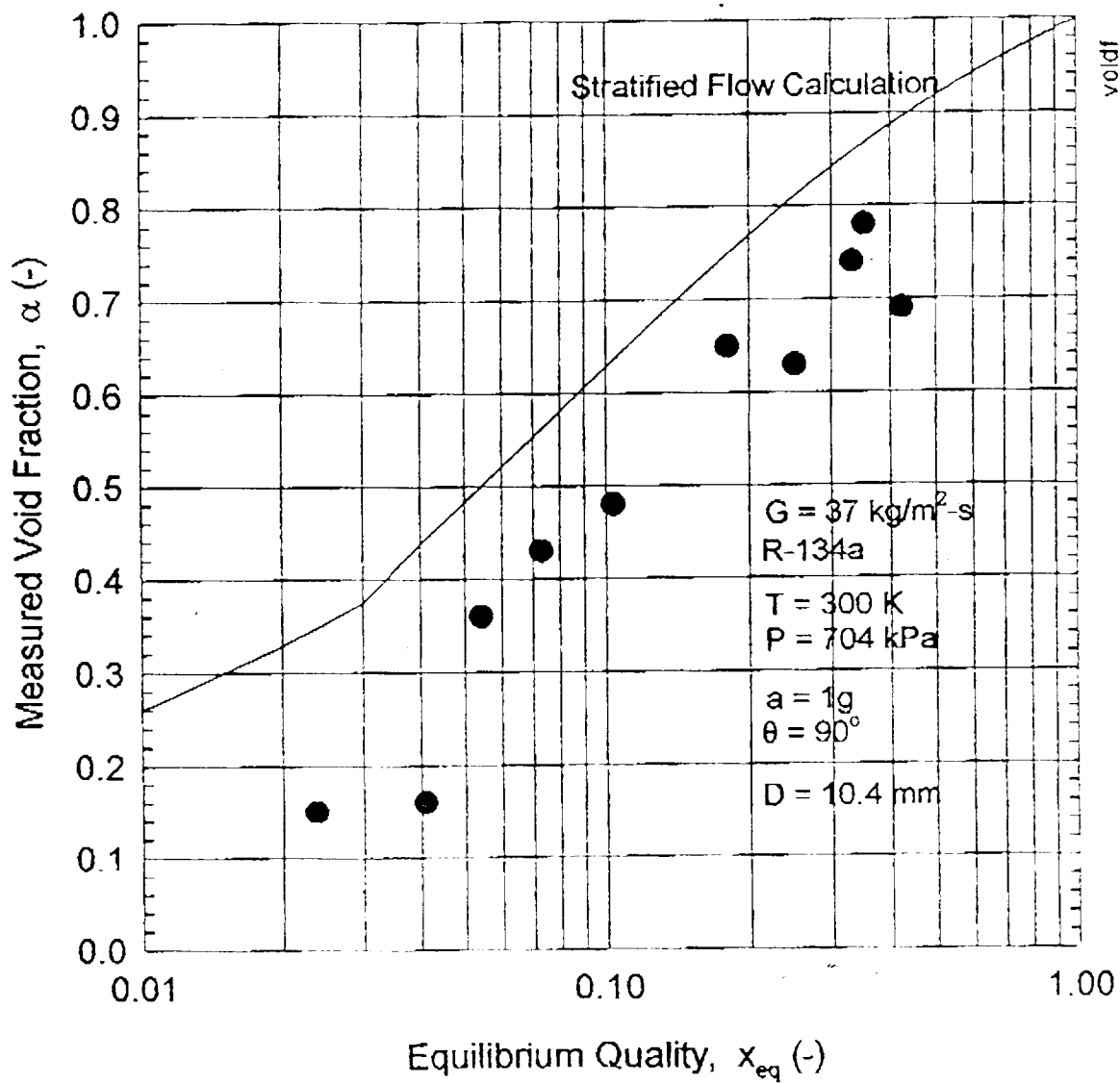
# Void Fraction Plot



11

Figure 3.

## R-134a Void Fraction





Engineering Research and Development Services  
30 Years of Technical Excellence

March 27, 1996

NASA Lewis Research Center  
Space Systems Branch  
Attn: Dr. Myron E. Hill  
Mail Stop 500-102  
21000 Brookpark Road  
Cleveland, OH 44135

**SUBJECT: LETTER REPORT ON FLIGHT TESTS (Contract NAS3-26552)**

Dear Myron:

Here is our letter report describing the second series of microgravity flight tests with the void fraction sensors delivered on our Phase II SBIR contract with NASA LeRC. This report completes our contractual obligations on the referenced contract.

Sincerely,

A handwritten signature in cursive script that reads "Christopher J. Crowley".

Christopher J. Crowley  
Principal Engineer

7598/amh

cc: Patrick Magari, Creare  
Christine Martin, Creare  
Christopher Signorino, LeRC  
Fred Best, CSP ✓  
Katy Miller-Hurlbert, JSC  
Steve Benner, GSFC

## Letter Report

**LOW-GRAVITY TESTING OF VOID FRACTION SENSORS:  
RESULTS FROM THE SECOND FLIGHT SERIES**

C.J. Crowley  
P.J. Magari  
C. Martin

**1. INTRODUCTION**

As part of our Phase II SBIR contract NAS3-26552 to develop a capacitive void fraction sensor for dielectric liquids, Creare participated in a second campaign of low-gravity flight tests aboard the NASA KC-135. The ongoing series of tests involves JSC (primary sponsor), GSFC (two-phase flow hardware), LeRC (void meter hardware), and Texas A&M University (manager of the flight tests and flow loop). Our role is to operate the void fraction instruments during the flights and to evaluate the void meter data. The overall objective of the testing is to demonstrate that the void fraction instrument works in the low-gravity environment.

The first campaign was conducted in July of 1995, and we documented the results in a letter report October 6, 1995. The tests focused upon the higher end of the void fraction range—50% or more. Tests were mostly in the annular flow regime, and results from the void fraction meters compared quite well with the independent measurement of void fraction.

The second test campaign was conducted in January 1996, with flights on January 23, 24, 25, and 27. The focus of these tests was upon test conditions which would produce void fractions of less than 50%, *i.e.* lower power tests in the slug or bubbly flow regimes.

**2. SUMMARY**

We found it difficult to draw quantitative conclusions about the results from these tests because it proved to be difficult to operate the facility in steady flow conditions at the low power. Transient behavior and non-uniform distribution of vapor and liquid across the length of the test section during the low-gravity period was observed nearly all of the time. Nevertheless, we can say that:

- The transient records of void fraction from these tests are in qualitative agreement with the visual observations.

- The void fraction from the upstream meter tends to be in better agreement, on average, than the downstream meter relative to void fraction measurements via the trapped volume.
- The calibration of both instruments in the test loop was remarkably stable in the period between ground tests at GSFC in May 1995, through the July 1995 flights, and through the January 1996 flights.

### 3. TEST CONDITIONS

The best test conditions were achieved on the final day of testing (January 27). On the previous days, it was difficult to achieve steady conditions in the facility.

The difficulty during the first three days was in creating steady, uniform two-phase conditions in the test section at low heat input. At low power input (in the range of 15 W to 40 W), the heat input for phase change, heat removal in the condenser, heat addition to overcome the subcooling, and heat losses (or gains) from the ambient are all of the same order of magnitude. A delicate balance needs to be maintained to achieve steady heat transfer conditions, and it is difficult to do so when the conditions such as the temperature of the heat sink coolant and the ambient temperature on the plane are changing with time. Texas A&M is implementing some facility modifications which should improve this situation in future campaigns.

There is also the possible influence of transverse acceleration, due to atmospheric conditions and the trajectory of the plane. This was noted especially on Day 2 (January 24), when vapor bubbles appeared to be migrating against the direction of flow.

On the first three days of this flight campaign, the approach was to control the energy balance by varying the flow rate of the coolant. By the fourth day of testing, a better balance was achieved by using warmer coolant water—a lower subcooling in the heat sink—and varying the coolant flow rate rather than evaporator power. Our evaluation focuses on the results from Day 4, since they are illustrative of the best test behavior during this flight campaign. Table 1 summarizes the test conditions and measured void fractions.

As shown in the table, 15 test points were obtained during this test day of 64 parabolas. The test procedure was to obtain a data point approximately every fourth parabola, although at least one break in the flight path of the KC-135 disrupted this pattern. Conditions were observed through three parabolas, isolation of the quick-closing valves was initiated at the end of the third parabola, and the trapped volume was measured during the fourth parabola in each group. The table identifies the parabolas during which the quick-closing valves were activated. We analyzed the output from the void fraction sensors, recorded on a portable PC, during the low-gravity periods. We have looked at both time-averaged and transient data records.

**Table 1. Low-Gravity Test Results**  
(Day 4, January 27, 1996)

Parabola	Pressure (kPa)	Flow Rate (kg/s)	Power (W) <sup>1</sup>	Average Upstream Void Fraction (-)	Average Downstream Void Fraction (-)	Void Fraction from Trapped Liquid (-)	Regime
3	646.0	0.00303	40 (29)	0.457	0.489	0.47	Slug
8	625.4	0.00301	35 (35)	0.412	0.877	0.33	Slug
11	604.8	0.00305	31 (31)	0.505	0.284	0.43	Slug
16	604.8	0.00298	25 (25)	0.384	0.302	0.34	Slug
19	604.8	0.00305	25 (25)	0.422	0.864	0.55	Slug
24	591.0	0.00308	25 (25)	0.439	0.896	0.39	Slug
27	591.0	0.00308	25 (18)	0.577	0.004	0.76	Slug
32	591.0	0.00311	25 (20)	0.462	0.112	0.69	Slug
35	591.0	0.00311	25 (16)	0.495	0.005	0.39	Slug
40	591.0	0.00312	25 (17)	0.482	0.004	0.50	Slug
43	591.0	0.00312	25 (16)	0.541	0.005	0.56	Slug
48	591.0	0.00312	25 (11)	0.227	0.005	0.15	Slug
56	591.0	0.00311	33 (16)	0	0.004	0.18	Slug
59	591.0	0.00310	33 (17)	0.552	0.481	0.73	Slug
64	591.0	0.00309	33 (16)	0.475	0.425	0.73	Slug

<sup>1</sup> Values in brackets are power input adjusted to account for inlet subcooling.

Rows with shading indicate tests with higher transit velocities (2 in/s) observed in videos. Unshaded rows had 1 in/s velocities.

One thing that becomes apparent in the data listed in Table 1 is that void fractions in excess of 50%, some over 70%, were measured in the volume between the quick-closing valves. These high void fractions were obtained even though the power input was 25 W to 35 W. With that amount of heat input, the *maximum* quality of the fluid entering the test section—assuming saturated liquid entering the evaporator—would be  $x = 0.055$ . The effect of inlet subcooling would be to reduce the quality and the void fraction. In the slug flow regime, the void fraction at that quality should be no larger than about 40%. Thus, it is difficult to fathom how the void fraction could be larger than this value for steady, two-phase flow conditions. This first order check indicates that there might have been a problem achieving steady flow conditions in the test section, and we will see that the transient data support this.

#### 4. FLOW REGIMES

The flow regime is slug flow during the low-gravity period in all of the tests. Video records of the flow were also made using digital imagery during this time, and those images confirm that the flow regime is slug flow. Ignoring subcooling effects or heat losses, the maximum possible quality for the flow is  $x = 0.055$ , and the corresponding void fraction is 40%. This is insufficient to produce an annular flow. In terms of void fraction, generally a void fraction of  $\alpha > 0.7$  is needed for an annular flow regime. Slug flow was the only flow regime observed during the tests, and this is corroborated by the video records from the digital imager.

#### 5. OBSERVED BEHAVIOR

Qualitatively, we observed the following sequence of events visually in the test section:

- During the 2-g period, the flow was stratified, often with a much larger void fraction indicated at the upstream than the downstream end.
- Upon entering the low-g period, and for some seconds thereafter, the void fraction was apparently much larger near the upstream end of the test section (near Meter 1) than in the downstream end of the test section (near Meter 2). Often, the downstream end of the test section appeared to be entirely liquid-filled, with no visible vapor bubbles.
- During the course of the low-g period, liquid and vapor bubbles gradually migrated from the upstream to the downstream section. In some cases, the vapor bubbles reached the end of the downstream section, but we could not visually determine whether the vapor bubbles had reached as far downstream as the second void fraction sensor by the end of the low-gravity period.

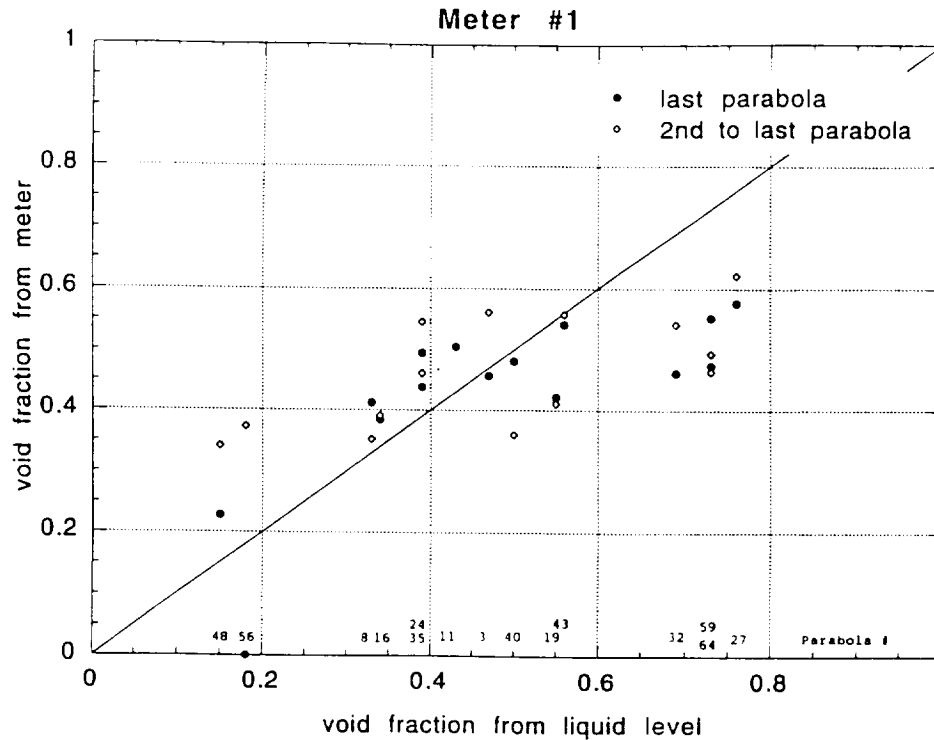
With that general picture in mind, we will first look at the time-averaged measurements from the void fraction meters. Then we will return to a more detailed look at the transient behavior as recorded by the void fraction sensors.

Time-Averaged Behavior. Figure 1 compares the time-averaged void fraction from the upstream meter (Meter 1), with the void fraction obtained by measuring the liquid level in the test section. The same analysis procedure as used in the evaluations for the July flights was applied here. Basically, the output of the void fraction meter is averaged during the last 15 to 20 seconds of the 25-second period of reduced gravity. Results are shown here for both the penultimate (second to last) parabola before valve closure and the parabola ("last" parabola) during valve closure. Results are consistent between the successive parabolas in the same series, but we see a general trend for the void fraction meters to read higher than the trapped volume at low void fraction and vice versa at higher void fractions. Void Meter 1 indicates that void fractions are in the range of 45% to 60%, when the void fractions from the liquid level are higher than 60%. Recall from the earlier discussion that void fractions greater than 40% from the liquid level in the trapped volume are suspect, because the power input is insufficient to justify that large a void fraction.

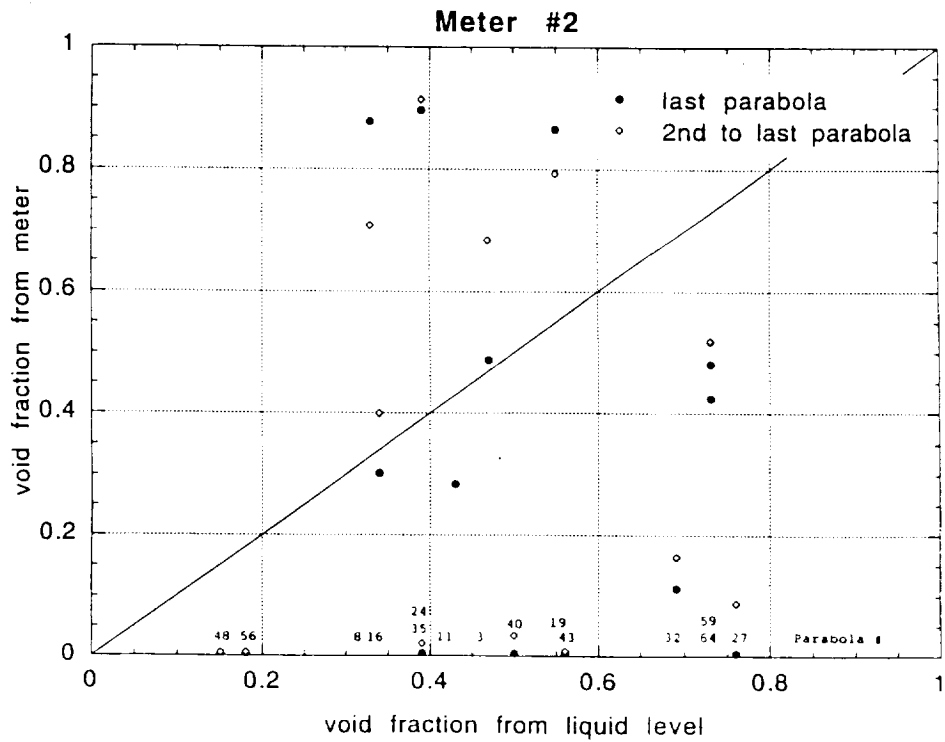
The approach of plotting the data versus the void fraction from the liquid level measurement may be a misleading one, because it assumes that the trapped volume is a good basis for comparison. If there is a significant transient behavior in the flow, the void fraction from the volume trapped in the test section may not represent a true average. Parabolas 35, 43, 56, and 64 represent nominally the same net input power of 16 W to the fluid (evaporator input power less heat input to overcome subcooling). Yet, the void fraction from the trapped volume is 39%, 56%, 18%, and 73%, respectively—quite a large variation for ostensibly the same power input. Similarly, Parabolas 16, 19, and 24 represent a net input power of 25 W to the fluid, and the void fraction from the trapped volume is 34%, 55%, and 39%. In addition, if we look at the tests in the order of increasing net input power, there is no monotonic trend toward increasing void fraction in the trapped volume with increasing power, as one would expect.

Figure 2 shows the corresponding data for the downstream meter (Meter 2). There is no good correlation between the downstream meter and the trapped liquid volume, or the void fraction as measured by Meter 1. The results for a number of the tests show nearly zero void fraction at this Meter, some show nearly all void, and some are in between. We believe that this quantitative evidence supports the qualitative observation that vapor bubbles were initially distributed upstream at the start of the low-g period and achieved varying degrees of success in reaching the downstream end during the low-gravity period. Examination of the transient behavior will shed some light on these results.

Transient Behavior. In Figure 3 we again show the data from Meter 1 (see Figure 1), but the minimum and maximum values of the void fraction during the low-g period are shown. Values range from near 10% to near 90% void fraction in every test. Thus, it is important to look at the transient behavior in the tests.



**Figure 1. Time-Averaged Void Fraction Measurements from Meter 1 (Upstream)**



**Figure 2. Time-Averaged Void Fraction Measurements from Meter 2 (Downstream)**

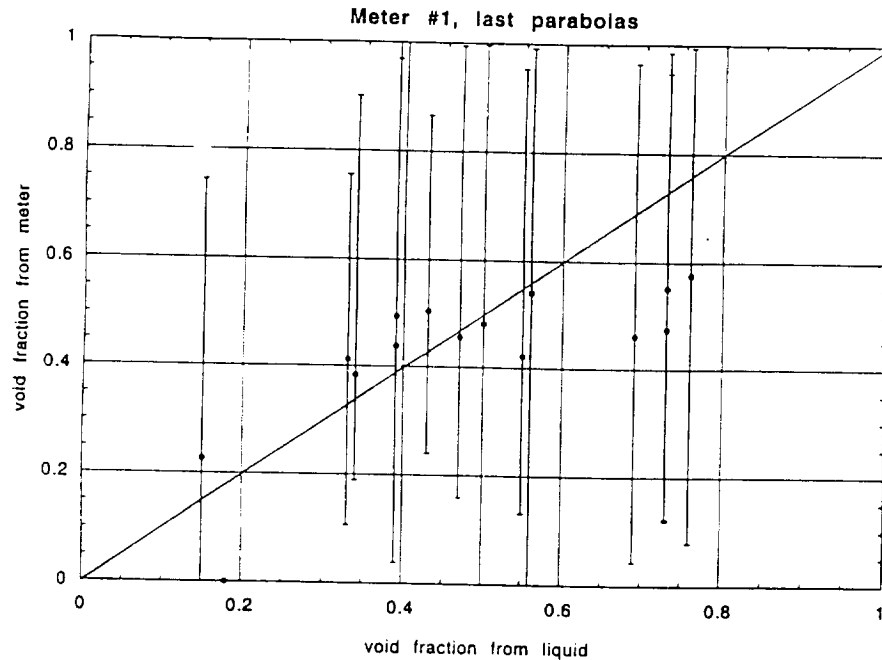


**Figure 3. Minimum and Maximum Void Fraction Measurements from Meter 1**

Figures 4 through 11 plot the transient results through the low-g period for selected tests. In each plot, we show the

- Acceleration (trace noted by an arrow to the right-hand scale)
- Void fraction from Meter 1 (solid trace)
- Void fraction from Meter 2 (dashed trace)
- Measured void fraction from the trapped liquid (horizontal dashed line  $\alpha_{liq}$ )

The specific parabolas are identified at the top of each Figure. See Table 1 for the test conditions. These parabolas are also identified in Figures 1 and 2. These figures are grouped by net power input to the fluid:

- Figure 4 (Parabola 3) is for 29 W
- Figures 5, 6, 7, and 8 (Parabolas 35, 43, 56, and 64) are for about 16 W
- Figures 9, 10, and 11 (Parabolas 16, 19, and 27) are for about 25 W

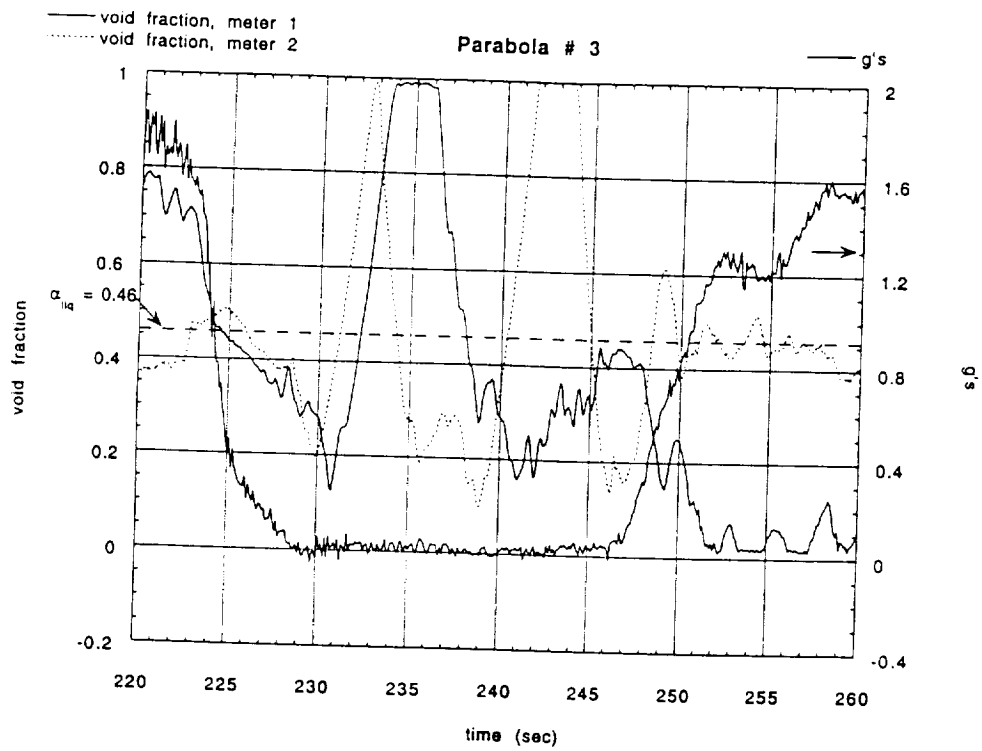


Figure 4. Transient Void Fractions for Parabola 3 (29 W)

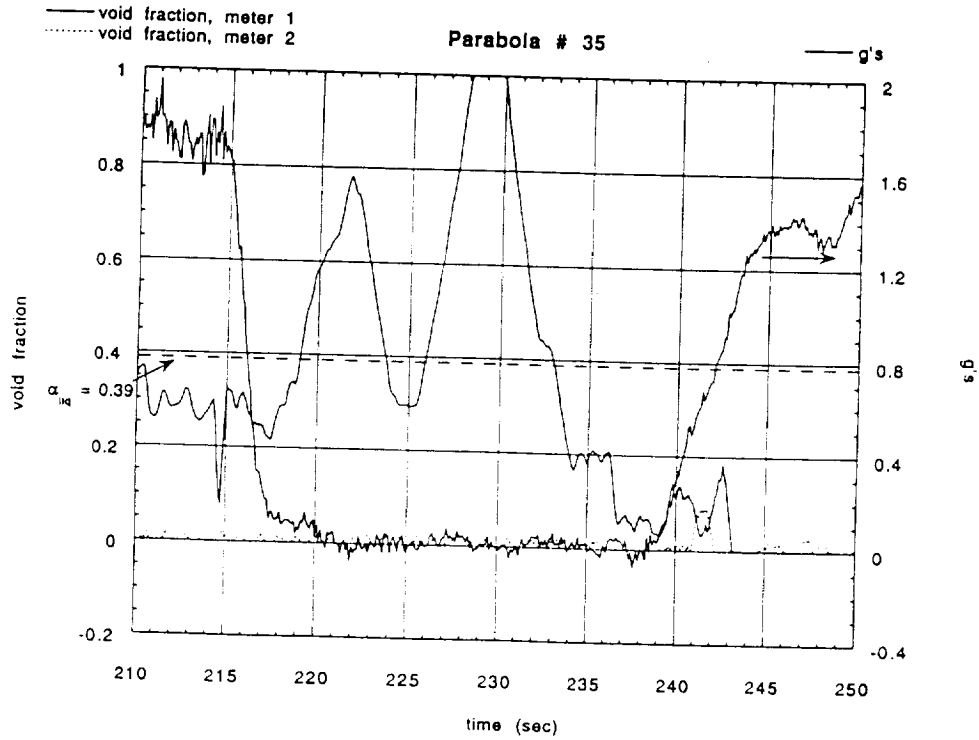


Figure 5. Transient Void Fractions for Parabola 35 (16 W)

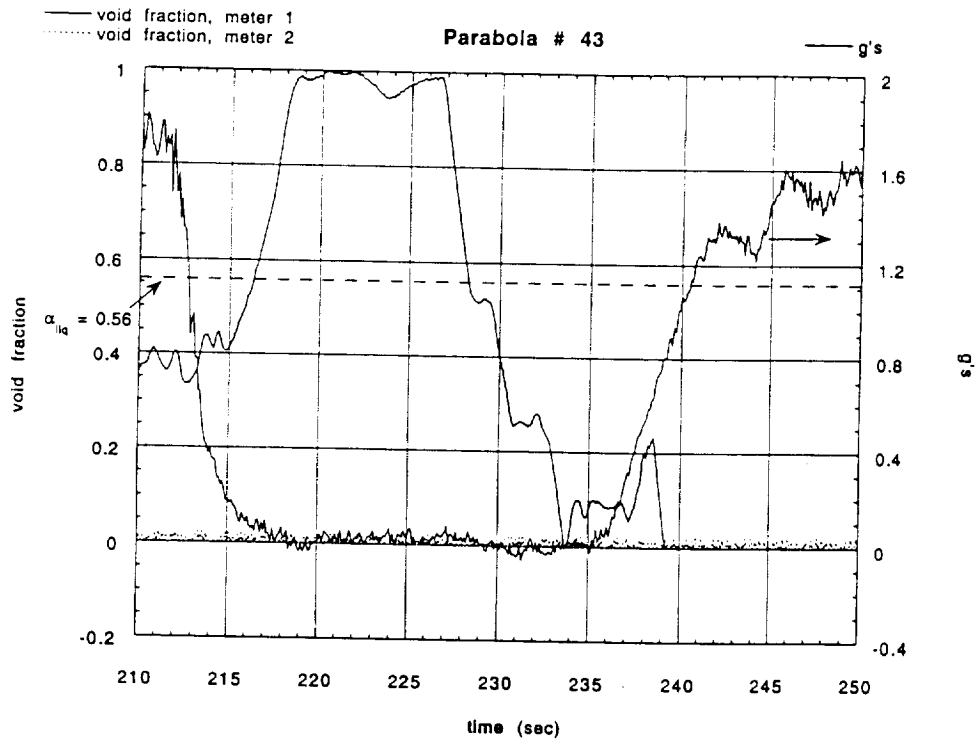


Figure 6. Transient Void Fractions for Parabola 43 (16 W)

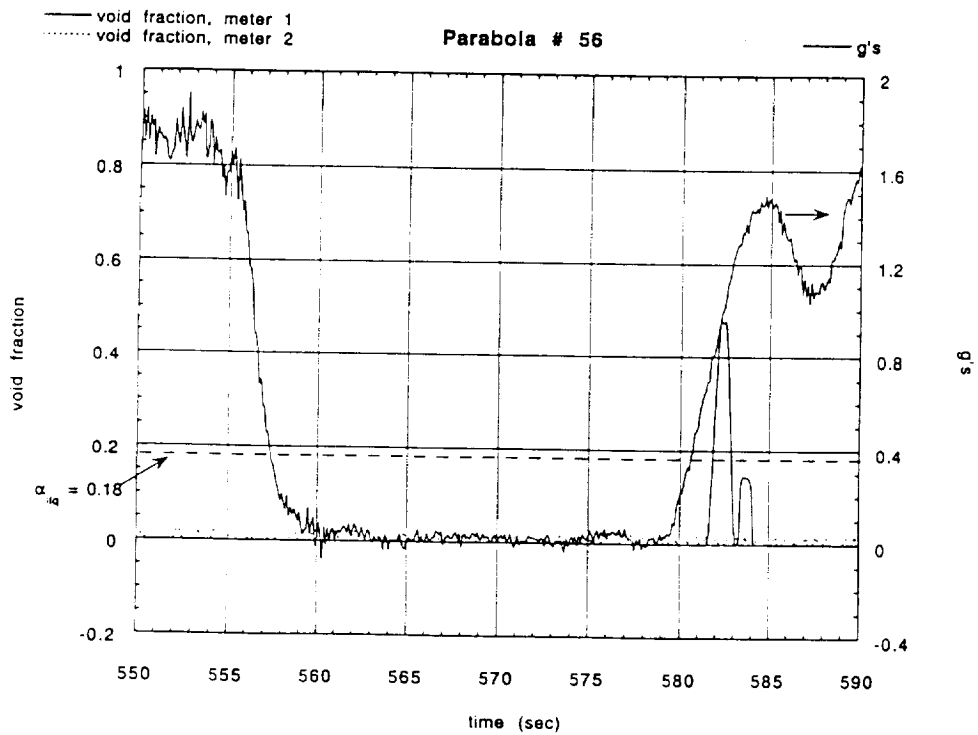


Figure 7. Transient Void Fractions for Parabola 56 (16 W)

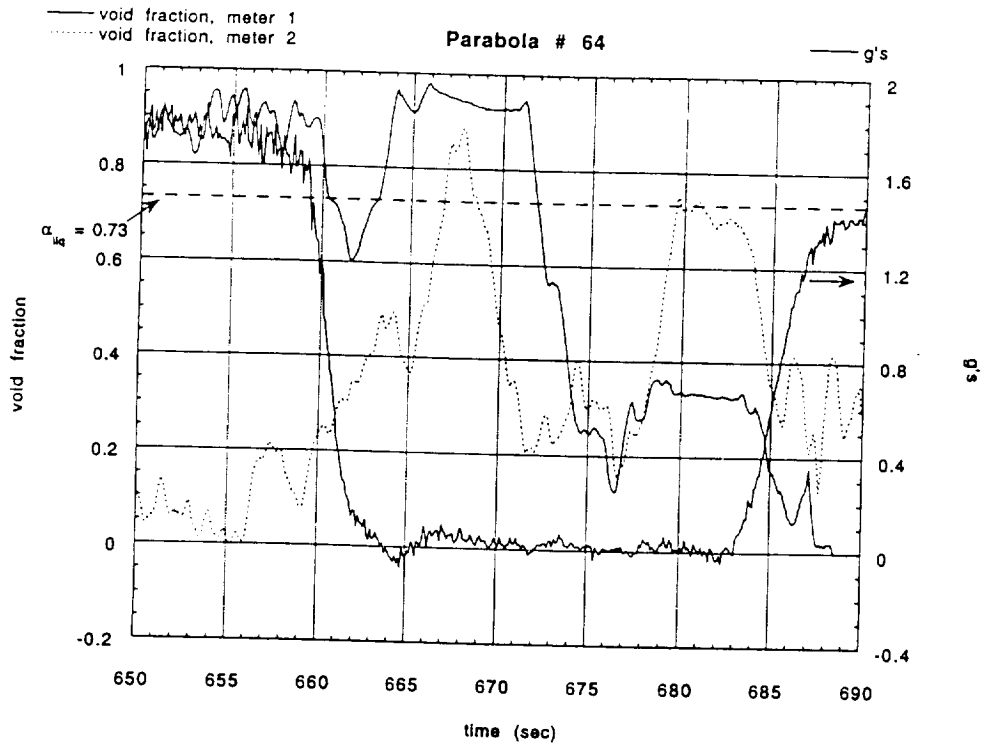


Figure 8. Transient Void Fractions for Parabola 64 (16 W)

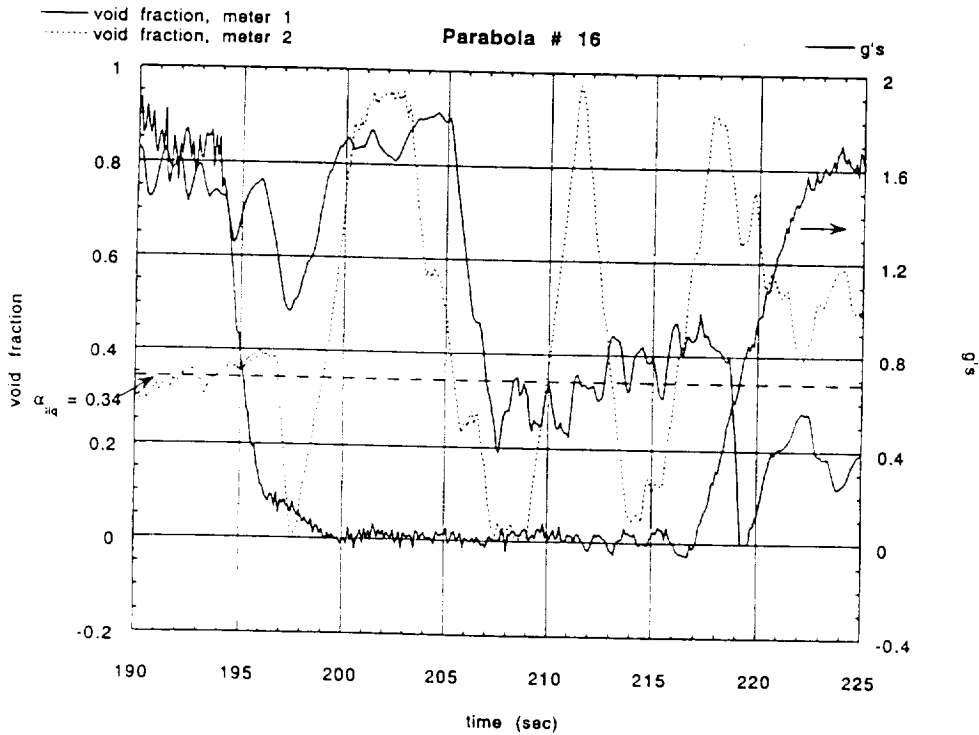


Figure 9. Transient Void Fractions for Parabola 16 (25 W)

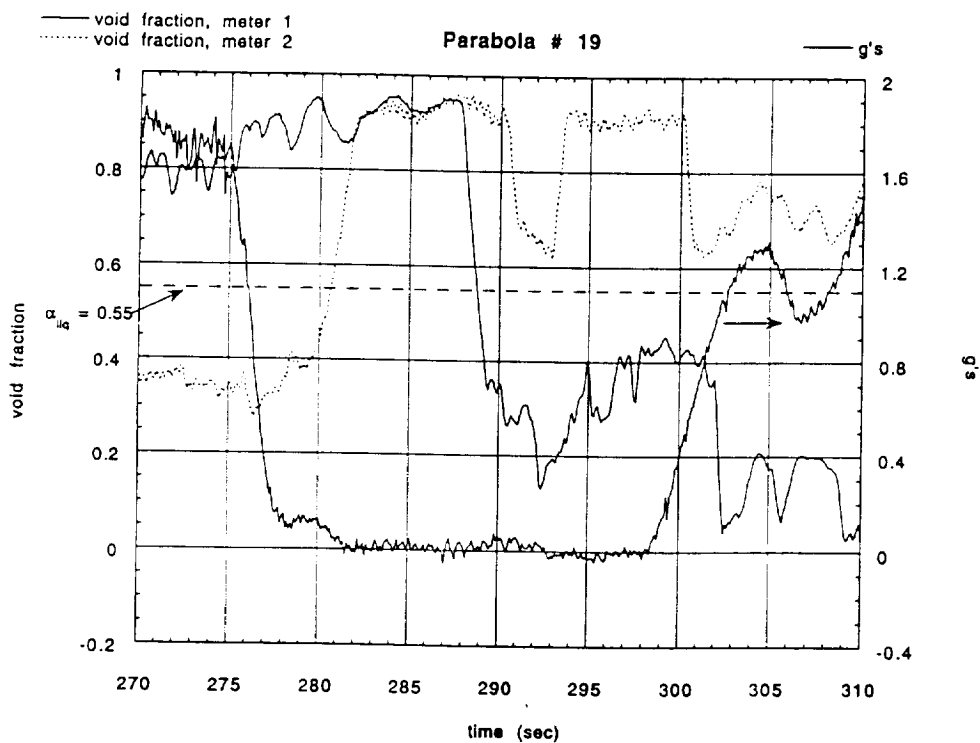


Figure 10. Transient Void Fractions for Parabola 19 (25 W)

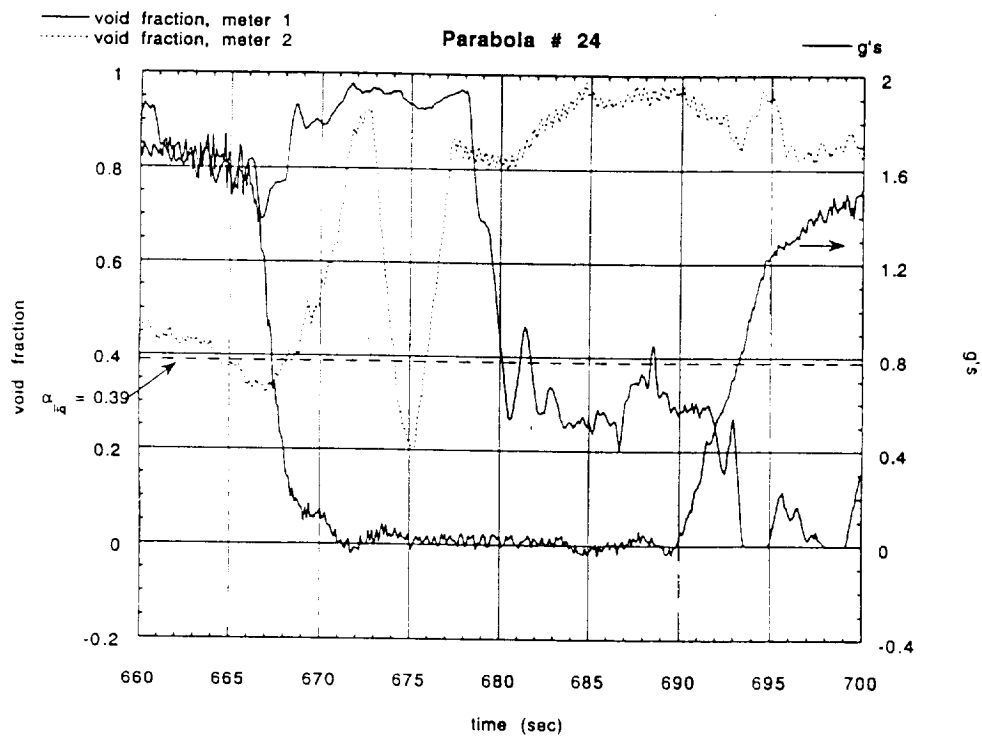


Figure 11. Transient Void Fractions for Parabola 24 (25 W)

In every case (Figures 4 through 11), there is a large difference in the void fraction between the upstream and downstream meters at the start of the transition to low-g. (The left-hand side of each plot is at about 1.8-g. Typically, the difference is about 40%, but is as high as 60%. For Parabolas 3, 64, 16, 19 and 24 (Figures 4, 8, 9, 10 and, 11), the void fraction at the upstream meter is around 80%. A heat input of 25 W corresponds to about a 40% void fraction in horizontal, stratified flow at 2-g. We therefore cannot explain from the power input how the void fraction at the upstream end of the test section could be greater than 40% in these parabolas. Other parabolas, such as Parabolas 35 and 43 (Figures 5 and 6), have a void fraction of about 40% at the upstream meter. This could be consistent with the heat input. In all cases, there is about a 40% change in void fraction across the test section. This corresponds to a loss of all the input power to the evaporator, about 25 W. Other mechanisms that could account for a gradient or a change in void fraction across the test section are: inclination of the test section or transverse acceleration. The important point for the purposes of our discussion here is that the low-g period consistently starts with a very large lengthwise distribution of the void fraction in the test section, and often with an impossibly large void fraction at the upstream end.

Now look at the period when the acceleration drops to near zero. In most cases, all but Parabola 56 (Figure 7), the void fraction seen by the upstream meter increases sharply for about the first ten seconds—the first half of the low-gravity period. This is consistent with our visual observation of vapor bubbles preferentially forming at the upstream end of the test section at the start of the low-gravity period. During the first half of the low-gravity period, Meter 2 tends to indicate an increase in the void fraction in some cases such as Parabolas 3, 64, 16, 19, and 24 (Figures 4, 8, 9, 10 and 11), while it shows only liquid in others (Figures 5, 6, and 7). That is, the results are highly variable from one test to the next. Note that this breakdown exactly corresponds to the tests with very high upstream void fraction and more reasonable upstream void fraction, respectively.

During the second half of the low-gravity period, the void fraction in Meter 1 decreases to a much lower value, about 10% to 40%. It is as if the vapor bubbles forming preferentially in the upstream end of the test section have migrated out into the test section. During this same time period, Meter 2 exhibits widely varying behavior—as we might expect, based upon the averages in Figure 2:

- In some tests, the void fraction at Meter 2 fluctuates widely (Figures 4, 8, and 9)
- In some tests the void fraction at Meter 2 goes to a large value (Figures 10 and 11)
- In some tests the void fraction at Meter 2 stays near zero (Figures 5, 6, and 7)

Since Figures 5, 6, 7, and 8 are for parabolas at nearly the same power input, and so are Figures 9, 10, and 11, it is evident that results can vary widely for similar test conditions.

We looked at the video records from the digital imager to estimate the observed void fractions from these visual data. The visual images are from a region 14 inches to 15 inches along the test section, which is very near to the downstream end. Table 2 summarizes the data obtained from the imager tapes. We looked at the velocities of bubbles and slugs, as well as the approximate lengths of each during the period of the video records, which was usually the last half of the low-gravity period. The total of the lengths of the bubbles is divided by the total of the lengths of the bubbles plus the liquid slugs to get an approximate value of the void fraction from the visual records. We found that the video analysis confirmed the unusually large void fractions measured at Meter 2 for Parabolas 19 and 24 (Figures 10 and 11). We found some small amounts of vapor in the video analysis for Parabolas 35 and 43 (Figures 5 and 6) where the meter shows no vapor at all. There is a void fraction from the liquid level measurements, but not a good correlation between the values. There is some correlation with trapped liquid measurements for cases with fluctuating values of the void fraction, such as Parabolas 3 and 64 (Figures 4 and 8), but not for Parabola 16 (Figure 9).

## 6. CONCLUSIONS

From the detailed look at the transient behavior recorded by the void fraction meters, we see that the test section begins the low-g period with a large gradient of about 40% void fraction between the upstream and downstream ends of the test section. Moreover, the initial void fraction at the upstream end of the test section is larger than can be accounted for by the heat input. This indicates that there is a significant and uneven distribution of the void fraction entering the low-gravity period. The subsequent behavior at the downstream end of the test section seems to be correlated in some way to this starting condition.

There are a couple of tests (see Parabola 3, Figure 5, for example) when the upstream and downstream conditions tend to converge to similar behavior during the low-g period. Although large fluctuations due to slug flows are evident, the time-averaged void fractions from both meters agree with the liquid level in these tests when the behaviors look similar upstream and downstream.

In other tests, the behavior in the upstream and downstream meters diverges. The behavior in the upstream meter tends to show an early period of large void fraction followed by a dramatic decline in the void fraction to a much lower level. The downstream meter sometimes sees no vapor at all, or else it sees a large vapor fraction that appears to correspond with transport of the large void region from the upstream meter to the downstream meter. Thus, a region of high void fraction (large amount of vapor) appears to travel from the upstream end of the test section to the downstream end of the test section during the low-g period. When this occurs, the void fraction from the trapped volume may be higher than steady-state consideration would permit, if the region of high void fraction is still in transit through the test section at the time that the fluid is trapped in the test section. The downstream void fraction meter tends to read either a

**Table 2. Low-Gravity Test Results from Video Images  
(Day 4, January 27, 1996)**

Parabola	Net Power (W)	Void Fraction from Trapped Liquid (-)	Length of Vapor Bubbles (in.)	Length of Liquid Slugs (in.)	Void Fraction from Video Images (-)	Velocity (in/s)
48	11	<0.15	No Vapor	All Liquid	0	1.1
35	16	0.39	1.25, 1, 0.75	2.8, 1.6, 3.3	0.28	1.0
43	16	0.56	0.3, 0.4, 0.6	5, 2.5, 1, >1.9	0.12	1.0
56	16	0.18	(no video)	(no video)	--	--
64	16	0.73	1.5, 10, 0.4, >8	3, 3.75, 1.8	0.70	1.4
40	17	0.50	2.2, 2.2	1, 6.5, 0.5	0.35	1.1
59	17	0.73	>13	0	(large)	--
27	18	0.76	6.3, 0.4, 3.2	1.1, 0.5	0.86	1.2
32	20	0.69	>12, 2.7	2	0.88	1.2
16	25	0.34	>2, 0.4, 0.5, 15.6	4.6, 0.75, 1.4, >0.4	0.73	2.0
19	25	0.55	>13, >3.6	1.25	0.92	1.7
24	25	0.39	>5.7	1.25	0.81	3.3
3	29	0.43	>5, 0.5, 1.5, 1, 0.5	4, 0.5, 1.5, 0.75, >1.5	0.51	2.0
11	31	0.33	1.8, 1.5, >6.2	3, 2.8, 3.2	0.51	2.0
8	35	0.47	>11.5, 5, 2.5	5, 7.5	0.59	2.5

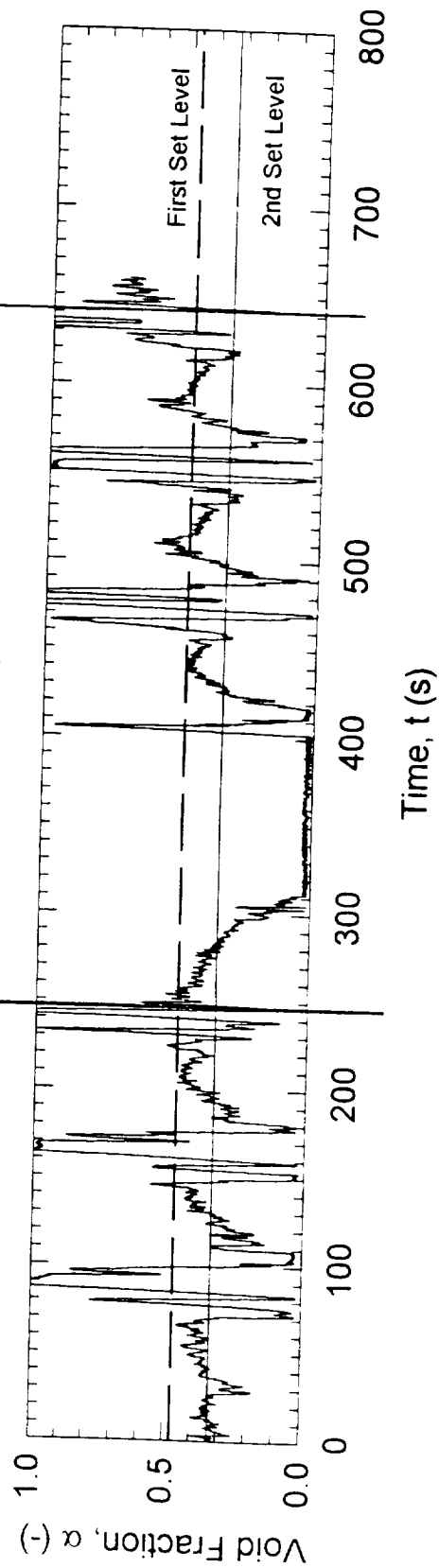
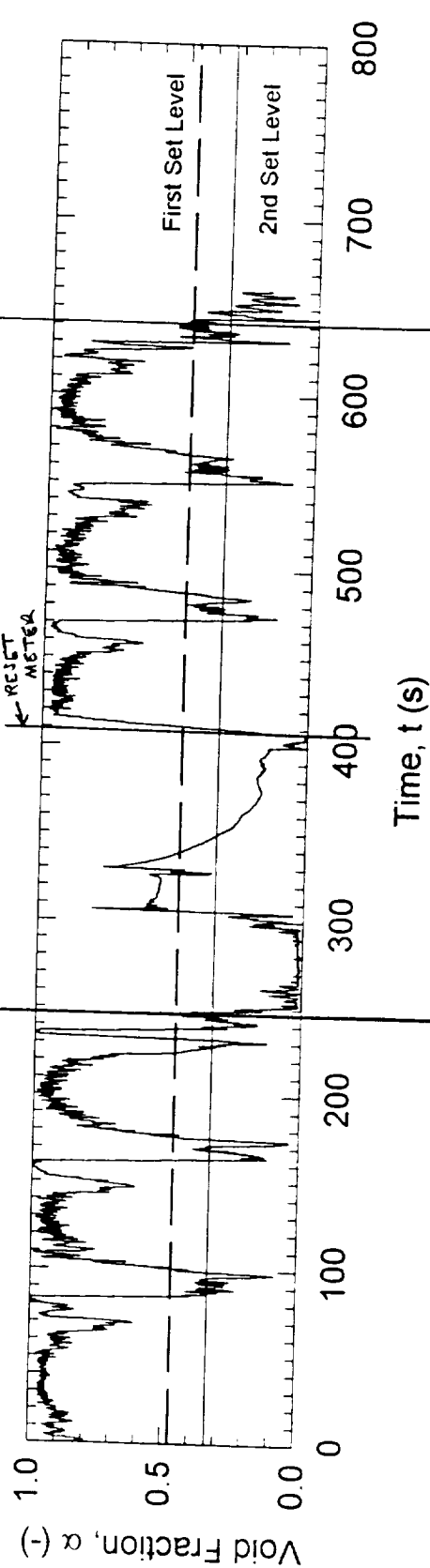
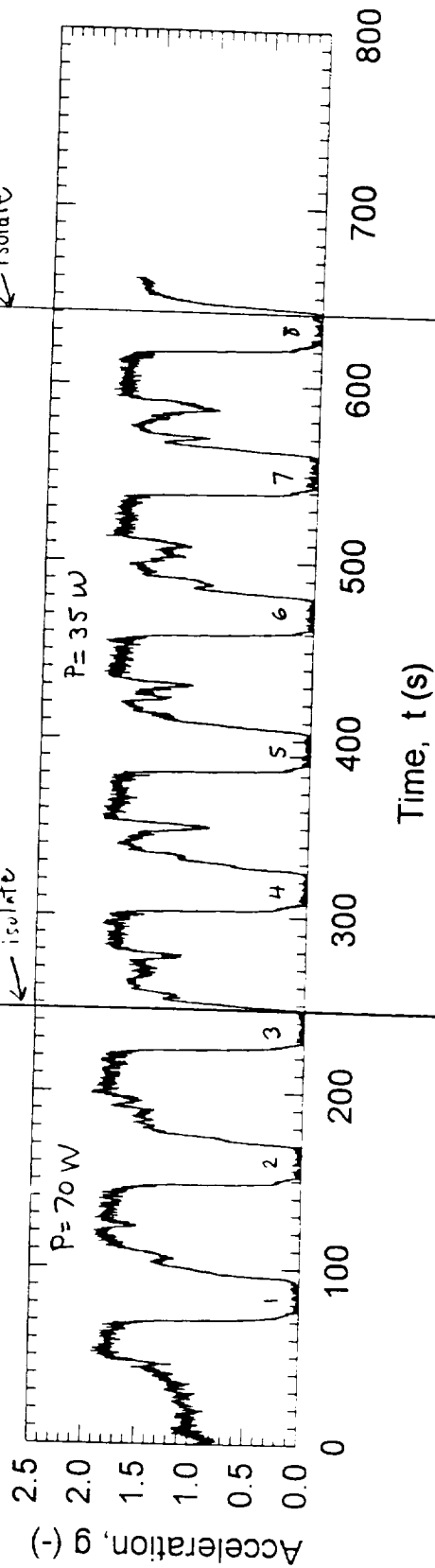
very high or very low void fraction, depending upon the progress of the high void fraction region through the test section—sometimes it reaches the meter and sometimes it doesn't. The measured behavior is consistent with video images with respect to which case occurs. With a continuous transient during the low-g period, rather than steady, uniform behavior from one end of the test section to the other, it is difficult to interpret whether the time-averaged "steady state" results are at all meaningful, even for the trapped volume.

From the video images, we can see that the velocity of bubbles and slugs of liquid is about 1 to 2 in/s. Since the test section is 16 in long, the transit time of fluid in the test section is about 16 seconds for the lower velocity and 8 seconds for the higher velocity. (The distance and transit time between the void fraction meters would be longer.) There does seem to be some correlation between those tests with higher observed velocities (Parabolas 8, 16, 24, 11, 3, and 19, at the bottom of Table 2, at higher power) and good comparisons of the average void fractions. See Figure 1, where these tests cluster in the middle group. The tests showing poorer comparisons—void fraction comparisons too high or too low—had low velocities and transit times of the same duration as the low-gravity period. Higher flow rates would reduce the transit time and could therefore lead to steadier, more uniform conditions in the test section during future tests.

## **APPENDIX A. COMPLETE DATA**

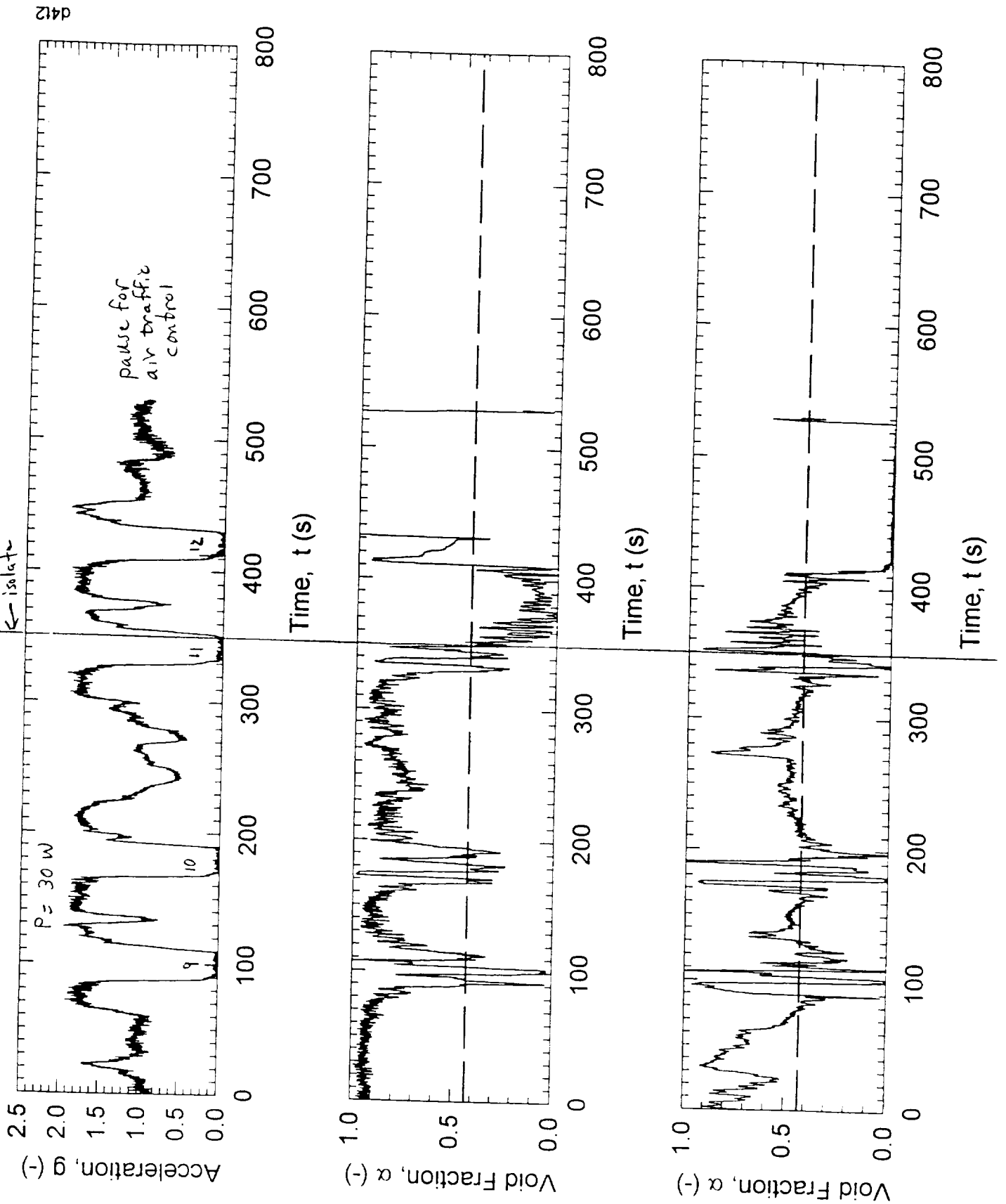
The detailed results from each group of parabolas flown on January 27, 1996 is included here. Some corrections have been made since the draft version issued in February.

# January 27, Parabolas 1 to 8

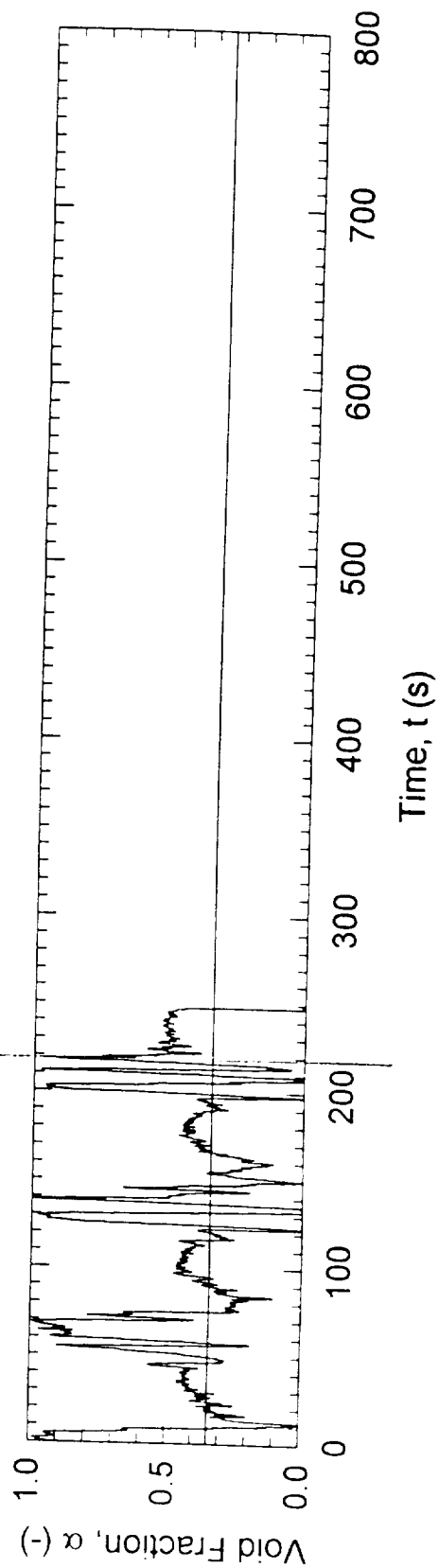
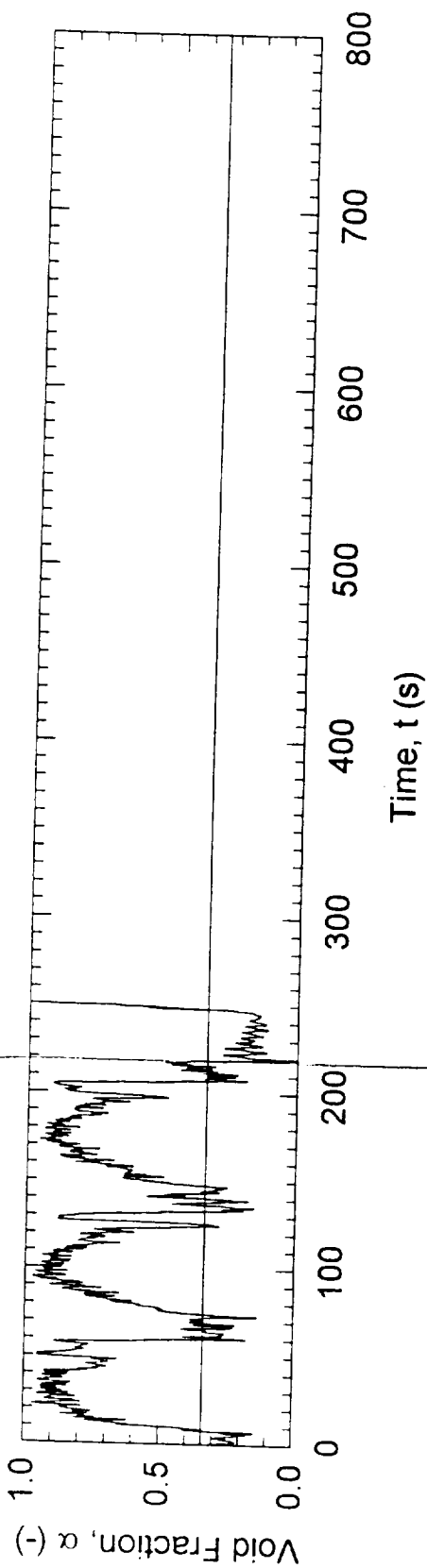
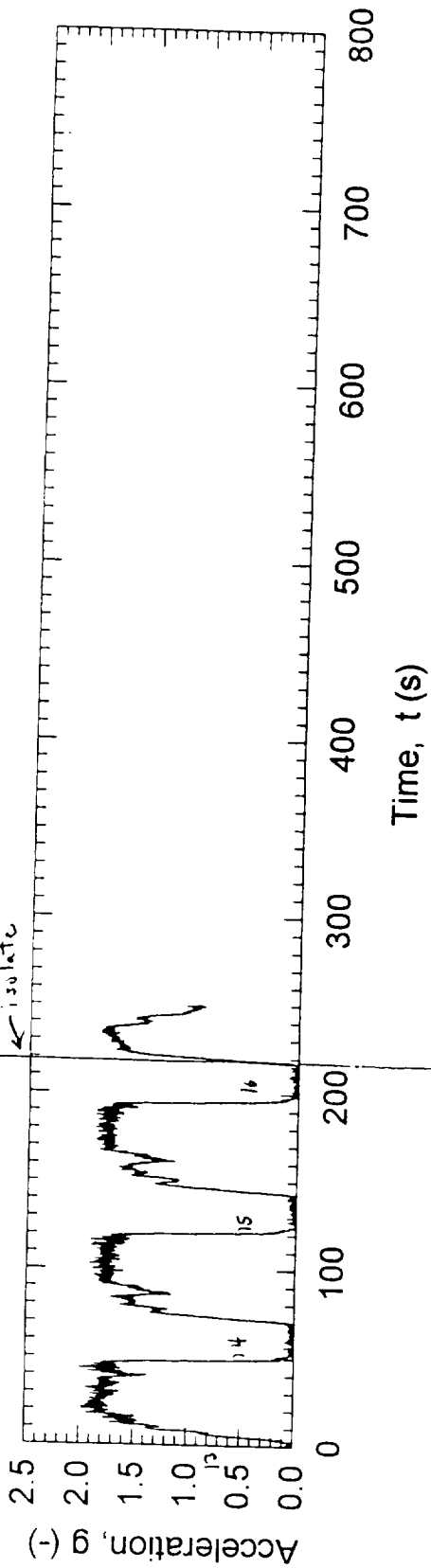


# January 27, Parabolas 9 to 12

78  
SLUG  
17-2" SLUG  
TRON LONG  
SLUG



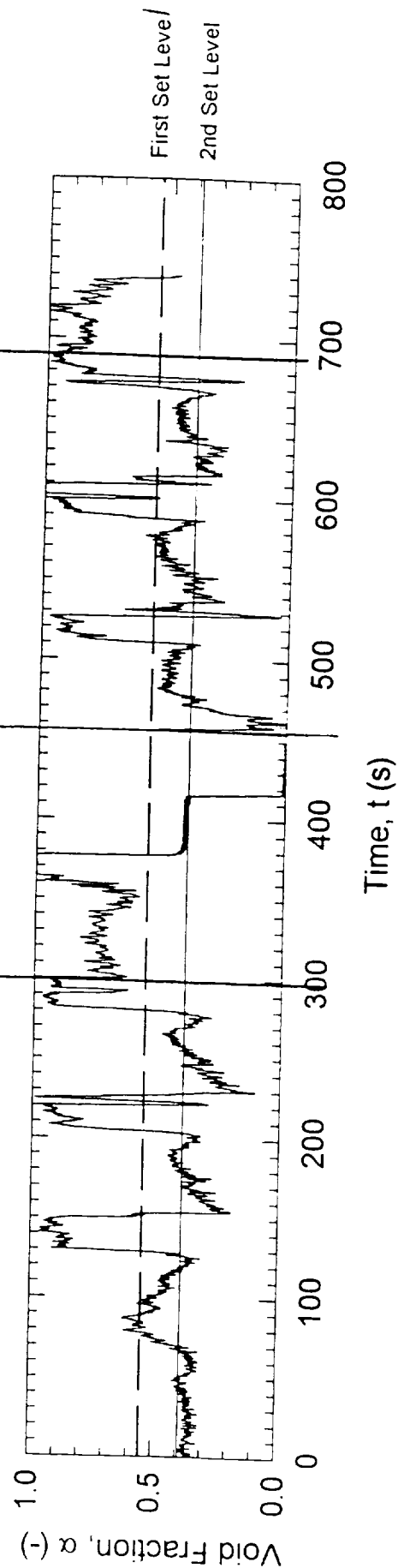
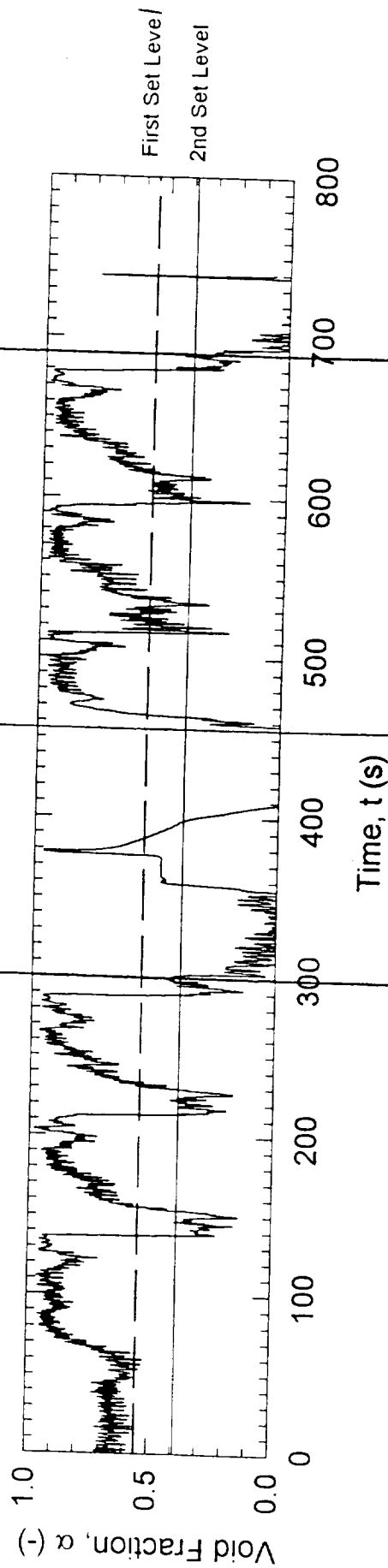
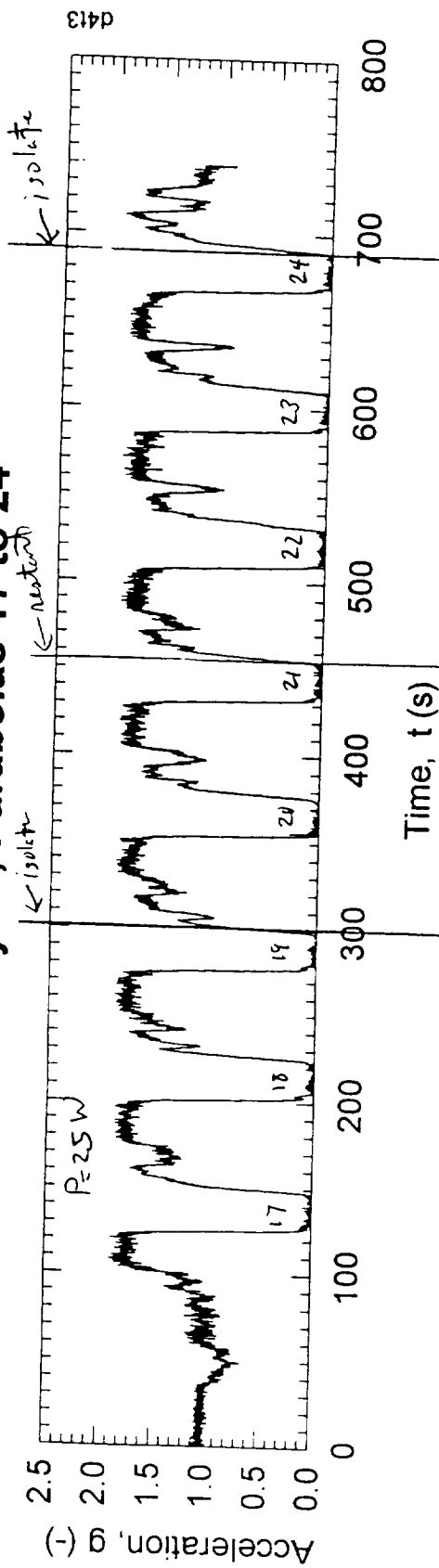
January 27, Parabolas 13 to 16



#99  
BUBBLE  
LEVE SLUG

d412a

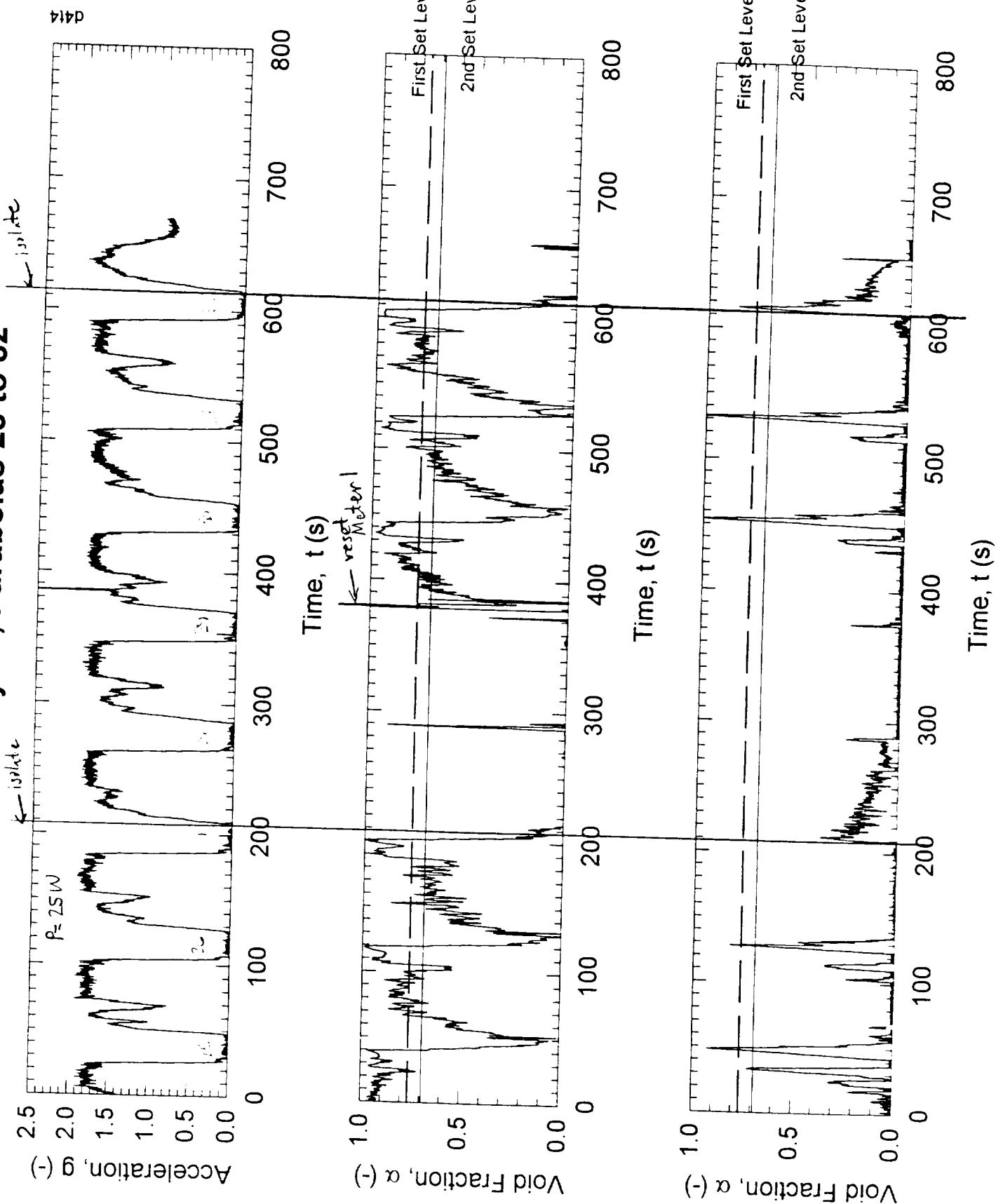
# January 27, Parabolas 17 to 24



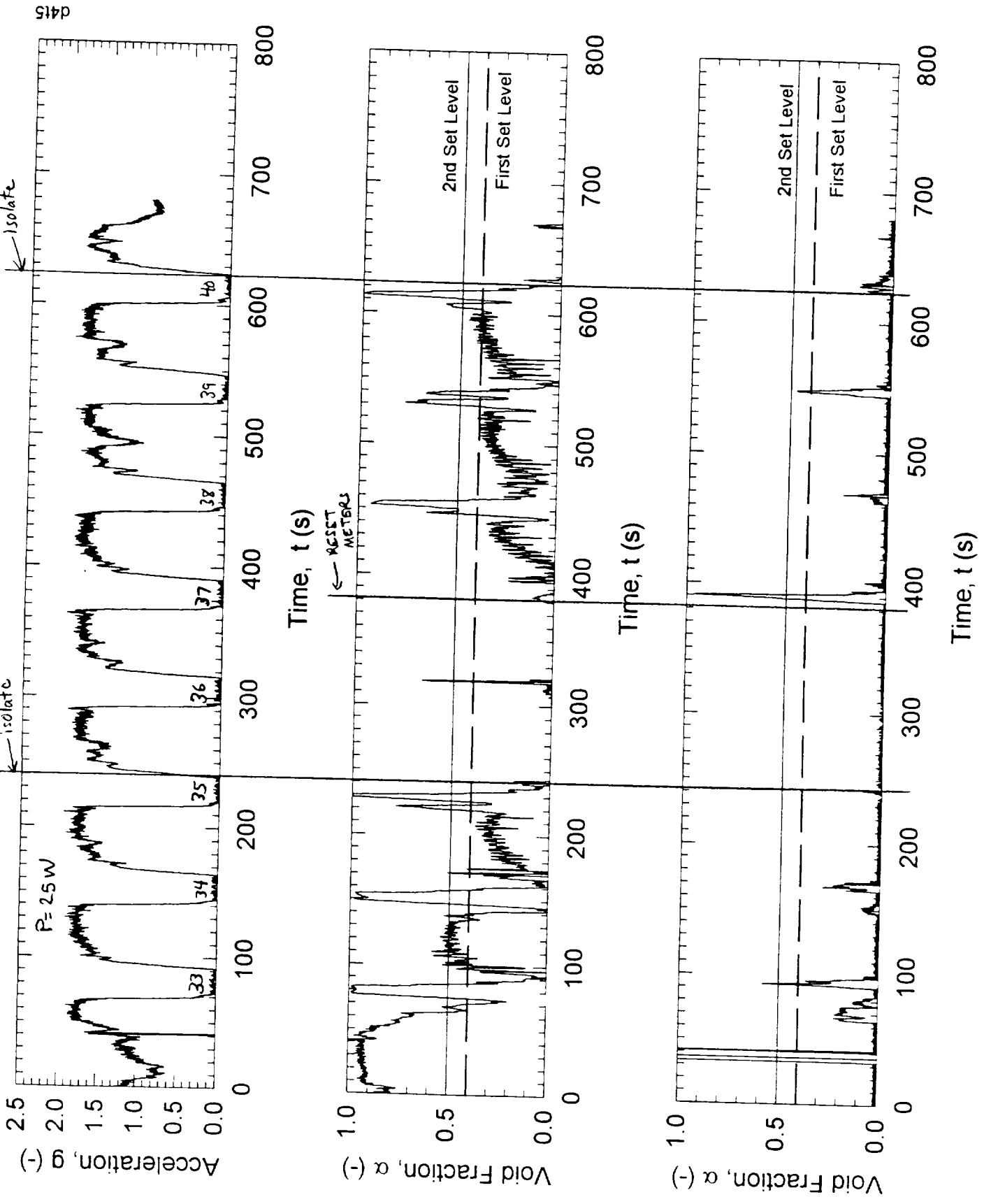
#101  
LONG  
B41336

LONG, LONG  
B41336

# January 27, Parabolas 25 to 32

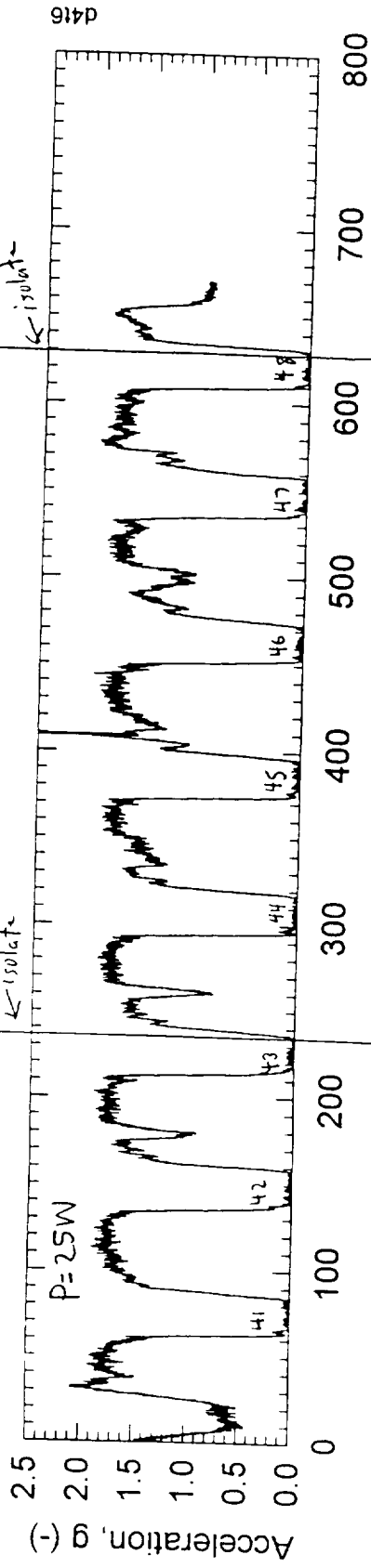


# January 27, Parabolas 33 to 40



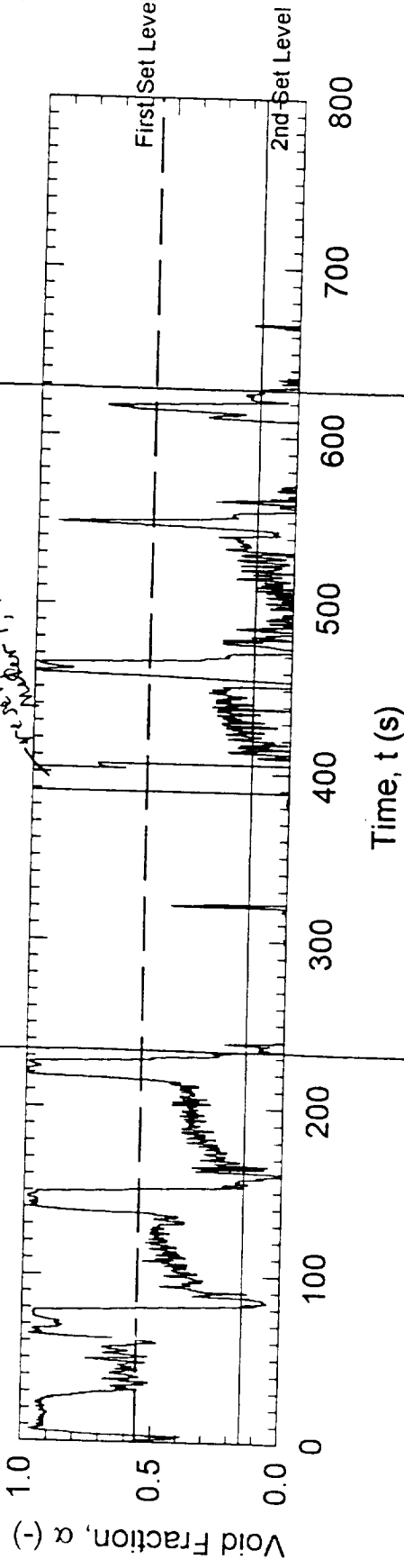
d415

# January 27, Parabolas 41 to 48

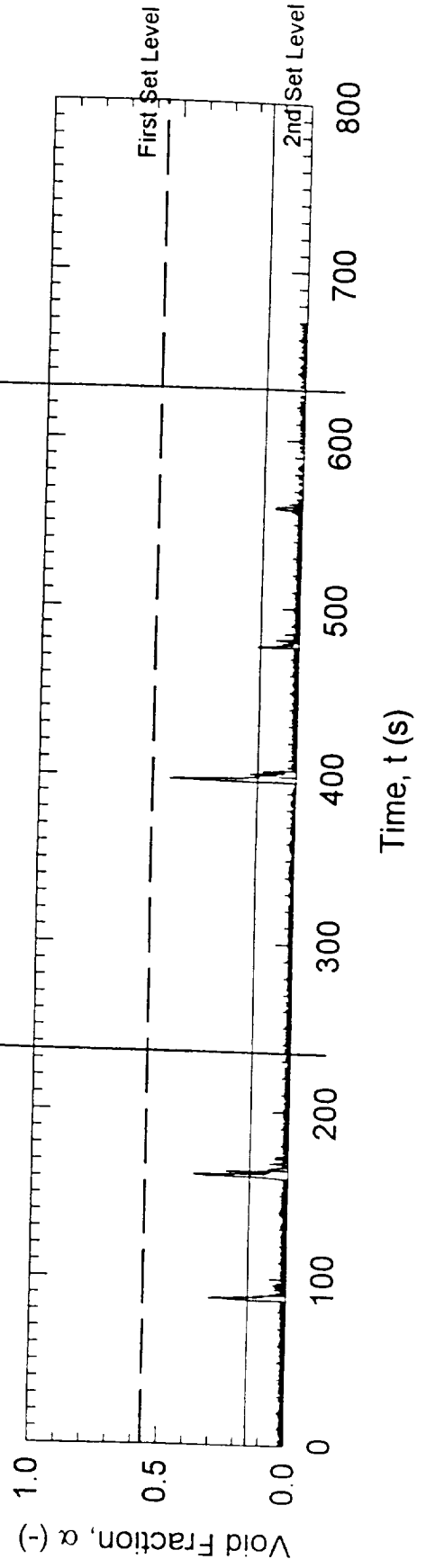


#107  
5M02-  
84B065

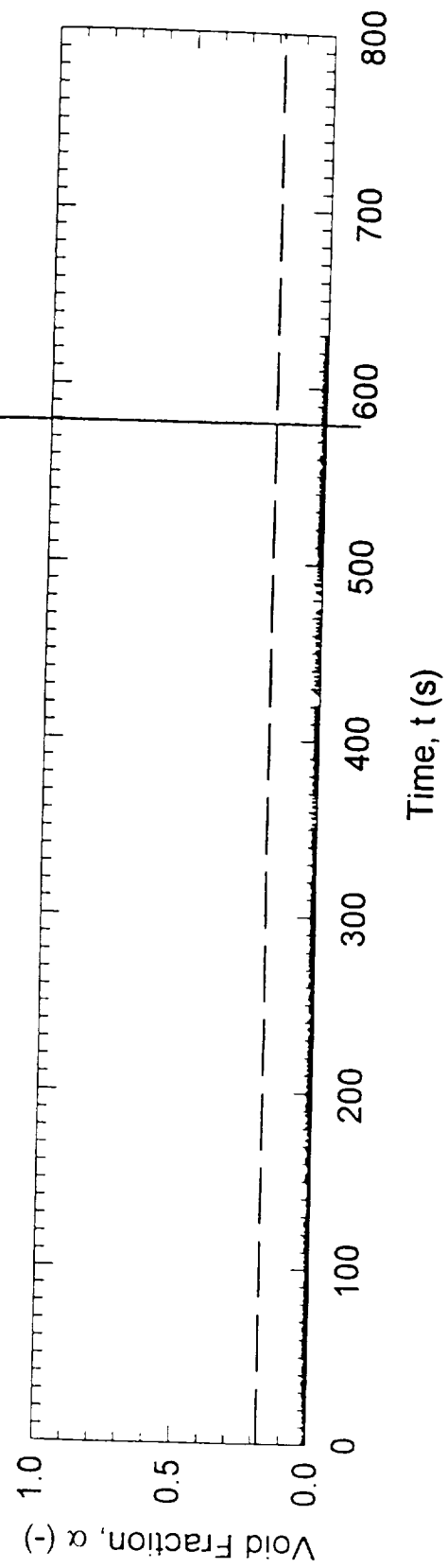
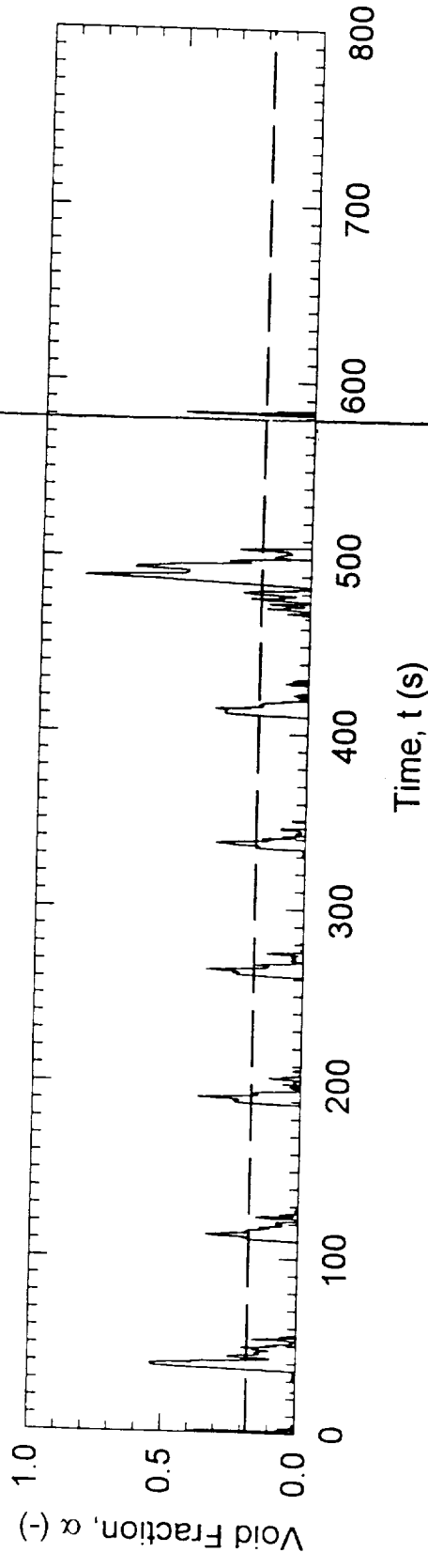
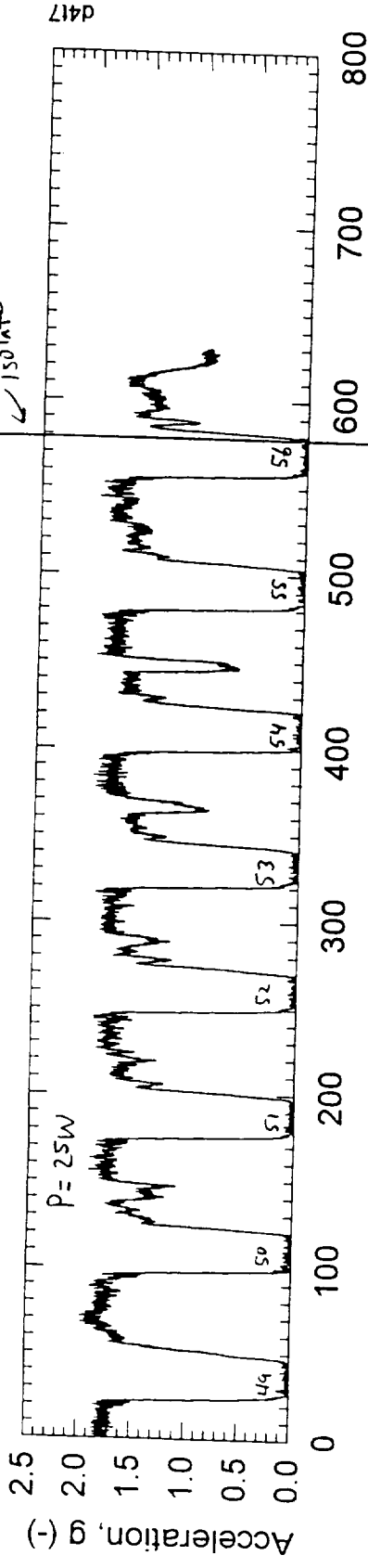
reducer; restart



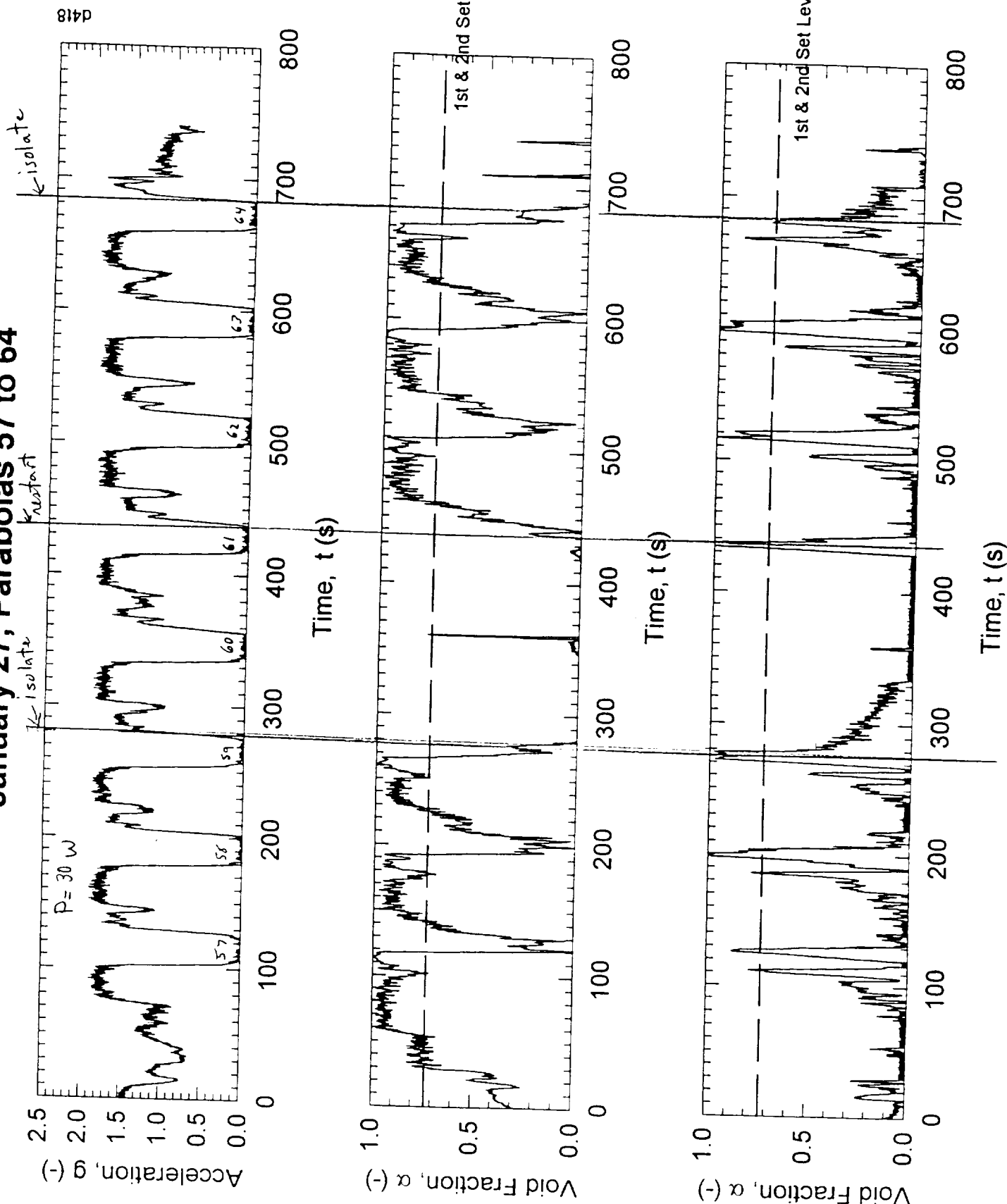
#108  
L.O. MID



# January 27, Parabolas 49 to 56



# January 27, Parabolas 57 to 64



## APPENDIX B. CALIBRATION RESULTS

We did “empty” and “full” calibrations on the ground. We recorded the first two series of parabolas—which were basically liquid-full. Results are shown in Figures B-1, B-2, and B-3. These tests basically confirm the empty and full calibrations. The values haven’t changed significantly since the July flight campaign.

One observation of possible interest: acceleration and void meter instrument signals are clearly more noisy during flight than on the ground. The accelerometer may be providing EM cross-talk to other instruments (including housekeeping?).

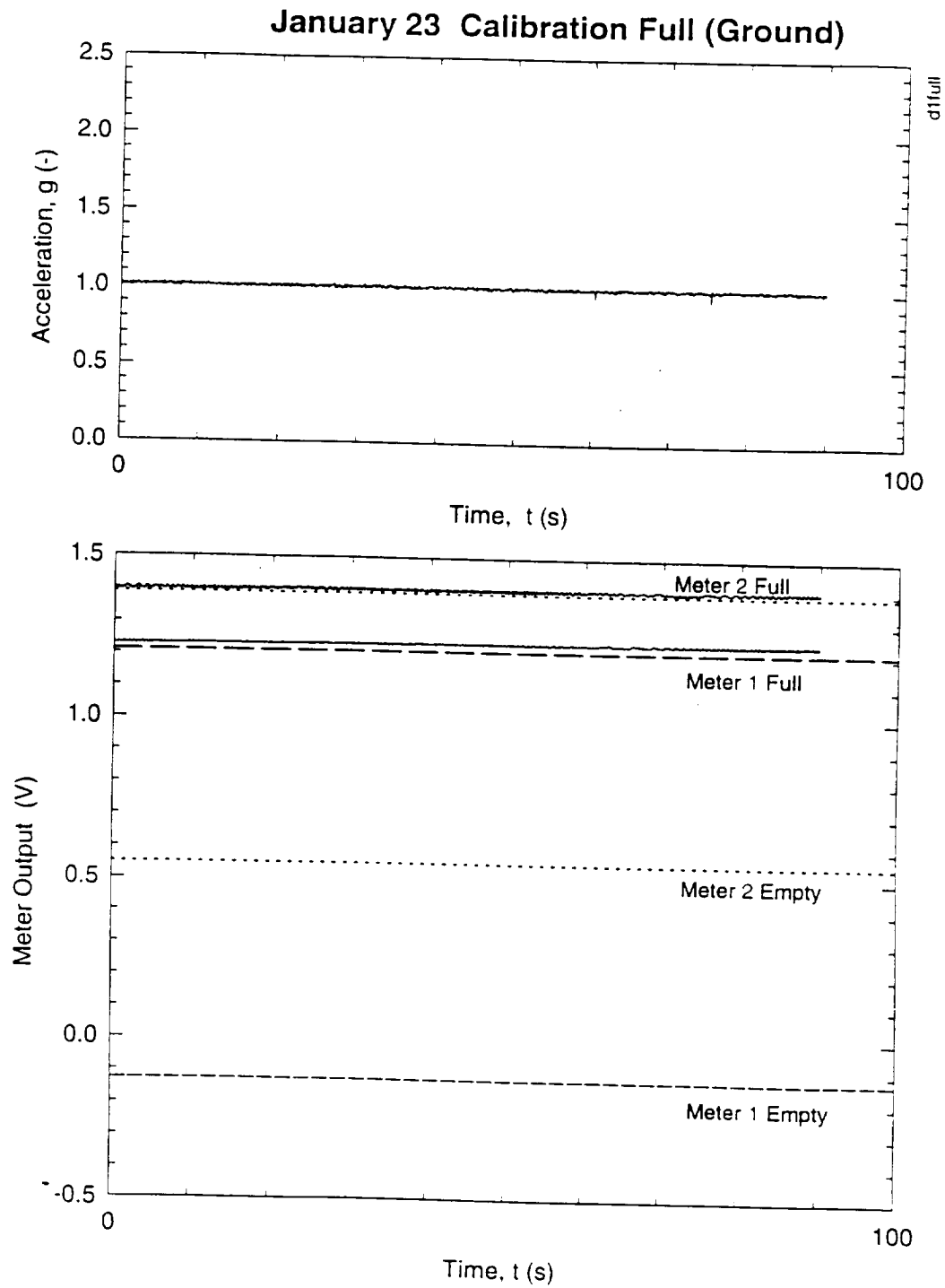


**Figure B-1. Ground Test Calibrations of "Full" Condition**

# January 23 Calibration Empty (Ground)

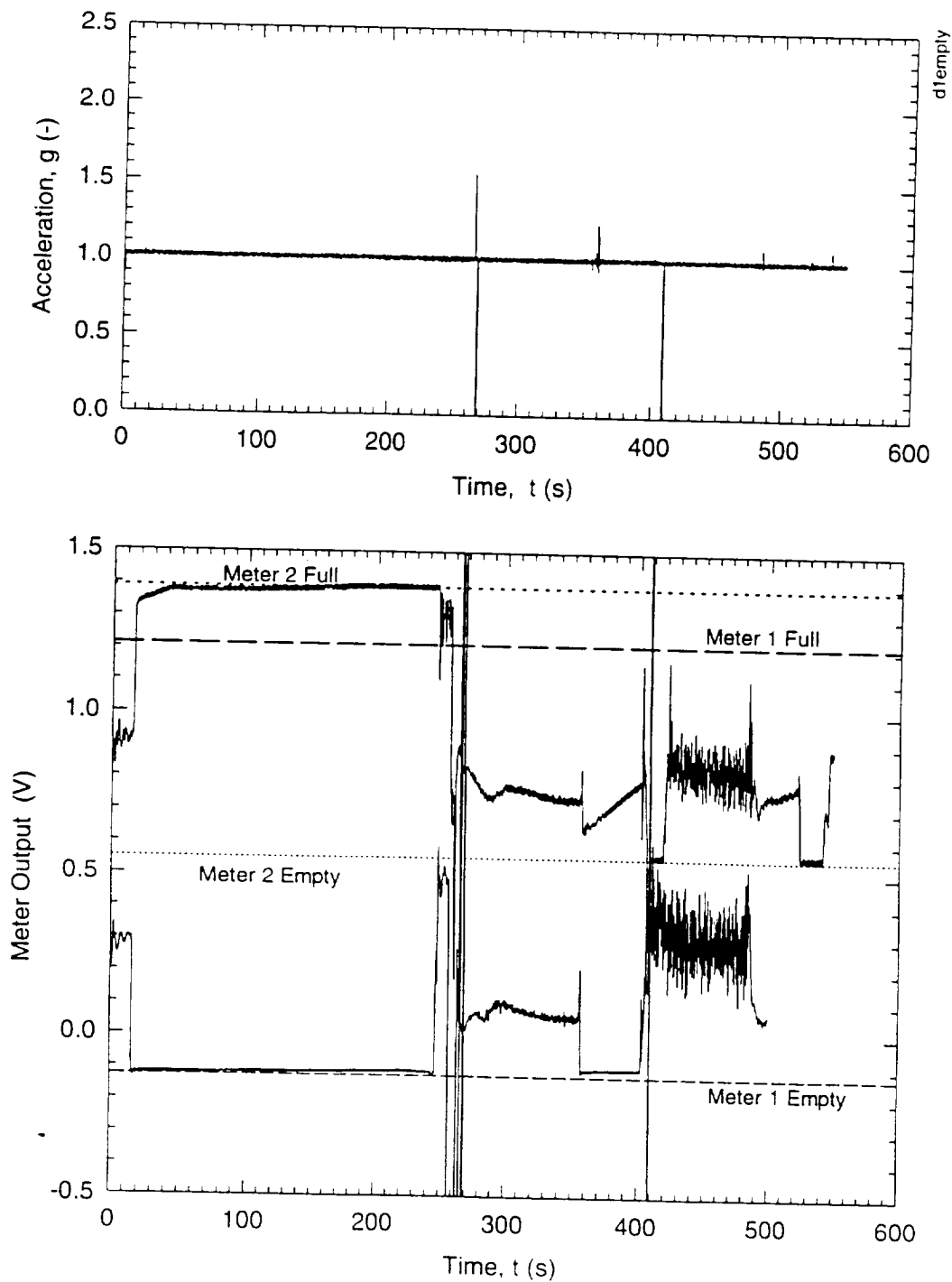


Figure B-2. Ground Test Calibrations of "Empty" Condition

January 23, Parabolas 1 to 8 (Null)

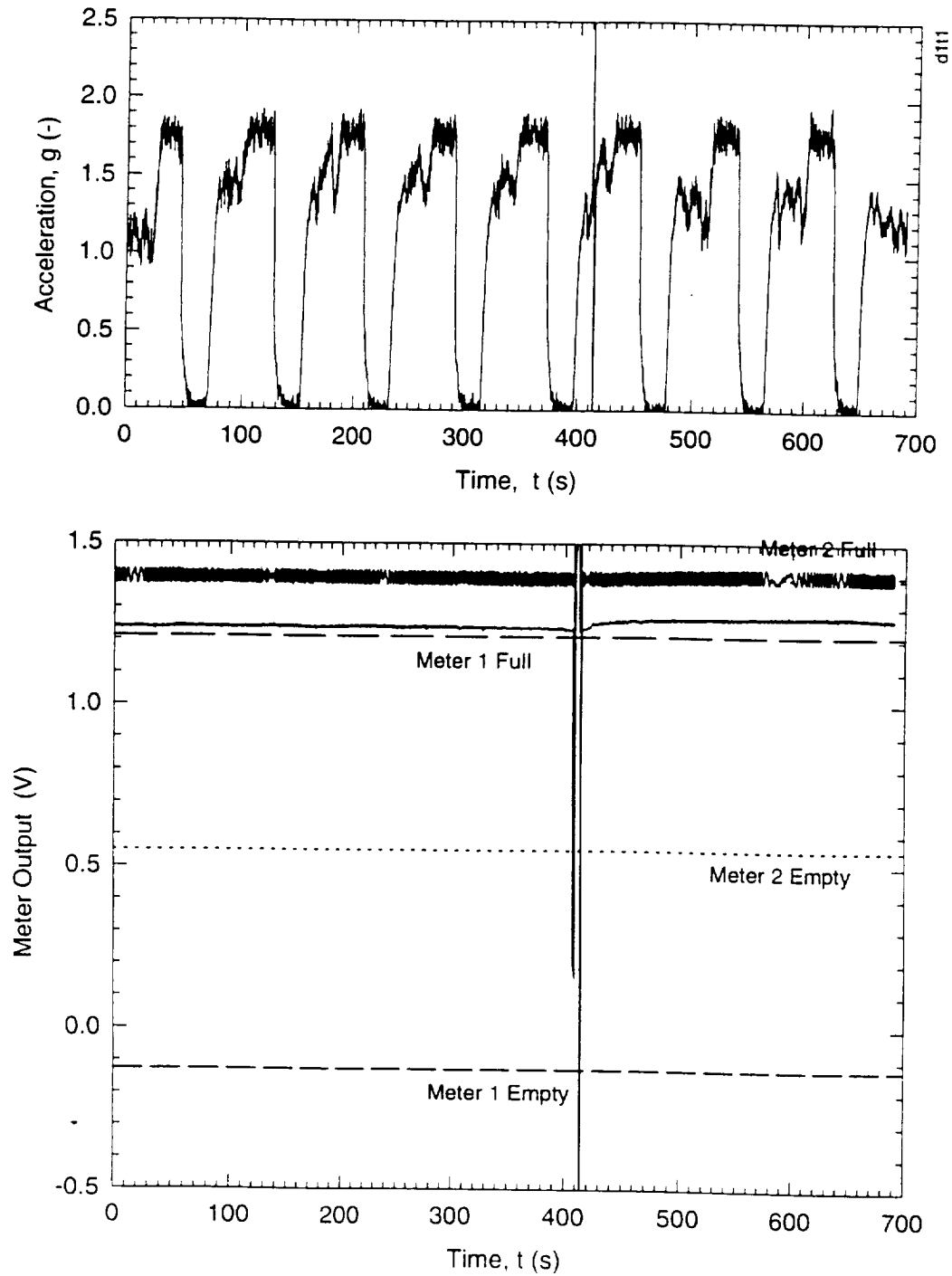


Figure B-3. Null Parabola with "Full Condition

## APPENDIX C

### Two-phase flow transit time calculation

A simple calculation was conducted to quantify the transit time of the liquid/vapor front from the exit of the evaporator to the second void fraction sensor to help understand the unusual results obtained from the flight series. During the flights, void fractions of 50% and greater were measured from the isolation of the quick acting valves for evaporator power inputs of 25 W to 35 W. Under these evaporator power conditions, the maximum void fractions should not exceed 40%. This may indicate that steady two-phase flow conditions were not achieved.

It is assumed that the vapor and liquid phases re-orient under the 2-g period to stratified flow. The transient time for the liquid/vapor front from the evaporator to the second void fraction sensor during 0-g is calculated. Transient times for two mass flow rates, 0.416 lb/min and 1.0 lb/min, were calculated. The first mass flow was the maximum flow rate obtained during the flight series. The mass flow of 1.0 lb/min is proposed for the next flight series.

Problem: Calculate velocities of liquid/vapor front for different evaporator power input.

Given: mass flow rates of 0.416 lb/min & 1.0 lb/min  
diameter = 0.010312 m

Assumptions:

1. saturated liquid entering evaporator
2. homogenous model; slip = 1
3. no losses to ambient from the evaporator
4. saturation properties of suva at 80 °F

$$\rho_f = 1199.9 \text{ kg/m}^3 \quad \rho_g = 33.97 \text{ kg/m}^3$$

$$h_f = 88.337 \text{ kJ/kg} \quad h_g = 264.88 \text{ kJ/kg}$$

mass flow rate:

$$m_1 = 0.416 \text{ lb/min} = 0.003145 \text{ kg/s}$$

$$m_2 = 1.000 \text{ lb/min} = 0.007560 \text{ kg/s}$$

Since the slip is 1, the void fraction ( $\alpha$ ) can be calculated if the quality ( $x$ ) is known:

$$\alpha = \frac{1}{1 + \frac{1-x}{x} \frac{\rho_g}{\rho_f}} \quad (\text{Eq. 1})$$

Figure 1 is a plot of quality vs. void fraction for Suva at 80 °F.

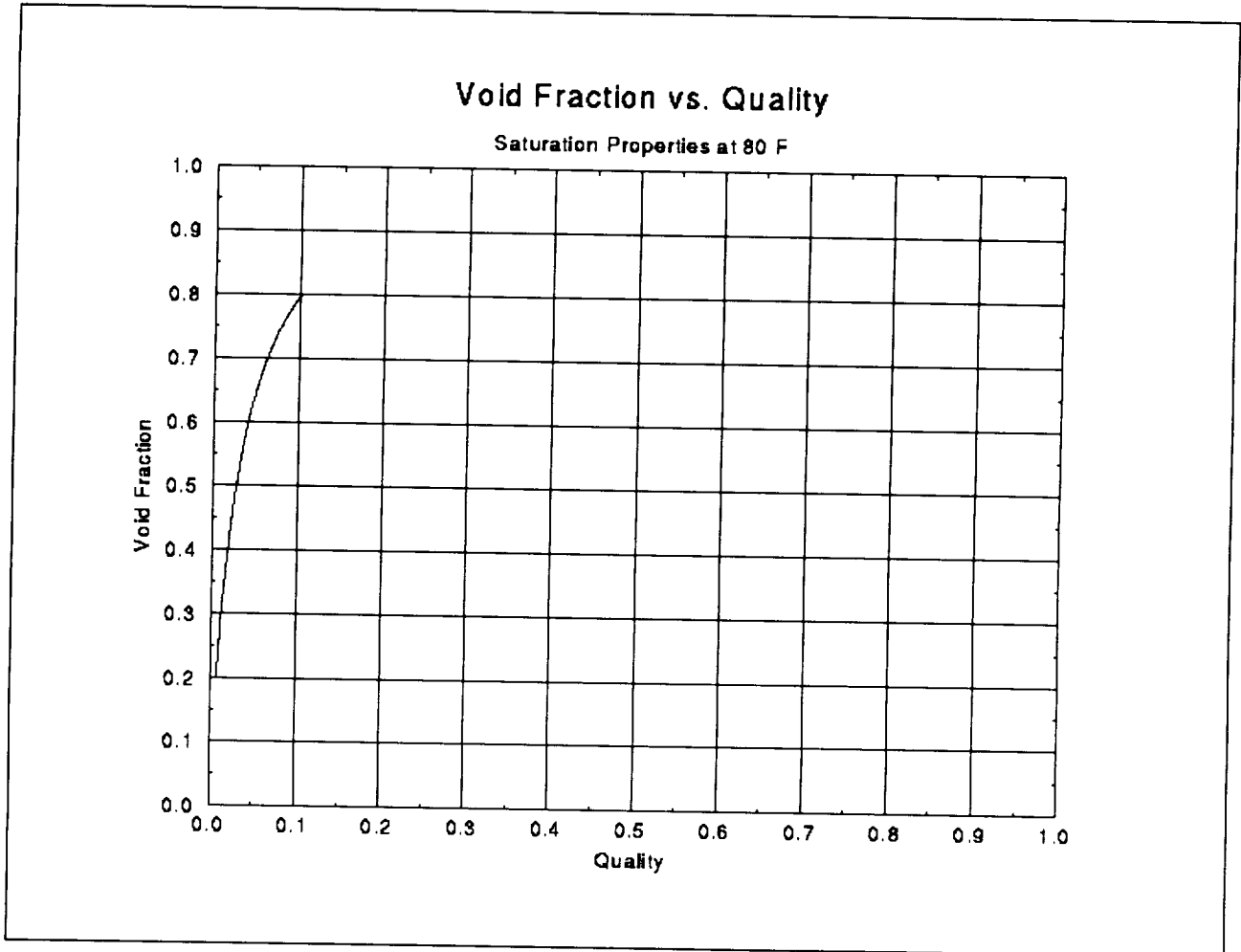


**Figure 1. Relationship between quality and void fraction for Suva @ 80 °F.**

To produce void fractions of 20% and 80% (limits of the visual test section), qualities of 0.7% and 10.2% must be produced by the system, which corresponds with evaporator power of 4 W and 56 W, respectively.

The quality of the Suva exiting the evaporator is calculated with the following equation:

$$x = \frac{\frac{Q}{\dot{m}}}{h_{fg}} \quad (\text{Eq. 2})$$

where

$Q$  - power (W)

$\dot{m}$  - mass flow rate (kg/s)

$h_{fg}$  - latent heat of vaporization (J/kg).

Figure 2 is a plot of power vs. quality.

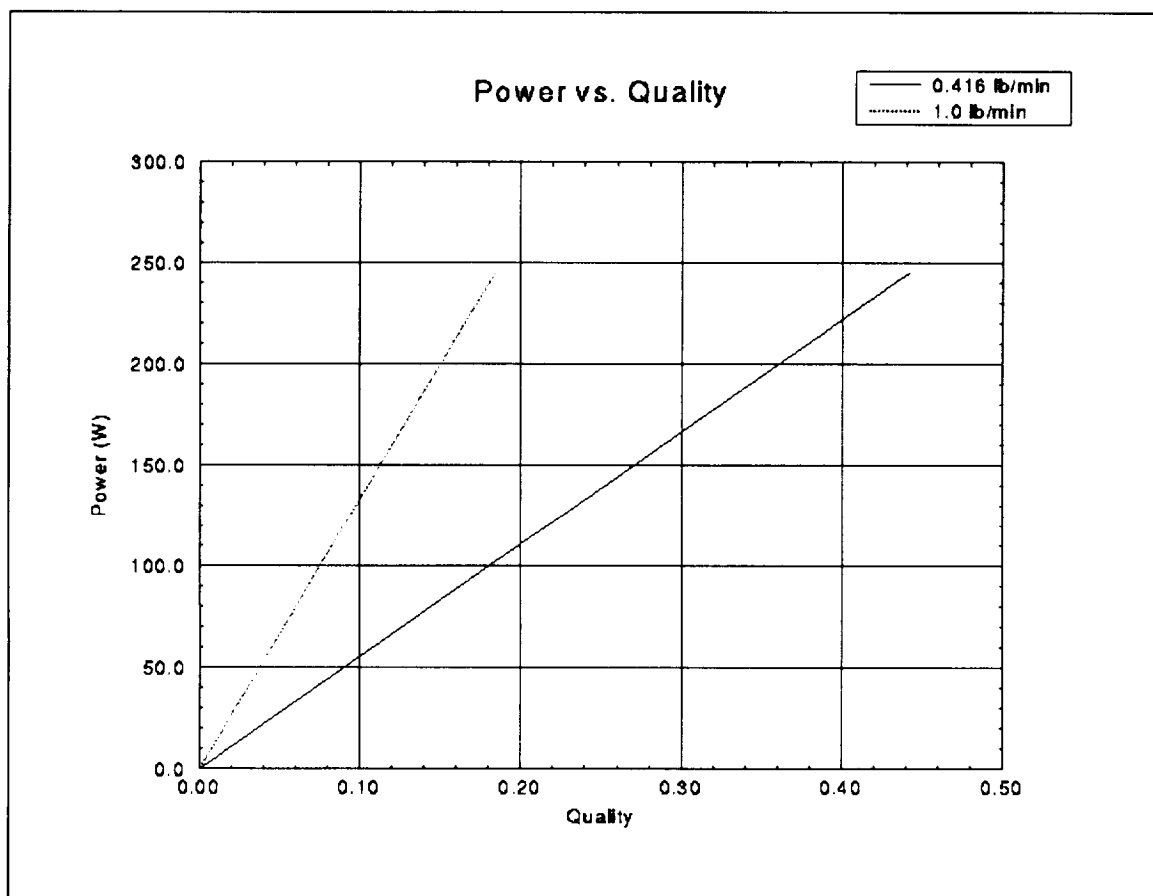


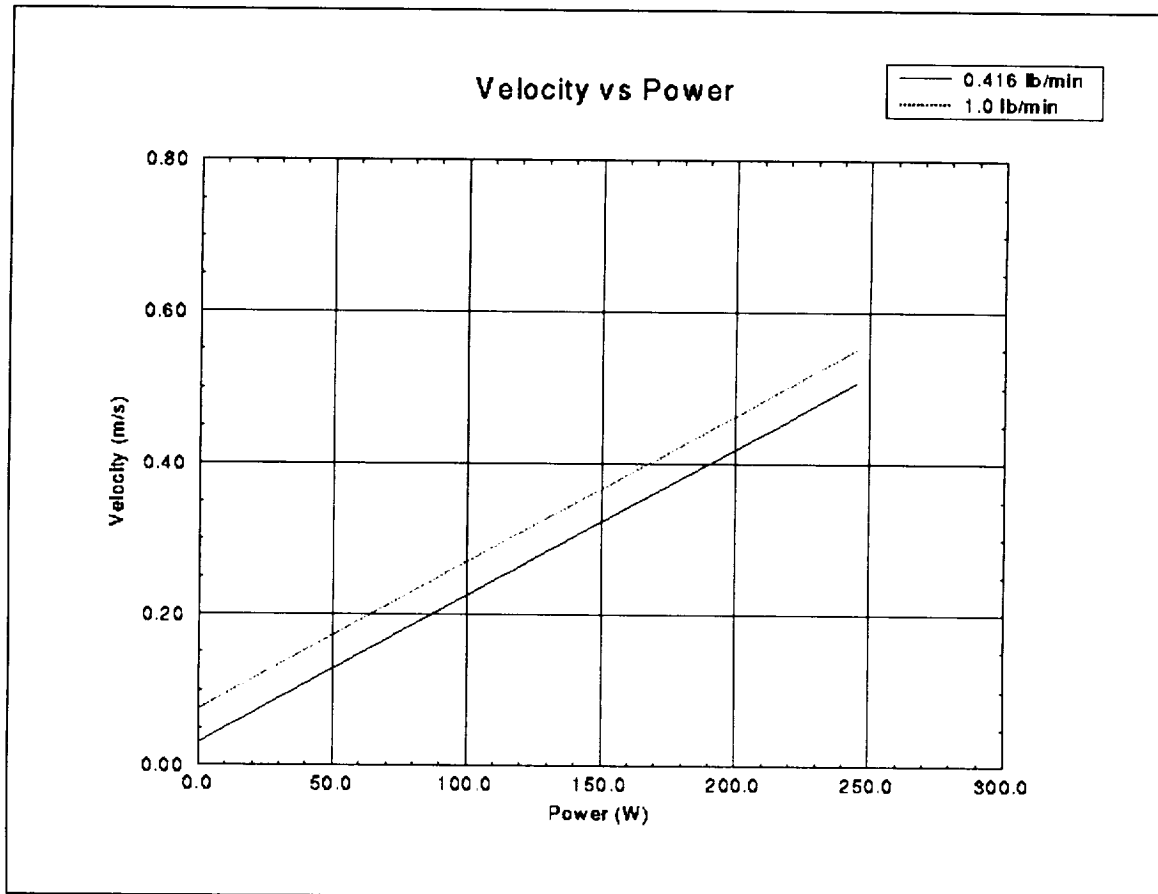
Figure 2. Power vs. quality for suva @ 80°F for 0.416 lb/min and 1.0 lb/min.

The superficial velocities are calculated using the following equation:

$$j = \frac{Gx}{\rho_g \alpha} \quad (\text{Eq. 3})$$

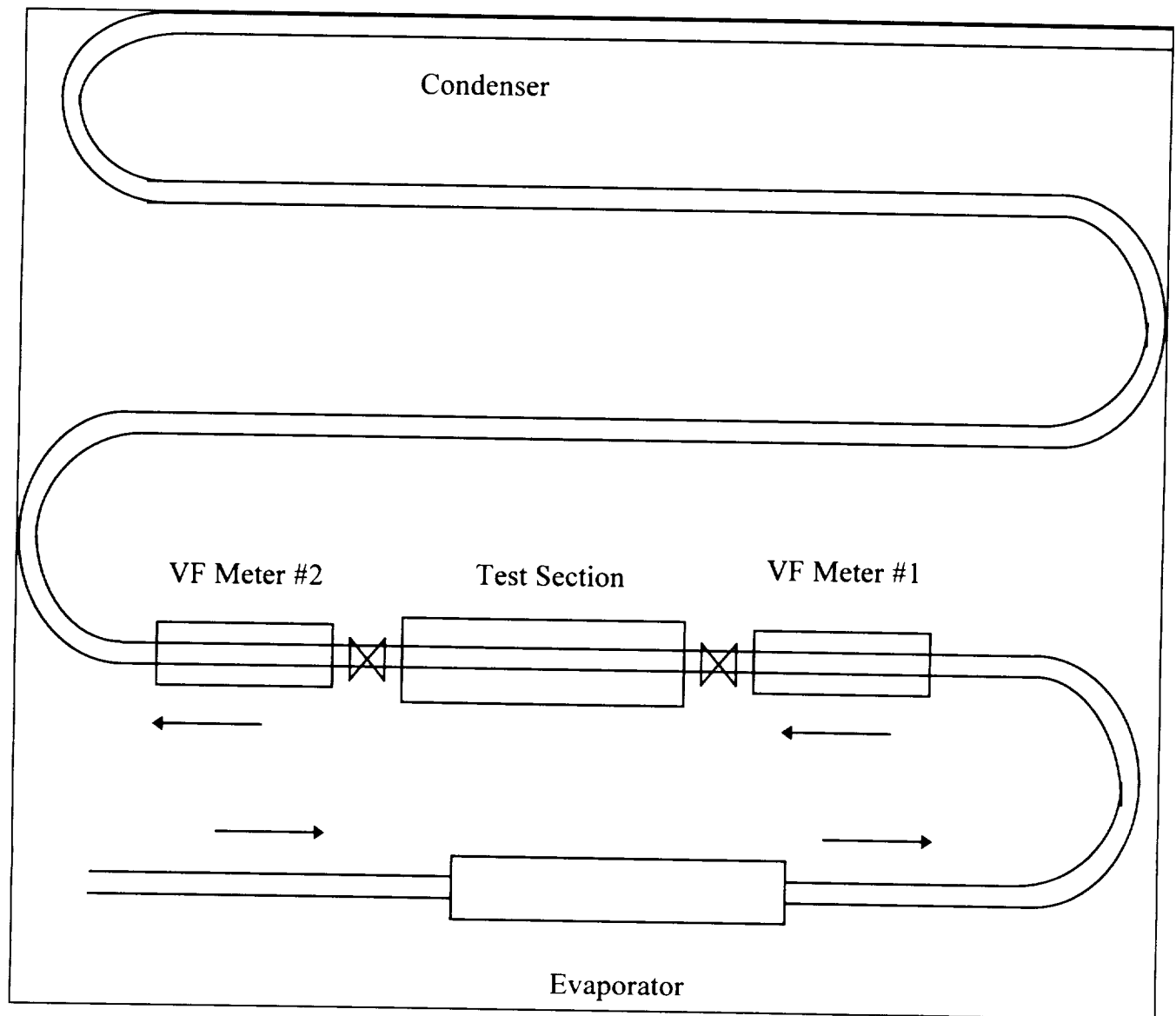
where  $G$  is the mass velocity ( $G = \frac{\dot{m}}{a}$ ) and  $a$  is the cross-sectional area.

Figure 3 is a plot of power vs superficial velocity.



**Figure 3. Superficial velocities for power inputs.**

The approximate distance between the entrance of the evaporator to the outlet of the second void fraction sensor is about 2.54 meter (see Figure 4).



**Figure 4. Schematic of flow path from evaporator to condenser**

Therefore, transit time for the liquid/vapor front from the evaporator after the reorientation in 2-g to the second void fraction sensor is calculated and plotted in Figure 5.

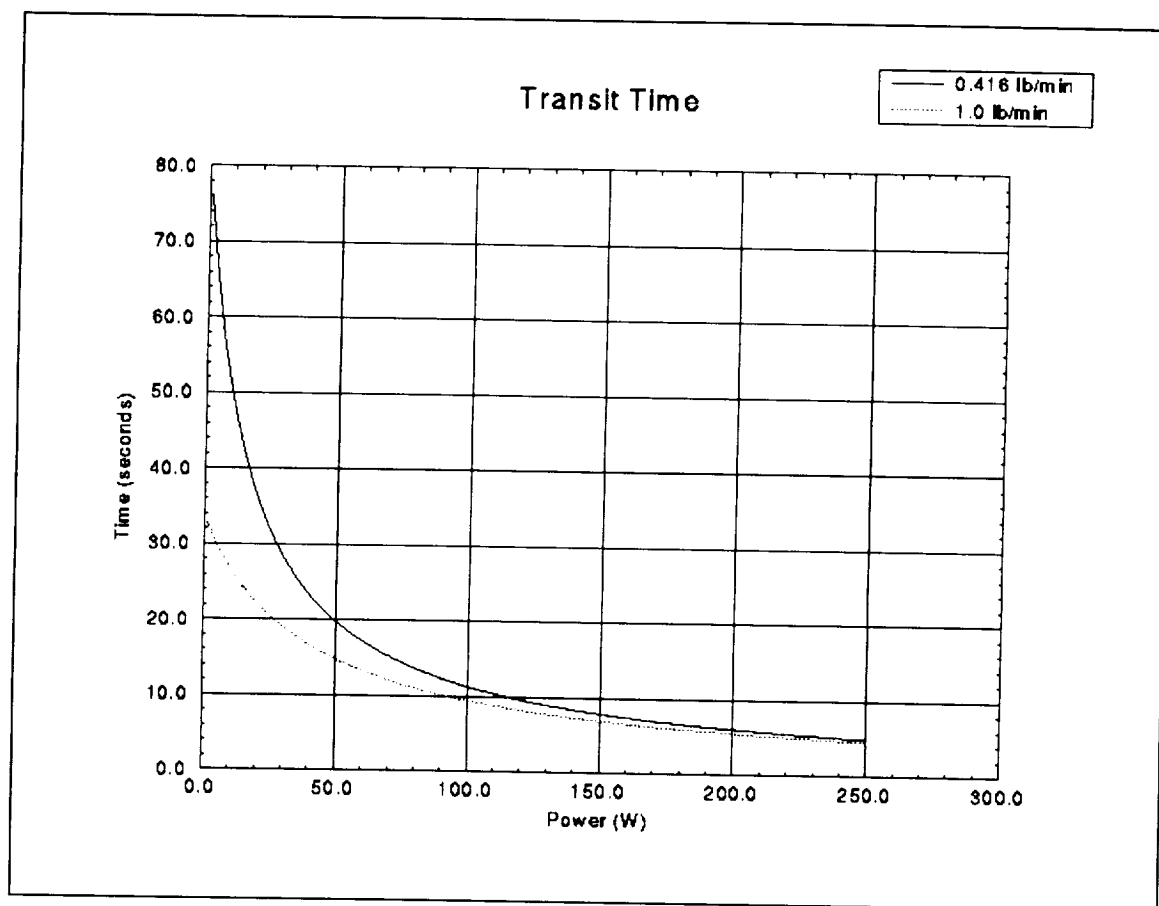


**Figure 5. Transit times for different power input.**

The linear relationship between velocity and power observed from Figure 3 can be shown by the following derivation.

$$j = \frac{Gx}{\rho_g \alpha}$$

Substituting for  $\alpha$  (Eq. 1)

$$j = \frac{Gx}{\rho_g \left[ \frac{1}{1 + \frac{(1-x) \rho_g}{x \rho_f}} \right]}$$

$$j = \frac{Gx}{\frac{x \rho_g \rho_f}{x(\rho_f - \rho_g) + \rho_g}}$$

$$j = \frac{G \left[ x(\rho_f - \rho_g) + \rho_g \right]}{\rho_f \rho_g}$$

Substituting for  $x$  (Eq. 2)

$$j = \frac{G \left[ \frac{Q}{\dot{m} h_{fg}} (\rho_f - \rho_g) + \rho_g \right]}{\rho_f \rho_g}$$

Therefore, for constant mass flow rate and properties, the superficial velocity is linearly dependent to evaporator power.

As shown in Figure 5, the transient time for evaporator power of 30 W is 28 seconds, which is longer than the 0-g period of 20 seconds. Therefore, steady two-phase flow conditions were not achieved. Even at the proposed mass flow rate of 1.0 lb/min, it will be difficult to obtain steady two-phase flow conditions to measure flow void fractions under 0-g period. It should be noted that this

analysis assumes no sub-cooling of the Suva prior to entering the evaporator. With sub-cooling, the transit times will be greater.